Aus dem
MUM – Muskuloskelettales Universitätszentrum München
Klinikum der Ludwig-Maximilians-Universität München
Direktor: Prof. Dr. med. Boris Holzapfel
Geschäftsführender Direktor: Prof. Dr. Wolfgang Böcker

Identification of Possible RNA Markers in Musculoskeletal Regeneration and Degeneration

Dissertation
zum Erwerb des Doktorgrades der Naturwissenschaften
an der Medizinischen Fakultät der
Ludwig-Maximilians-Universität München

vorgelegt von
Elif Akova Ölken
aus
Ankara, Turkei

Jahr
2024

Mit Genehmigung der Medizinischen Fakultät
der Universität München

Betreuer:	PD Dr. Attila Aszodi
Zweitgutachter:	Prof. Dr. Heiko Hermeking
Dekan:	Prof. Dr. med. Thomas Gudermann
Tag der mündlichen Prüfung:	25. September 2024

LMU LUDWIG-MAXIMILIANS-UNIVERSITÄT MÜNCHEN

Dekanat Medizinische Fakultät
Promotionsbüro

Affidavit

Akova Ölken, Elif

Surname, first name

I hereby declare, that the submitted thesis entitled

Identification of Possible RNA Markers in Musculoskeletal Regeneration and Degeneration

is my own work. I have only used the sources indicated and have not made unauthorised use of services of a third party. Where the work of others has been quoted or reproduced, the source is always given.

I further declare that the dissertation presented here has not been submitted in the same or similar form to any other institution for the purpose of obtaining an academic degree.

Munich, 26.09.2024

Place, Date

Elif Akova Ölken

Signature doctoral candidate

Table of content

List of abbreviations

MSC: Human Mesenchymal Stem Cell

SFRP2: Secreted Frizzled Related Protein 2

PC3: Caucasian prostate adenocarcinoma cell line

EMT: Epithelial to Mesenchymal Transition

COL1: Collagen Type 1

PCA: Principal Component Analysis

DEG: Differentially Expressed Genes

MA Plots: Log Mean Ratio (M) and Mean Average (MA) Plot

P-adj: Adjusted P value

GO Pathway: Gene Ontology Pathway

SC: Satellite Cells

List of publications

1. **Akova Ölken, E.**, Aszodi, A., Taipaleenmäki, H., Saito, H., Schönitzer, V., Chaloupka, M., ... & Saller, M. M. (2022). SFRP2 Overexpression Induces an Osteoblast-like Phenotype in Prostate Cancer Cells. Cells, 11(24), 4081.
2. Reiprich, S., **Akova, E**., Aszódi, A., & Schönitzer, V. (2021). Hyaluronan Synthases' Expression and Activity Are Induced by Fluid Shear Stress in Bone Marrow-Derived Mesenchymal Stem Cells. International journal of molecular sciences, 22(6), 3123.
3. Pircher, T., Wackerhage, H**., Akova, E**., Böcker, W., Aszodi, A., & Saller, M. M. (2022). Fusion of Normoxic-and Hypoxic-Preconditioned Myoblasts Leads to Increased Hypertrophy. Cells, 11(6), 1059.

Other Publications

4. Schluessel, S., Hartmann, E. S., Koehler, M. I., Beck, F., Redeker, J. I., Saller, M. M., **Akova, E**., ... & Mayer-Wagner, S. (2022). Dental and Orthopaedic Implant Loosening: Overlap in Gene Expression Regulation. Frontiers in Immunology, 13, 820843-820843.
5. Taha, S.; **Akova, E**.; Saller, M.M.; Giunta, R.E.; Haas-Lützenberger, E.M. Early Transcriptional Changes of Adipose-Derived Stem Cells (ADSCs) in Cell Culture. Medicina (2022), 58, 1249.
6. Stocks, M., Walter, A. S., **Akova, E**., Gauglitz, G., Aszodi, A., Boecker, W., ... & Volkmer, E. (2023). RNA-seq unravels distinct expression profiles of keloids and Dupuytren's disease. Heliyon.

My contribution to the publications

1.1 Contribution to paper I

For the paper "SFRP2 Overexpression Induces an Osteoblast-like Phenotype in Prostate Cancer Cells", I performed both *in vitro* experiments and computational analysis. I created *SFRP2* overexpressed PC3 cell line by using Sleeping Beauty Transposon system. During cloning experiments, I supervised an MSc student named as Beyza Bozdag, where she also included the creation of stable $PC3^{SFRP2}$ cell line into her thesis. Also, Martina Burggraf (MTA) guided me during the nucleofection steps. After the creation of the cell lines, first I started with the verification of the overexpression on gene and protein expression level (Paper I – Figure 1). After that, I isolated the RNA from each group and Martina Burggraf prepared the library for sequencing.

After I received the sequencing results, I executed differential gene expression analysis on R programming to define the effect of *SFRP2* gene overexpression on PC3 cells that were seeded on the COL1-coated surface. As long as COL1-$PC3^{\boldsymbol{SFRP2}}$ cells showed unique clustering compared to other groups (Paper I – Figure 2), I performed gene set enrichment analysis (GSEA) to check the significant gene ontology biological pathways (Paper I – Figure 3A). The results showed that the *SFRP2* overexpression increases biological adhesion, taxis, locomotion, and morphologic differentiation-related pathways significantly. To verify these significant biologic pathways, I tested each property *in vitro.* Furthermore, to prove the contribution of *SFRP2* expression on osteogenesis I retrieved osteoblast differentiation-related genes from GSEA and matched them with my dataset to observe the clustering (Paper I – Figure 3B).

First, I checked the change in morphology that was triggered by COL1 surface and *SFRP2* overexpression to prove the EMT (Epithelial to Mesenchymal Transition) property of the osteomimicry phenomenon (Paper I – Figure 4). Then I checked proliferation, metabolic activity, colony formation (Paper I – Figure 5) and migration and adhesion properties in both surface types (Paper I – Figure 6). After I finished the *in vitro* experiments with at least 3 technical replicates, I performed statistical analysis with two-way ANOVA on R programming.

In the last stage, I created an illustration to summarize our hypothesis on the Biorender website for the manuscript. By using all results together, I got help from my supervisors Attila Aszodi, Maximillian Saller, Hanna Taipaleenmäki, Hiroaki Saito and Veronika Schönitzer to finalize the manuscript and published it. Furthermore, from Klinikum LMU

urology and orthopedics department, we got a consultation about prostate cancer bone metastasis patients' diagnosis and treatment strategies.

1.2 Contribution to paper II

For the paper "Hyaluronan Synthases' Expression and Activity Are Induced by Fluid Shear Stress in Bone Marrow-Derived Mesenchymal Stem Cells", my colleague Sebastian Reiprich (S.R) performed the *in vitro* experiments. He first created HAS2 overexpressed SCP1 cells and by using human bone derived mesenchymal stem cells (hMSC) and HAS2-SCP1 cells, he applied fluid shear stress by special mechanical equipment. To be able to observe the transcriptomic changes were triggered by fluid shear stress, next-generation (NGS) RNA sequencing was performed for control hMSCs and fluid shear stress applied hMSCs with Illumina HiSeq1500 device

After the sequencing results, I performed the bioinformatics analysis of NGS data. First, I demultiplexed the raw data with specific Illumina primers and aligned them with human-specific genome version GRCh.38.99 by using STAR to be able to obtain read per gene file required for R programming sequencing analysis. To analyze the clustering within each group and the initial difference between control and treatment I performed PCA analysis (Paper II - Figure 2A). To understand the change in gene expression with fluid shear stress application, differential gene expression analysis was performed with the DESeq2 package. Depending on the significance cutoffs defined as, log fold change below -2 or higher than 2 and p-adjusted value below 0.05, I filtered down significant up- and down-regulated genes that are affected by the treatment (Paper II – Figure 2B/2C). As the primary aim of the project is to observe the effect of fluid shear stress on hyaluronan synthases (HA) related gene expression I filtered the genes that are upregulated in the treated group (Paper II – Figure 2D).

To be able to understand what other pathways are affected by the fluid shear stress treatment, I formed gene set enrichment analysis (GSEA) for significantly up- and down-regulated genes. I filtered biological process gene ontology pathways (Paper II – Figure 3). As the highest score in GO Pathway results belongs to the cellular response to fluid shear stress" (GO:0071498), I filtered the genes belong to this group and matched them with our data set to observe the significance of these genes. It is used to verify the mechanotransduction effect on transcriptome and support *in vitro* findings of my colleague S.R. (Paper II – Figure 4A/4B). Then I applied the same procedure for the biosynthetic process (GO:0030213) gene set as well (Paper II – Figure 6A/6B).

After the verification of mechanotransduction, it is known to be important for the regulation of osteogenic differentiation of MSCs in the literature [1]. For this reason, I

filtered significantly upregulated genes related to bone formation to support our finding with the well-known literature (Paper II – Figure 5A/5B).

In overall, the important morphological and biological changes were observed *in vitro* by my successful colleague Sebastian, I support his findings *in vitro* and his literature review with RNA Sequencing bioinformatics analysis and tried to translate these findings into a clinical point of view. We identified together possible RNA markers contributing to the bone biomineralization process that was triggered by mechanical stimuli and try to discover possible treatment options for bone fractures.

1.3 Contribution to paper III

For the paper "Fusion of Normoxic- and Hypoxic-Preconditioned My-oblasts Leads to Increased Hypertrophy", my colleague Tamara Pircher investigated hypoxia and normoxia condition on C2C12 myoblast biological properties and transcriptome. She co-cultured preconditioned hypoxic and normoxic C2C12 cells that are expressing GFP and RFP protein respectively. Sequencing libraries were prepared from these co-cultures in different time zone as 24h, 72h, 96h and 144h. I performed bioinformatic analysis and compared the effect of different co-culturing methods in different time zones. I performed PCA for the comparison of hypoxic-conditioned $C2C12^{RFP}$ my-oblasts in normoxia 21% (H-Diff_N) and normoxic-conditioned $C2C12^{GFP}$ cells in 2% hypoxia (N-Diff-H) at 4 different time points (Paper III – Fig7A). Then I calculated significantly upregulated genes belong specifically to each time point and common gene set (Paper III – Fig7B). I performed GSEA to detect matched hallmark gene sets in each time point (Paper III – Fig7C). I checked the Top 50 DEG expressed in be-tween two groups at each time point (Paper III – Fig7D) and from that list, I filtered 9 genes that were the most promising ones contributing to the myogenesis pathway (Paper III – Fig7E).

Introduction

1.4 Musculoskeletal System Development

The musculoskeletal system plays a vital role in the development and functioning of the human body. From infancy to adulthood, this complex system undergoes remarkable changes, enabling movement, support and protection. In early childhood, bones gradually grow and ossify, increasing in size and density. At the same time, muscles develop and strengthen through a combination of genetic factors and physical activity. As adolescence approaches, the skeletal structure matures further, the growth plates close and the bones reach their final shape. Certain diseases cause the musculoskeletal system to undergo detrimental changes in the functional parts of the body. In musculoskeletal research, the aim is to analyze these patient-specific changes, which are influenced by 'regeneration and degeneration of the musculoskeletal system', and to translate these findings into clinical applications as therapeutic options.

1.4.1 Musculoskeletal Regeneration

Musculoskeletal regeneration in healthy vertebrates is an ongoing process to regulate bone and muscle mass. Although a promising therapeutic target for the treatment of bone and muscle wasting diseases, from a cancer perspective, the excessive regeneration process, like many other pathways, must be suppressed.

Stem cells are emerging as one of the most promising individual therapeutic modalities for the treatment of musculoskeletal diseases due to their ability to differentiate into other lineages and self-renew [2]. Because stem cells are derived from the patient themselves, the immune response is relatively smaller than other treatment modalities [3], making cell-based regenerative therapy the promising "aspirin" of the modern world. The full pathway of stem cell differentiation and its precise localization are not yet fully understood. Although somewhat predictable under *in vitro* conditions, translational research is a prerequisite for the development of cell-based therapies. Understanding the biochemical and mechanistic stimuli that promote mesenchymal stem cell differentiation and the detection of potential biomarkers are essential.

1.4.1.1 Mesenchymal Stem Cells

Mesenchymal Stem Cells (MSCs) were first discovered by their differentiation and self-renewal potential around 1960s in mouse bone marrow [4], and the prerequisites for MSCs were defined in 2006 as differentiating into adipocytes, chondrocytes and osteoblasts [5-6]. In a transcriptomic manner, MSCs have signature cell surface antigens such as CD90, CD105 and CD73, and the lack of CD45, CD34, CD14, CD79 and HLA-DR [7]. Recently, it has been shown that not only the three lineages but also MSCs can differentiate into cell types that form muscle, tendons and other connective tissues [8].

Although first discovered in bone marrow and referred to in the literature as "bone stromal cells", later it was found that MSCs can also be also isolated from another tissues including the fat, dental pulp and muscle [9]. The different sources of MSCs in the human body for isolation make them highly attractive for regenerative medicine to treat musculoskeletal diseases, despite that multiple factors are involved in the differentiation process for a cell certain linage. Furthermore, targeting MSCs to the right place and precisely transplanting them is also extremely critical. Despite being administered intravenously, only a small percentage of infused mesenchymal stem cells (MSCs) are able to successfully reach the target tissue [10]. In many cases, this percentage is less than 1%, indicating the challenges involved in delivering MSCs to the desired site in the body. The low targeting efficiency of MSCs is a major limitation in their use for therapeutic purposes, and this has stimulated continued research into methods to improve the targeted administration of these cells.

Syngeneic mesenchymal stem cell transplantation represents a breakthrough in the treatment of musculoskeletal diseases. As a cell-based personalized medicine treatment, MSCs are immunosuppressive and immune rejection to other transplants are relatively low. With translational biomarker discovery, it is possible to identify MSCs and induce their differentiation into the desired lineage for treatment, even for allogeneic transplants. Still, it is important to identify novel RNA biomarkers for translational musculoskeletal diseases treatments.

1.4.1.2 Bone Formation and Bone Microenvironment

Human bone is a complex mixture of minerals and organic substances. Minerals make up 60% of bone, of which hydroxyapatite (calcium phosphate) is the primary component [11]. The remaining 20-40% is made up of organic material, primarily type I collagen

fibers. The process of bone mineralization, also known as calcification, is a vital and ongoing process in the human body. Collagen is a major structural protein of bone tissue, making up more than 90% of the extracellular matrix [12]. Collagen type I (Col-I) is the most abundant type of collagen in bone tissue, while type V collagen is present in smaller amounts [13]. The collagen fibers in bone tissue provide a structural framework for the deposition of minerals such as hydroxyapatite. These minerals, together with the collagen fibers, give bone strength and toughness. In addition to its structural role in bone tissue, collagen also plays a role in bone growth and development, as well as in the regulation of bone metabolism.

Osteogenesis is the process of bone formation that starts in the embryonic stage and continues until early adulthood. After this period the process switch to bone remodeling, where bone formation and bone resorption are in a balance to maintain the integrity of bone structure.

Osteoblasts are bone-forming cells that secretes extracellular matrix (ECM) proteins as Col-I [14] and promote bone mineralization by controlling the production and alignment of calcium phosphate crystals within the collagen-based matrix. The osteogenic differentiation both *in vitro* and *in vivo* is marked by the deposition of hydroxyapatite crystals at the late stage of development [15].

Skeletal diseases affecting adults often result from imbalances in bone remodeling caused by excessive activity of osteoclasts or osteoblast. This can lead to a range of conditions, including osteoporosis, which causes bones to become weak and brittle; periodontal disease, which affects the gums and other tissues that support teeth; rheumatoid arthritis, an autoimmune disorder that causes inflammation in the joints; multiple myeloma, a cancer that affects the bone marrow; and metastatic cancers, which are cancers that have spread from their original location to the bones [16]. In order to maintain the structural integrity of bone mass, there must be well-protected balance between the osteoblast and osteoclast activity.

The up or down regulation of markers or ligands that control osteogenesis and osteoclastogenesis are upstream targets for the maintenance of biological balance. MSCs can differentiate into osteoblasts for bone formation. This complex process involves a series of signaling pathways, transcription factors and extracellular matrix interactions (Figure 1). Bone morphogenetic protein-2 (BMP-2), transforming growth factor beta 1 (TGFß-1) [17] and the transcription factor Runx2, which govern the expression of genes associated with osteoblast maturation [18] are well-defined regulators of osteoblast differentiation.

The synthesis and secretion and subsequent mineralization of extracellular matrix components contribute to the formation of new bone tissue. Even if the regulatory pathways are known for osteoblast differentiation, it is still an ongoing challenge to implement this knowledge into a translational therapeutic method.

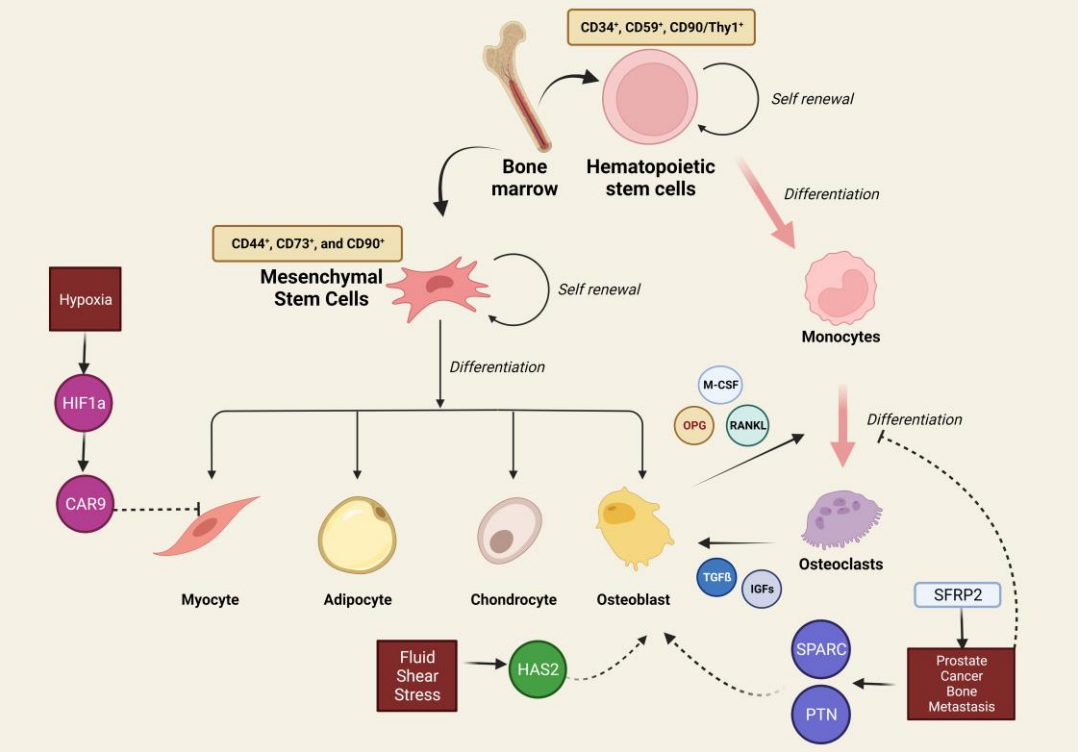

Figure 1: Illustration of musculoskeletal system development and the contribution of potential RNA markers in regenerative (dashed line) and degenerative (dashed inhibitor lines) musculoskeletal diseases. Created with BioRender.

1.4.1.2.1 Fluid Shear Stress

The complex process of osteoblast differentiation plays a key role in bone homeostasis, and mechanical stimuli such as fluid shear stress (FSS) contribute to this differentiation process. Fluid shear stress is a mechanical stimulus defined as the stress exerted by flowing fluids on cells. Basically, it is caused by accumulation of fluid in between bone cells during blood circulation and bending of bones. Cells can sense FSS through mechanoreceptors such as integrins and ion channels [19]. This sensing process triggers a series of intracellular signaling pathways that influence cell differentiation and function. In other words, cells use FSS to regulate their own differentiation into specific cell types. FSS has been shown to play a remarkable role in the differentiation and proliferation of MSCs [20]. Several studies have indicated that both continous fluid flow

(CFF) and pulsating fluid flow (PFF) enhance osteogenic differentiation compared to static culture [21].

Application of shear stress for MSC differentiation is a promising new therapeutic approach since as it provides a safer method to stimulate bone regeneration in destructive musculoskeletal diseases. Therefore, it is of utmost importance to understand the influence of the stimulus of FSS on MSCs *in vitro* and to make it feasible for clinical research through transcriptomic changes.

1.4.1.3 Myogenesis and Skeletal Muscle Development

Myogenesis is the process of skeletal muscle cell development and differentiation that occurs during both embryogenesis and postnatal life. Myogenesis involves the differentiation of multipotent stem cells into progenitor muscle cells, called myoblasts, and the fusion of those myoblasts into multinucleated muscle fibers. In adults, myogenesis occurs to repair and maintain muscle tissue.

The main cell types involved in myogenesis are satellite cells (SC – myogenic stem cells) and mesenchymal stem cells (MSCs), which are found in various tissues of the body. SCs are stem cells located between the sarcolemma and basal lamina of muscle fibers [22] and have *PAX3* as an identity marker [23]. Both satellite cells and MSCs have the ability to differentiate into myoblasts and contribute to the process of muscle repair and growth. Dysregulation of myogenesis can lead to muscle disorders such as muscular dystrophy. Research into myogenesis has implications for the treatment of muscle-wasting diseases and injuries, as well as for the understanding of muscle function in health and disease conditions.

Several studies have investigated the role of MSCs in muscle repair and regeneration. MSCs can express muscle-specific markers like *IGF-1* or *HGF* [24] and differentiate towards the myogenic lineage, but their ability to differentiate into muscle cells is limited and yet not fully understood.

1.4.2 Musculoskeletal Degeneration

Musculoskeletal degeneration alters the integrity and function of the musculoskeletal system. Ageing is one of the primary factors that contribute to the loss of bone and muscle mass [25], by altering the transcriptome and hormonal status of patients. In addition, due to genetic mutations, lifestyle choices or injuries, the musculoskeletal system can undergo degenerative changes that lead to pain, impaired mobility, and reduced quality of life.

Common examples of musculoskeletal degeneration include osteoarthritis, osteoporosis, tendinopathy, and muscular atrophy. According to the World Health Organization (WHO) declaration in 2022, 1.71 billion people still suffer from musculoskeletal conditions worldwide, which shows how far we are for finding potential therapies that can inhibit musculoskeletal degeneration or promote regeneration, depending on the disease. Yet, current advances in regenerative medicine are only just emerging.

1.4.2.1.1 Bone Degradation

During bone resorption, existing bone tissue by specialized cells called osteoclasts, which break down the bone matrix and release minerals into the bloodstream. I contrast to the bone-producing osteoblasts, which differentiate from mesenchymal progenitors, osteoclast are bone destructive cells derived from the monocyte/macrophage lineage [26] however, their differentiation is mediated by the osteoblasts gene expression (Figure 1). M-CSF (Macrophage colony stimulating factor) [27] and RANKL/TNSF11, which is recognized by the osteoclast precursor receptor RANK/TNFRSF11A [28], activates NF-κB pathway and regulates the formation of osteoclasts (Figure 1).

In diseases involving excessive bone formation, such as osteoporosis and certain type of bone metastasis, to enhance osteoclast differentiation for inducing degeneration is a promising therapeutic option that could completely change the direction of musculoskeletal research.

1.4.2.1.2 Muscle Degradation with Hypoxia

Oxygen is vital for the survival and proper functioning of aerobic cells, as it is required for various metabolic processes, energy production, proliferation, and even for the self-renewal and differentiation of certain cell types. It is an essential component of the environment in which these cells operate and is required to maintain their structural and functional integrity. However, most studies of the effects of oxygen on cellular behavior have been conducted using 21% oxygen levels that are much higher than those found in the body's tissues (3-5%) [29]. Thereby, this effects the morphology and biological properties of each cell type and makes it even more difficult to translate *in vitro* findings to clinical application.

The concentration of oxygen in muscle tissue tends is generally lower during embryonic development and in certain pathological conditions [30]. The decrease in oxygen levels have an impact on the development and function of muscle tissue, and can even lead to atrophy [31]. A reduction in oxygen levels, known as hypoxia, has been

observed to inhibit muscle stem cell differentiation by upregulating a transcription factor hypoxia-inducible 1a (HIF1a) [32]. This effect has been widely studied in the context of various diseases and injuries, as the ability of stem cells to respond to changes in oxygen availability may have important therapeutic implications. Furthermore, it has been shown that changes in oxygen concentration can affect the behavior of stem cells and the process of muscle differentiation, and may have implications for tissue repair and regeneration [33].

1.5 Regenerative and Degenerative RNA Markers in Musculoskeletal Diseases

The development of the bone, muscles and cartilage is well-defined in the literature, including the impact of stem cell differentiation on the formation of these tissue types. In term of regenerative medicine, however, there are still huge gaps in between laboratory research and clinical trials. As like other transitional research subjects, there are two primary goals; one is to use of these stem cells for the treatment of various musculoskeletal diseases such as osteoporosis, muscle atrophy, sarcopenia or even bone tumors. As long as the number of MSC in bone microenvironment is age dependent [34] and the loss can cause an imbalance in the differentiation rate, translational research in orthopedic related diseases is crucial. However, MSC transplantation is not promising for the time being, because of the failure of long term engraftment in *in vivo* mouse models [35]. The second goal is to fully the understand pathways that cause musculoskeletal diseases, metastatic or primary bone cancer, and to find potential biomarkers for drugs or diagnosis. Discovery of novel RNA biomarkers may increase patient survival and allow researchers to diagnose diseases/cancer at an early stage.

Translational research has a dual advantage in terms of current treatment of diseases of the musculoskeletal system; on the one hand, it can provide more examples for *in vitro* research, and on the other hand, it can increase the probability of finding biomarkers. Using RNA Sequencing analysis and Gene Set Enrichment Analysis (GSEA), the identified markers of osteogenic or myogenic differentiation pathways are well established and are constantly updated with new results. This up-to-date data analysis brings researchers one step closer to understanding the entire disease process with predictive early biomarkers and finding a potential cure.

1.5.1 Tumor Orthopedics

Tumor orthopedics is the field that covers primary and secondary musculoskeletal sarcomas. Primary tumors are formed inside or at surface of the bone, where chondrosarcomas account for 40% and osteosarcomas represent 28% of the diagnosed patients, respectively [36]. Osteosarcomas are mainly formed by malignant osteoblasts derived from MSCs or osteoblast precursor cells [37].

Secondary musculoskeletal sarcomas are generated by metastasis of aggressive epithelial tumors. The most common osteotropic tumors are breast, lung and prostate cancers, which are usually located close to the axial skeleton of the human body [38]. The main challenge is the early detection of metastatic cells with an osteotropic tendency and the timely interruption of bone metastasis which may result in fatal consequences. There are two types of osteotropic cancers; osteoclastic and osteoblastic bone metastasis. Unlike other common osteotropic metastatic cancers, such as breast or lung cancer, prostate cancer can metastasize either bone-destructive or bone-generative.

1.5.1.1 Prostate Cancer Bone Metastasis

Prostate cancer remains a major risk factor for men. In 2021, 248,530 new prostate cancer patients were diagnosed in the United States alone, far higher than any other type of cancer diagnosed and accounting for 13% of all cancer diagnoses [39]. Aging has a strong impact on the formation of prostate cancer, with 64% of diagnosed patients older than 65 years old [40]. Despite being so common, successful treatment rate and overall patient survival are high in the case of early diagnosis. However, when cancer cells leave the primary site and metastasize, patient survival is dramatically reduced. After the discovery of “prostate specific antigen” (PSA) in blood serum by Papsidero in the 1980s [41], it became a commonly used diagnostic biomarker for prostate cancer in men. Abundant expression of PSA encoded by *KLK3* gene in prostate cells is used for initial monitoring and staging of the patients, despite its relatively low specificity and the tendency cause false positive results [42]. Therefore, it is very important to find better biomarkers that are highly spesific for prostate cancer stages and even to detect metastasis.

The most common sites for prostate cancer metastasis are lymph nodes and bones. Therefore, early diagnostic markers are needed to detect osteoblast or osteoclast differentiation. For this purpose, besides the commonly used serum marker PSA for prostate cancer diagnosis, other possible serum or bone markers are required to identify patients with prognosis for advanced prostate cancer. In order to achieve this, it is important to

understand the difference between the transcriptome of primary and metastatic prostate cancer, and especially the influence of metastatic cancer cells on the differentiation of MSCs or the activity of osteoblast and osteoclasts.

1.5.1.1.1 *SFRP2* Expression in Prostate Cancer Bone Metastasis

Osteomimicry is a survival strategy for metastatic cancer cells to evade the immune response and invade bone to colonize at later stages [43]. Therefore, targeting osteomimicry with the help of novel biomarkers may be a potential solution to intervene in this pathway and increase survival in patients with prostate cancer bone metastasis. *Secreted frizzled-related protein 2* (*SFRP2*) is a potential osteomimic biomarker due to its dual function in cancer and bone cells.

WNT signaling is a double-edge sword that is crucial for the development of the cells, whereas aberrant WNT activity is observed mostly associated with cancer cells due to increased proliferation and metastasis [44]. Several regulators are responsible for the suppression of WNT signaling, such as Dickkopf-1 (DKK1) [45] and secreted frizzled-related proteins (sFRPs) [46]. These regulators are hypermethylated in their promoter region in most cancer types including prostate cancer, due to their tumor suppressor properties [47]. However, recent studies have shown that in addition to the function of SFRP2 as an antagonist of WNT signaling, it could also promote EMT (Epithelial to Mesenchymal Transition) and metastasis in various cancer cells [48-49].

In addition to the function of SFRP2 on cancer cells, it has been found that *SFRP2* deficiency causes a decrease in skeletal stem cell self-renewal and thus a decrease in bone healing [50]. Furthermore, *SFRP2* expression in blood shows poor prognosis in breast cancer [51] where, similar to prostate cancer, bone metastases are common in the latest stage of breast cancer. Therefore, there is a potential correlation between osteoblastic bone formation and bone metastasis. This correlation makes *SFRP2* as a potential diagnostic marker for secondary bone metastasis (Figure 1) that is not yet curable (Figure 1).

1.5.2 Osteological Diseases and Fractures

Skeletal development and fracture repair is a complex process involving the coordination of several events. This process involves the migration, differentiation and activation of several cell types and tissues. During the development of the skeleton, cells called osteoblasts and osteoclasts work together to form new bone tissue and shape it into the

desired structure, where osteoblasts are responsible for the synthesis and deposition of bone matrix and osteoclasts for the breakdown and resorption of bone tissue.

When there bone loss due to injury, the body responds by activating various cells and tissues to repair the damage. This process involves the activation of immune cells, the formation of a blood clot to stop bleeding, and the activation and differentiation of bone-forming osteoblasts. The coordinated action of these cells and tissues is essential for the successful repair of fractures. To this end, it is important to find potential biomarkers which could participate in the activation of osteogenesis. The differentiation of stem cells and their migration to the damaged site is a complex mechanism, which includes the combination of chemical and mechanical stimuli to induce osteoblast formation. Furthermore, the identification of RNA biomarkers is of utmost importance in the treatment of excessive osteoclast activity causing osteoporosis or periodontal disease.

For these purposes, translational research on MSCs has focused on developing MSC-based therapies that can be used to treat these diseases and conditions in clinical settings. This research has involved the isolation, expansion, and characterization of MSCs, as well as the development of strategies for their delivery and engraftment into the body. Next-generation sequencing technology may enhance this process by identifying potential RNA markers at each step. The knowledge gained from RNA biomarkers may pave the way for new treatment modalities to re-enforce differentiation in a fractured bone or in the case of osteogenesis imperfecta (OI), where the bone is brittle due to the absence or insufficient formation of the type I collagen network [52]. Furthermore, other factors contributing mechanically or chemically to the osteogenic differentiation pathway can be detected using biomarkers.

1.5.2.1 *HAS2* Expression in Osteogenesis

Hyaluronan (HA) is a large, linear glycosaminoglycan that is crucial for tissue development and regeneration. It is important for many tissue, including bone marrow, where hyaluronan is a key ECM component that promotes the stem cell differentiation [53]. Hyaluronan interacts with the cells via the cell surface receptor CD44 [54]. In bone marrow-derived MSCs, hyaluronan is produced the three major hyaluronan synthases (*HAS1, HAS2,* and *HAS3*), and the CD44-HA coat is maintained in an autocrine manner [55], yet much remains unknown about the exact function of HA in MSC differentiation. These enzymes contribute to the local production of hyaluronan in the bone

microenvironment, and studies have shown that especially the expression of *HAS2* is altered during osteoblast differentiation [56]. This observation making *HAS2* a potential diagnostic RNA marker for detecting an increase or decrease in osteogenesis in musculoskeletal diseases, as well as a potential therapeutic target in regenerative medicine.

1.5.3 Myopathy

Myopathy is a term that refers to a group of diseases that affect the muscles, such as cachexia, sarcopenia, muscular dystrophies. The skeletal muscle is the largest tissue in the body and when it is unable to function or regenerate properly, it can cause musculoskeletal disorders resulting in severe disability. These diseases can be caused by a variety of factors, including genetic mutations, metabolic disorders, and autoimmune conditions. The capacity for regeneration in this specific context is limited for minor wounds and injuries. In the case of major muscle loss due to trauma or surgery, a greater effort is required in order to achieve adequate repair and regeneration.

Depending on the identified markers in GSEA for myogenesis pathway, effectors molecules induced by chemical and mechanical stimuli can be identified for the treatment of common skeletal muscle diseases. MSCs is the remarkable, cell-based therapeutic option for the treatment of skeletal muscle diseases due to their differentiation potential for myoblasts. However, further research is needed to fully understand the mechanisms of myogenesis and to determine the optimal conditions for utilizing MSCs in muscle repair and regeneration therapies.

1.5.3.1 *CAR9* Expression in Myogenesis

Hypoxia is one of the major contributor of muscle atrophy. HIF-1α is the key transcription factor expressed by innate and adaptive immune cells in response to low oxygen concentration to initiate pro-inflammatory response [57]. In terms of severe hypoxia, this pro-inflammatory signaling reduces the proliferation of satellite cells and disturbs their differentiation [58]. *Carbonic anhydrase 9 (CA9/CAR9)* is a major target of HIF-1α, which regulates extracellular acidification by controlling pH in most cancer cells and is associated with poor cancer prognosis [59]. Therefore, it is expected to become a novel marker of hypoxia in cancer cells. Furthermore, it was found that chronic hypoxic conditions significantly upregulates *CAR9* expression in mouse gastrocnemius muscle *in vivo* and in the myoblastic C2C12 cell line *in vitro* [60]. Even it is a potential target in cancer, the effect of *CAR9* expression on downstream targets need to be investigated in

ischemic epithelial and endothelial cells. CAR9 is a promissing diagnostic biomarker for hypoxia induced muscular atrophy and it may identify cells effected by ischemia-reperfusion injury.

1.6 Computational Biology for the Identification of RNA Markers

Translational and clinical research plays a crucial role in the development and evaluation of new treatments and interventions for a range of diseases. Translational research is the translation of scientific findings into clinical practice, while clinical research is the testing of new treatments on human subjects through clinical trials. A key area of translational research is personalized medicine, which aims to tailor treatments to the specific genetic and molecular characteristics of individual patients. This approach has the potential to improve the effectiveness and safety of treatments and has been applied to a wide range of diseases including cancer, cardiovascular disease and neurodegenerative disorders [61].

A primary goal in modern medicine is to translate findings of basic science at the molecular or cellular level into a potential clinical treatment. This “bench to bedside” approach, coined by National Cancer Institute (NCI) [62], is the simplest definition of translational research and requires the integration of many research fields including “omics” to close the bridge between basic research and clinical practice.

The term “omics” refers to the study of large-scale sets of biological data, such as genomics (the study of the entire genome), transcriptomics (the study of the transcriptome, i.e. all RNA molecules in a cell), proteomics (the study of the proteome, i.e. all proteins in a cell) and metabolomics (the study of the metabolome, i.e. all small molecules involved in metabolism). These disciplines use high-throughput technologies to generate large amounts of data that can be effectively analyzed to gain insights into biological processes and diseases. Omics technologies are widely used in areas such as drug development, disease diagnosis and personalized medicine.

While genomics focuses on the common mutations on the genome level, transcriptomics explores the pattern of gene expression to understand the impact of biological (normal and pathological) conditions on the whole system. Transcriptomic analysis aims to identify possible RNA markers by RNA Sequencing (RNA-Seq) technology for early detection of a disease or a deep understanding of the molecular mechanisms of a condition. It shortens the duration for translating *in vitro* findings to the clinical application, which has revolutionized clinical research.

1.6.1 Next-Generation RNA Sequencing

RNA sequencing is a breakthrough in biological sciences that enables researchers to study the gene expression levels in a biological sample on bulk tissue or cellular levels. The first method was developed in the 1970s, using a technique called S1 mapping [63] which involves the digestion of RNA with S1 nuclease, followed by the separation of the resulting fragments by electrophoresis and the visualization of the fragments using autoradiography. In the 1990s, a new method, serial analysis of gene expression (SAGE), was developed, which allowed high-throughput analysis of gene expression [64]. This method is based on the digestion of RNA into short fragments with a set of specific restriction enzymes, followed by the amplification and sequencing of the resulting fragments [65]. However, it was still relatively slow and expensive compared to other DNA sequencing technologies.

Next-generation sequencing (NGS) is a revolution phase in the sequencing area, which refers to high-throughput sequencing technologies. The first marketed NGS platform (Roche 454) based on paralleled pyrosequencing was presented in 2004 [66]. It significantly improved the speed and accuracy of RNA sequencing and reduced the cost of the process, especially in the field of genetic diseases and cancer research [67]. In 2005, Solexa, a company later purchased by Illumina, introduced Genome Analyzer. This technology used a different approach to DNA sequencing, known as synthesis sequencing, which enabled much higher throughput and lower costs compared to pyrosequencing. Since then, several other NGS technologies have been developed, including Ion Torrent, Pacific Biosciences and Oxford Nanopore, which have further improved the speed, accuracy and cost of RNA sequencing.

Today, NGS technologies are widely used in a variety of applications, including the study of the whole transcriptome and the identification of potential biomarkers for cancer and other diseases. Moreover, NGS allows the identification of genetic variations associated with disease susceptibility, and the analysis of gene regulation and function.

1.6.2 RNA Biomarker Research

Advances in technology have had a significant impact on biological research, resulting in the evolution of diagnostic procedures and targeted drug development techniques. Biomarkers are used to assists diagnosis, prognosis and treatment of various diseases. Simply defining, a biomarker (biological marker) is an accurately measurable biological

entity that gives relevant information about the patient's medical status [68]. It is a "significant and meaningful" change in protein or gene expression that is triggered by a potential disease [69] that should be reproducible for the majority of the patients.

Biomarker research has been accelerated after the technical development of sequencing. It grounds the "filling the gap" position in translational research aiming to transfer *in vitro* findings to clinical application. Before the boost of sequencing technology, biomarker research is mainly performed via protein extraction and purification and antigen detection in tissues and body fluids. In addition, PCR technology has been used to detect predicted gene expressions, i.e., predicted biomarkers. However, these methods are mostly valid in the later stages of the disease and cannot be used in asymptomatic patients. With sequencing technology, not only a single biomarker can be detected, but the effect of a single gene mutation or a disease on to the whole transcriptome can also be observed.

The use of NGS has enabled researchers to analyze large quantities of tissue samples to identify potential RNA markers that can serve as indicators of specific biological processes or diseases. This cutting-edge technology allows rapid and comprehensive analysis of RNA, providing valuable insights into the underlying mechanisms of various biological systems and paving the way for the development of new therapeutic approaches. Moreover, with the improvement of sequencing technology in the last decade, single-cell RNA sequencing has been another breakthrough that led to an understanding of unique markers that represent individual cell types in bulk tissue [70]. Nevertheless, independent of the sequencing method, computational analysis is a prerequisite for the identification of RNA biomarkers.

1.6.3 Next-Generation RNA-Sequencing Bioinformatics Analysis

Bioinformatics is the modern-day enhancement in biological studies, where basic laboratory research is expanded with computational analysis. By using comprehensive omics data, researchers can now observe the effect of a treatment, genetic modification or disease status on genomic, transcriptomic, proteomic and metabolomics levels.

RNA-Seq data is typically stored in a text-based file format called FASTA, which represents nucleotide sequence data in a compressed format. FASTA files contain four lines of text for each sequence read, including the sequence identifier, the nucleotide sequence, a quality score identifier, and the quality scores for each nucleotide [71].

The initial step of bioinformatics analysis is to demultiplex the FASTA files based on sample-specific barcodes used in the library construction. Demultiplexing typically

involves the decoding of barcodes, which are unique sequences added to the RNA-Seq reads of each sample during library preparation, in sequencing results [72]. To identify read per gene counts, an alignment step is performed on the demultiplexed sequence. Alignment refers to the process of aligning the reads (short nucleotide sequences) generated by the sequencing process to the reference genome provided by the Ensembl Project [73]. One of the advantages of the Ensembl genome has been the ability to keep bioinformatics analysis up-to-date. Alignment allows researchers to align reads to specific locations in the genome and identify the transcripts from which the reads are derived [74]. STAR (Spliced Transcripts Alignment to a Reference) is at well-known software tool for aligning RNA-Seq reads to a reference genome with high speed and sensitivity [75]. STAR uses a two-step alignment process to align RNA-Seq reads to a reference genome. In the first step, it searches for splice junctions in the reads and uses these junctions to align the reads to the genome. This approach allows STAR to more accurately align reads across splice junctions than other alignment tools. [76].

After the read per gene counts have been determined from STAR alignment, R programming packages can be used to calculate the differential gene expression between samples or treatment methods. The purpose of the calculations is the "production of a list of genes passing multiple-test adjustment and ranked by P value" [77]. The DESeq2 package is one of the well-established solutions for next-generation RNA sequencing analysis, offering higher sensitivity while controlling false positive rate [78] compared to other Differential Expression Analysis methods such as the edgeR or limma packages [79].

Log Fold Change (LFC) measures the difference in gene expression between two samples or conditions. A positive LFC value indicates that the gene is better expressed in one sample, while a negative LFC indicates that the gene is better expressed in the other sample. Significant up- or down-regulation of a gene can be assessed using the LFC and the adjusted p-value (p-adj). The most widely accepted general confidence interval in the scientific community is 95%, so the p-adj cut-off is usually set at 0.05. For the LFC cut-off, depending on how rigorously the difference between samples is to be assessed, LFC cut-offs are usually defined as less than -1 (or -2) and greater than 1 (or 2) for calculations.

By identifying significant differentially expressed genes (DEGs), bioinformatics analysis leads to the generation of meaningful transcriptomic patterns needed to understand a disease or condition. Gene set enrichment analysis (GSEA) is a statistical method used to match DEG genes to gene set groups of genes with common biological or chromosomal characteristics [80]. It is a widely used approach in the field of genomics

and transcriptomics for identifying functional relationships among genes and for understanding the biological mechanisms underlying complex diseases and other biological phenomena. Gene Ontology (GO) Pathways are biological predefined gene sets according to the literature that are used in GSEA [81]. For analyzing differential gene expressions, GO Pathway analysis is more straightforward to make a correlation of the genes with each other. Moreover, it simplifies the results in a comprehensive way to every researcher that has no experience with bioinformatics analysis.

Ultimately, bioinformatic analysis takes the traditional methods of wet laboratory experiments a step further to achieve the noble goal of clinical research. It is important to find potential therapeutic targets or the main origin of disease to extend the lifespan of individual patients. Therefore, as translational research aims to translate *in vitro* laboratory results into clinical application, the importance of computational bioinformatics analysis is undeniable.

2. References

1- Stewart, Sarah et al. “Mechanotransduction in osteogenesis.” *Bone & joint research* vol. 9,1 1-14. 16 May. 2020, doi:10.1302/2046-3758.91.BJR-2019-0043.R2

2- Ding, Dah-Ching et al. “Mesenchymal stem cells.” *Cell transplantation* vol. 20,1 (2011): 5-14. doi:10.3727/096368910X

3- Lovell-Badge, R. “The future for stem cell research.” *Nature* vol. 414,6859 (2001): 88-91. doi:10.1038/35102150

4- Friedenstein, A J et al. “Osteogenesis in transplants of bone marrow cells.” *Journal of embryology and experimental morphology* vol. 16,3 (1966): 381-90.

5- Dominici, M et al. “Minimal criteria for defining multipotent mesenchymal stromal cells. The International Society for Cellular Therapy position statement.” *Cytotherapy* vol. 8,4 (2006): 315-7. doi:10.1080/14653240600855905

6- Sun, Yuyang et al. “Mechanical Stimulation on Mesenchymal Stem Cells and Surrounding Microenvironments in Bone Regeneration: Regulations and Applications.” *Frontiers in cell and developmental biology* vol. 10 808303. 21 Jan. 2022, doi:10.3389/fcell.2022.8083037

7- Ankrum, James A et al. “Mesenchymal stem cells: immune evasive, not immune privileged.” *Nature biotechnology* vol. 32,3 (2014): 252-60. doi:10.1038/nbt.2816

8- Marion, Nicholas W, and Jeremy J Mao. “Mesenchymal stem cells and tissue engineering.” *Methods in enzymology* vol. 420 (2006): 339-61. doi:10.1016/S0076-6879(06)20016-8

9- Kisiel, Agatha H et al. “Isolation, characterization, and in vitro proliferation of canine mesenchymal stem cells derived from bone marrow, adipose tissue, muscle, and periosteum.” *American journal of veterinary research* vol. 73,8 (2012): 1305-17. doi:10.2460/ajvr.73.8.1305

10- Ankrum, James, and Jeffrey M Karp. “Mesenchymal stem cell therapy: Two steps forward, one step back.” *Trends in molecular medicine* vol. 16,5 (2010): 203-9. doi:10.1016/j.molmed.2010.02.005

11- Feng, Xu. “Chemical and Biochemical Basis of Cell-Bone Matrix Interaction in Health and Disease.” *Current chemical biology* vol. 3,2 (2009): 189-196. doi:10.2174/187231309788166398

12- Rico-Llanos, Gustavo A et al. “Collagen Type I Biomaterials as Scaffolds for Bone Tissue Engineering.” *Polymers* vol. 13,4 599. 17 Feb. 2021, doi:10.3390/polym13040599

13- Amirrah, Ibrahim N et al. “A Comprehensive Review on Collagen Type I Development of Biomaterials for Tissue Engineering: From Biosynthesis to Bioscaffold.” *Biomedicines* vol. 10,9 2307. 16 Sep. 2022, doi:10.3390/biomedicines10092307

14- Wittkowske, Claudia et al. “*In Vitro* Bone Cell Models: Impact of Fluid Shear Stress on Bone Formation.” *Frontiers in bioengineering and biotechnology* vol. 4 87. 15 Nov. 2016, doi:10.3389/fbioe.2016.00087

15- Quarles, L D et al. “Distinct proliferative and differentiated stages of murine MC3T3-E1 cells in culture: an in vitro model of osteoblast development.” *Journal of bone and mineral research : the official journal of the American Society for Bone and Mineral Research* vol. 7,6 (1992): 683-92. doi:10.1002/jbmr.5650070613

16- Boyle, William J et al. “Osteoclast differentiation and activation.” *Nature* vol. 423,6937 (2003): 337-42. doi:10.1038/nature01658
17- Wu, Mengrui et al. “TGF-β and BMP signaling in osteoblast, skeletal development, and bone formation, homeostasis and disease.” *Bone research* vol. 4 16009. 26 Apr. 2016, doi:10.1038/boneres.2016.9
18- Komori, Toshihisa. “Regulation of Proliferation, Differentiation and Functions of Osteoblasts by Runx2.” *International journal of molecular sciences* vol. 20,7 1694. 4 Apr. 2019, doi:10.3390/ijms20071694
19- Huang, Xiaobin et al. “Physical Stimulations for Bone and Cartilage Regeneration.” *Regenerative engineering and translational medicine* vol. 4,4 (2018): 216-237. doi:10.1007/s40883-018-0064-0
20- Elashry, Mohamed I et al. “Influence of mechanical fluid shear stress on the osteogenic differentiation protocols for Equine adipose tissue-derived mesenchymal stem cells.” *Acta histochemica* vol. 121,3 (2019): 344-353. doi:10.1016/j.acthis.2019.02.002
21- Huang, Xiaobin et al. “Physical Stimulations for Bone and Cartilage Regeneration.” *Regenerative engineering and translational medicine* vol. 4,4 (2018): 216-237. doi:10.1007/s40883-018-0064-0
22- Morgan, Jennifer E, and Terence A Partridge. “Muscle satellite cells.” *The international journal of biochemistry & cell biology* vol. 35,8 (2003): 1151-6. doi:10.1016/s1357-2725(03)00042-6
23- Motohashi, Norio, and Atsushi Asakura. “Muscle satellite cell heterogeneity and self-renewal.” *Frontiers in cell and developmental biology* vol. 2 1. 30 Jan. 2014, doi:10.3389/fcell.2014.00001
24- Witt, R et al. “Mesenchymal stem cells and myoblast differentiation under HGF and IGF-1 stimulation for 3D skeletal muscle tissue engineering.” *BMC cell biology* vol. 18,1 15. 28 Feb. 2017, doi:10.1186/s12860-017-0131-2
25- Roberts, Sally et al. “Ageing in the musculoskeletal system.” *Acta orthopaedica* vol. 87,sup363 (2016): 15-25. doi:10.1080/17453674.2016.1244750
26- Udagawa, N et al. “Origin of osteoclasts: mature monocytes and macrophages are capable of differentiating into osteoclasts under a suitable microenvironment prepared by bone marrow-derived stromal cells.” *Proceedings of the National Academy of Sciences of the United States of America* vol. 87,18 (1990): 7260-4. doi:10.1073/pnas.87.18.7260
27- Yoshida, H et al. “The murine mutation osteopetrosis is in the coding region of the macrophage colony stimulating factor gene.” *Nature* vol. 345,6274 (1990): 442-4. doi:10.1038/345442a0
28- Pérez-Sayáns, Mario et al. “RANK/RANKL/OPG role in distraction osteogenesis.” *Oral surgery, oral medicine, oral pathology, oral radiology, and endodontics* vol. 109,5 (2010): 679-86. doi:10.1016/j.tripleo.2009.10.042
29- Carreau, Aude et al. “Why is the partial oxygen pressure of human tissues a crucial parameter? Small molecules and hypoxia.” *Journal of cellular and molecular medicine* vol. 15,6 (2011): 1239-53. doi:10.1111/j.1582-4934.2011.01258.x
30- Pircher, Tamara et al. “Hypoxic Signaling in Skeletal Muscle Maintenance and Regeneration: A Systematic Review.” *Frontiers in physiology* vol. 12 684899. 23 Jun. 2021, doi:10.3389/fphys.2021.684899
31- Barreiro, Esther, and Ariel Jaitovich. “Muscle atrophy in chronic obstructive pulmonary disease: molecular basis and potential therapeutic targets.” *Journal of thoracic disease* vol. 10,Suppl 12 (2018): S1415-S1424. doi:10.21037/jtd.2018.04.168

32- Sinha, Krishna M et al. “Hypoxia-inducible factor 1α (HIF-1α) is a major determinant in the enhanced function of muscle-derived progenitors from MRL/MpJ mice.” *FASEB journal : official publication of the Federation of American Societies for Experimental Biology* vol. 33,7 (2019): 8321-8334. doi:10.1096/fj.201801794R
33- Redshaw, Zoe, and Paul T Loughna. “Oxygen concentration modulates the differentiation of muscle stem cells toward myogenic and adipogenic fates.” *Differentiation; research in biological diversity* vol. 84,2 (2012): 193-202. doi:10.1016/j.diff.2012.06.001
34- Guan, Min et al. “Directing mesenchymal stem cells to bone to augment bone formation and increase bone mass.” *Nature medicine* vol. 18,3 456-62. 5 Feb. 2012, doi:10.1038/nm.2665
35- Meyerrose, Todd E et al. “In vivo distribution of human adipose-derived mesenchymal stem cells in novel xenotransplantation models.” *Stem cells (Dayton, Ohio)* vol. 25,1 (2007): 220-7. doi:10.1634/stemcells.2006-0243
36- Mediouni, Mohamed, and Daniel R Schlatterer. “Orthopaedic tumors: What problems are we solving, and are universities and major medical centers doing enough?.” *Journal of orthopaedics* vol. 14,2 319-321. 4 May. 2017, doi:10.1016/j.jor.2017.03.014
37- Mutsaers, Anthony J, and Carl R Walkley. “Cells of origin in osteosarcoma: mesenchymal stem cells or osteoblast committed cells?.” *Bone* vol. 62 (2014): 56-63. doi:10.1016/j.bone.2014.02.003
38- Macedo, Filipa et al. “Bone Metastases: An Overview.” *Oncology reviews* vol. 11,1 321. 9 May. 2017, doi:10.4081/oncol.2017.321
39- “Erratum to "Cancer statistics, 2021".” *CA: a cancer journal for clinicians* vol. 71,4 (2021): 359. doi:10.3322/caac.21669
40- Heinzer, Hans, and Thomas Steuber. “Prostate cancer in the elderly.” *Urologic oncology* vol. 27,6 (2009): 668-72. doi:10.1016/j.urolonc.2009.07.015
41- Rao, Amrith Raj et al. “The discovery of prostate-specific antigen.” *BJU international* vol. 101,1 (2008): 5-10. doi:10.1111/j.1464-410X.2007.07138.x
42- Filella, Xavier, and Laura Foj. “Prostate Cancer Detection and Prognosis: From Prostate Specific Antigen (PSA) to Exosomal Biomarkers.” *International journal of molecular sciences* vol. 17,11 1784. 26 Oct. 2016, doi:10.3390/ijms17111784
43- Rucci, Nadia, and Anna Teti. “Osteomimicry: how tumor cells try to deceive the bone.” *Frontiers in bioscience (Scholar edition)* vol. 2,3 907-15. 1 Jun. 2010, doi:10.2741/s110
44- Zhan, T et al. “Wnt signaling in cancer.” *Oncogene* vol. 36,11 (2017): 1461-1473. doi:10.1038/onc.2016.304
45- Niida, Atsushi et al. “DKK1, a negative regulator of Wnt signaling, is a target of the beta-catenin/TCF pathway.” *Oncogene* vol. 23,52 (2004): 8520-6. doi:10.1038/sj.onc.1207892
46- Nathan, Elisha, and Eldad Tzahor. “sFRPs: a declaration of (Wnt) independence.” *Nature cell biology* vol. 11,1 (2009): 13. doi:10.1038/ncb0109-13
47- Perry, Antoinette S et al. “Gene expression and epigenetic discovery screen reveal methylation of SFRP2 in prostate cancer.” *International journal of cancer* vol. 132,8 (2013): 1771-80. doi:10.1002/ijc.27798
48- Lai, Hong-Yue et al. “High Stromal SFRP2 Expression in Urothelial Carcinoma Confers an Unfavorable Prognosis.” *Frontiers in oncology* vol. 12 834249. 16 Mar. 2022, doi:10.3389/fonc.2022.834249

49- Techavichit, Piti et al. “Secreted Frizzled-Related Protein 2 (sFRP2) promotes osteosarcoma invasion and metastatic potential.” *BMC cancer* vol. 16,1 869. 8 Nov. 2016, doi:10.1186/s12885-016-2909-6
50- de Castro, Luis Fernandez et al. “Secreted frizzled related-protein 2 (Sfrp2) deficiency decreases adult skeletal stem cell function in mice.” *Bone research* vol. 9,1 49. 2 Dec. 2021, doi:10.1038/s41413-021-00169-7
51- Huang, Chumei et al. “Secreted Frizzled-Related Protein 2 Is Associated with Disease Progression and Poor Prognosis in Breast Cancer.” *Disease markers* vol. 2019 6149381. 3 Mar. 2019, doi:10.1155/2019/6149381
52- Morello, Roy. “Osteogenesis imperfecta and therapeutics.” *Matrix biology : journal of the International Society for Matrix Biology* vol. 71-72 (2018): 294-312. doi:10.1016/j.matbio.2018.03.010
53- Solis, Mairim Alexandra et al. “Hyaluronan regulates cell behavior: a potential niche matrix for stem cells.” *Biochemistry research international* vol. 2012 (2012): 346972. doi:10.1155/2012/346972
54- Vogeley, Christian et al. “The regulatory effect of hyaluronan on human mesenchymal stem cells' fate modulates their interaction with cancer cells in vitro.” *Scientific reports* vol. 11,1 21229. 27 Oct. 2021, doi:10.1038/s41598-021-00754-0
55- Qu, Chengjuan et al. “Extensive CD44-dependent hyaluronan coats on human bone marrow-derived mesenchymal stem cells produced by hyaluronan synthases HAS1, HAS2 and HAS3.” *The international journal of biochemistry & cell biology* vol. 48 (2014): 45-54. doi:10.1016/j.biocel.2013.12.016
56- Falconi, Dominic, and Jane E Aubin. “LIF inhibits osteoblast differentiation at least in part by regulation of HAS2 and its product hyaluronan.” *Journal of bone and mineral research : the official journal of the American Society for Bone and Mineral Research* vol. 22,8 (2007): 1289-300. doi:10.1359/jbmr.070417
57- Palazon, Asis et al. “HIF transcription factors, inflammation, and immunity.” *Immunity* vol. 41,4 (2014): 518-28. doi:10.1016/j.immuni.2014.09.008
58- Ziemkiewicz, Natalia et al. “The Role of Innate and Adaptive Immune Cells in Skeletal Muscle Regeneration.” *International journal of molecular sciences* vol. 22,6 3265. 23 Mar. 2021, doi:10.3390/ijms22063265
59- Pastorekova, Silvia et al. “Tumor-associated carbonic anhydrases and their clinical significance.” *Advances in clinical chemistry* vol. 42 (2006): 167-216.
60- de Theije, Chiel C et al. “Distinct responses of protein turnover regulatory pathways in hypoxia- and semistarvation-induced muscle atrophy.” *American journal of physiology. Lung cellular and molecular physiology* vol. 305,1 (2013): L82-91. doi:10.1152/ajplung.00354.2012
61- Chin, Lip Ket et al. “Plasmonic Sensors for Extracellular Vesicle Analysis: From Scientific Development to Translational Research.” *ACS nano* vol. 14,11 (2020): 14528-14548. doi:10.1021/acsnano.0c07581
62- Keramaris, N C et al. “Translational research: from benchside to bedside.” *Injury* vol. 39,6 (2008): 643-50. doi:10.1016/j.injury.2008.01.051
63- Kapler, G M et al. “Sequence and S1 nuclease mapping of the 5' region of the dihydrofolate reductase-thymidylate synthase gene of Leishmania major.” *Nucleic acids research* vol. 15,8 (1987): 3369-83. doi:10.1093/nar/15.8.3369
64- Velculescu, V E et al. “Serial analysis of gene expression.” *Science (New York, N.Y.)* vol. 270,5235 (1995): 484-7. doi:10.1126/science.270.5235.484
65- Tuteja, Renu, and Narendra Tuteja. “Serial Analysis of Gene Expression: Applications in Human Studies.” *Journal of biomedicine & biotechnology* vol. 2004,2 (2004): 113-120. doi:10.1155/S1110724304308119

66- Hitzemann, R et al. “Genes, behavior and next-generation RNA sequencing.” *Genes, brain, and behavior* vol. 12,1 (2013): 1-12. doi:10.1111/gbb.12007
67- Shyr, Derek, and Qi Liu. “Next generation sequencing in cancer research and clinical application.” *Biological procedures online* vol. 15,1 4. 13 Feb. 2013, doi:10.1186/1480-9222-15-4
68- Strimbu, Kyle, and Jorge A Tavel. “What are biomarkers?.” *Current opinion in HIV and AIDS* vol. 5,6 (2010): 463-6. doi:10.1097/COH.0b013e32833ed177
69- Shariat, Shahrokh F et al. “Statistical consideration for clinical biomarker research in bladder cancer.” *Urologic oncology* vol. 28,4 (2010): 389-400. doi:10.1016/j.urolonc.2010.02.011
70- Jovic, Dragomirka et al. “Single-cell RNA sequencing technologies and applications: A brief overview.” *Clinical and translational medicine* vol. 12,3 (2022): e694. doi:10.1002/ctm2.694
71- Cock, Peter J A et al. “The Sanger FASTQ file format for sequences with quality scores, and the Solexa/Illumina FASTQ variants.” *Nucleic acids research* vol. 38,6 (2010): 1767-71. doi:10.1093/nar/gkp1137
72- Pereira, Rute et al. “Bioinformatics and Computational Tools for Next-Generation Sequencing Analysis in Clinical Genetics.” *Journal of clinical medicine* vol. 9,1 132. 3 Jan. 2020, doi:10.3390/jcm9010132
73- Cunningham, Fiona et al. “Ensembl 2022.” *Nucleic acids research* vol. 50,D1 (2022): D988-D995. doi:10.1093/nar/gkab1049
74- Berglund, Eva C et al. “Next-generation sequencing technologies and applications for human genetic history and forensics.” *Investigative genetics* vol. 2 23. 24 Nov. 2011, doi:10.1186/2041-2223-2-23
75- Dobin, Alexander, and Thomas R Gingeras. “Mapping RNA-seq Reads with STAR.” *Current protocols in bioinformatics* vol. 51 11.14.1-11.14.19. 3 Sep. 2015, doi:10.1002/0471250953.bi1114s51
76- Dobin, Alexander et al. “STAR: ultrafast universal RNA-seq aligner.” *Bioinformatics (Oxford, England)* vol. 29,1 (2013): 15-21. doi:10.1093/bioinformatics/bts635
77- Love, Michael I et al. “Moderated estimation of fold change and dispersion for RNA-seq data with DESeq2.” *Genome biology* vol. 15,12 (2014): 550. doi:10.1186/s13059-014-0550-8
78- Love, Michael I et al. “Moderated estimation of fold change and dispersion for RNA-seq data with DESeq2.” *Genome biology* vol. 15,12 (2014): 550. doi:10.1186/s13059-014-0550-8
79- Liu, Shiyi et al. “Three Differential Expression Analysis Methods for RNA Sequencing: limma, EdgeR, DESeq2.” *Journal of visualized experiments : JoVE* ,175 10.3791/62528. 18 Sep. 2021, doi:10.3791/62528
80- Subramanian, Aravind et al. “Gene set enrichment analysis: a knowledge-based approach for interpreting genome-wide expression profiles.” *Proceedings of the National Academy of Sciences of the United States of America* vol. 102,43 (2005): 15545-50. doi:10.1073/pnas.0506580102
81- Werner, Thomas. “Bioinformatics applications for pathway analysis of microarray data.” *Current opinion in biotechnology* vol. 19,1 (2008): 50-4. doi:10.1016/j.copbio.2007.11.005

3. Summary

The rapid development of technology in recent years has had a major impact on biological re-search, leading to advances in diagnostic techniques and the development of new drugs. The integration of technological innovations has enabled more efficient and accurate diagnostic methods and facilitated the creation of more targeted and effective drugs. This demonstrates the important role that technology plays in advancing biology and medicine.

This role has provided scientists with a unique opportunity to bridge the gap between the scattered, previous experimental knowledge accumulated over time and opened the door to solid results. One such door facilitates the discovery of potential biomarkers for the progression of diseases, drugs or cell therapy targets. Even in basic laboratory experiments, where researchers are able to observe the effects of a few genes or proteins individually using traditional methods such as PCR or Western blot, multi-omics and computational bioinformatics analysis are advancing our knowledge to gain insights into entire biological pathways. The aim of this thesis is to investigate potential RNA markers involved in the pathway or treatment of musculoskeletal diseases such as bone metastasis, skeletal fractures, and myopathies. In all three papers presented in this thesis, next generation RNA sequencing was performed after specific treatments to observe the change in gene expressions.

The first part of my thesis focuses on my first authored study entitled "SFRP2 Overexpression Induces an Osteoblast-like Phenotype in Prostate Cancer Cells" (Paper I), which includes *in vitro* experiments and RNA sequencing computational analysis in R programming. The aim is to investigate the role of a potential biomarker, SFRP2, in the pathway of prostate cancer bone metastasis. According to the literature, SFRP2 plays a role in osteogenesis and a potential marker for prognosis in different cancer types. *SFRP2* is known to be hypermethylated in most cancer types, but no re-search has been performed to date on its association with prostate cancer bone metastasis. In our work, we have shown that *SFRP2* overexpression increases osteomimic properties of the prostate cancer cell line PC3, in bone-like environment recapitulated with Collagen 1-coated surface. Osteomimicry is a deceptive strategy for cancer cells to evade the immune response in bone metastasis, where they exhibit osteoblastic properties. This finding is a promising translational study to under-stand the impact of a potential biomarker on the pathway and its effect on other gene expressions. Further applications of this biomarker in diagnosis are possible, for example, to detect bone metastasis in prostate cancer at an early stage.

The second part of my thesis focuses on my co-authored paper named as “Hyaluronan Synthases’ Expression and Activity Are Induced by Fluid Shear Stress in Bone Marrow-Derived Mesenchymal Stem Cells” (Paper II). Bone biomineralization is a key mechanism in bone formation that ensures the maintenance of stiffness and rigidity and the balance between the activity of bone forming osteoblast and bone resorbing osteoclast is necessary for healthy bone structure. Bone remodeling and mineralization is modulated by mechanical stimuli by activating mechanotransduction path-ways in bone cells and MSCs in the bone marrow. The paper aimed to investigate the effect of fluid shear stress on gene expression profile and activity of hyaluronan synthases in bone marrow-derived MSCs. RNA sequencing and bioinformatics analysis revealed that fluid shear stress induces pronounced transcriptomic changes characterized by upregulation of genes and biological processes associated with osteogenesis and hyaluronan biosynthesis. Hyaluronan, a non-branching polysaccharide, is involved in bone development and mineralization, and is expressed by MSCs in the bone marrow. Exposure of MSCs to fluid shear stress increased the expression of the hyaluronan synthase genes, in particular *HAS1* and *HAS2*, and genes encoding their receptors, and these gene expression changes were associated with increased HAS activity. Our study demonstrated the first time a clear link between *HAS* expression and osteogenic gene expression of bone marrow-derived MSCs, and may identify hyaluronan synthase genes as biomarkers marking MSCs with osteogenic potential.

The third part of my thesis is based on the article “Fusion of Normoxic- and Hypoxic-Preconditioned Myoblasts Leads to Increased Hypertrophy” (Paper III). Regeneration of the skeletal muscle takes place in an environment exposed to different oxygen tension. The aim of our study was to elucidate the effect of normoxic/hypoxic preconditioning on the morphology, proliferation, myogenesis and transcriptomic profile of myoblastic C2C12 cells. We found that prolonged exposure to hypoxia (2% oxygen) causes cell rounding and inhibits myoblast fusion, but does not influence my-oblast proliferation compared to normoxic condition (21% oxygen). Interestingly, when we mimicked the mixed oxygen tension of an *in vivo* injury situation, we observed that when normoxic/hypoxic preconditioned C2C12 were differentiated together, they showed significantly increased myotubes size but smaller areas and number of myotubes, suggesting a synergistic effect of oxygen-dependent myoblast subpopulations on myotube hypertrophy. Transcriptomic profiling of these myotubes differentiated from the mixture of normoxic/hy-

poxic preconditioned myoblast under normoxia or hypoxia revealed numerous differentially expressed genes in a time-dependent manner. A hierarchical cluster analysis of the top 50 DEGs identified candidate genes for the control of myogenic fusion at various oxygen tensions, including *Car9 (Carboxy anhydrase 9)*, a tumor hypoxia-associated gene, which was the most upregulated gene under the hypoxic differentiation condition. Thus, we identified a gene expression cascade associated with hypoxia during oxygen-dependent myogenesis *in vitro*, which may represent therapeutic targets for the management of hypoxia-induced skeletal muscle damage *in vivo*.

The primary aim of this thesis was to combine *in vitro* laboratory experiments with computer analysis as part of translational research. Overall, understanding which potential markers are perturbed or required for tissue regeneration was addressed using a combination of bioinformatics and wet-lab research.

4. Zusammenfassung

Die rasante Entwicklung der Technologie in den letzten Jahren hat die biologische Forschung stark beeinflusst und zu Fortschritten in der Entwicklung von Diagnosetechniken und neuer Arzneimittel geführt. Die Integration technologischer Innovationen hat effizientere und genauere Diagnosemethoden ermöglicht und die Entwicklung gezielterer und wirksamerer Medikamente erleichtert. Dies zeigt, welch wichtige Rolle die Technologie für den Fortschritt in Biologie und Medizin spielt.

Diese Rolle hat den Wissenschaftlern die einzigartige Möglichkeit gegeben, die Lücke zwischen dem verstreuten, im Laufe der Zeit angesammelten, experimentellen Wissen zu schließen und die Brücke zu soliden Ergebnissen herzustellen. Diese neue Möglichkeit erleichtert die Entdeckung potenzieller Biomarker für den Verlauf von Krankheiten, Medikamenten oder Zelltherapiezielen. Selbst bei grundlegenden Laborexperimenten, bei denen Forscher die Auswirkungen einiger weniger Gene oder Proteine einzeln mit traditionellen Methoden wie PCR oder Western Blot untersuchen erweitern Multi-Omics und computergestützte Bioinformatik-Analysen das Wissen, um Einblicke in ganze biologische Signaltransduktionswege zu gewinnen. Ziel dieser Arbeit ist es, potenzielle RNA-Marker zu untersuchen, die an der Entstehung oder Behandlung von Muskel-Skelett-Erkrankungen wie Knochenmetastasen, Skelettfrakturen und Myopathien beteiligt sind. In allen drei in dieser Arbeit vorgestellten Projekten wurde nach bestimmten Behandlungen eine RNA-Next Generation Sequencing. durchgeführt, um die Veränderung der Genexpressionen zu studieren.

Der erste Teil meiner Dissertation befasst sich mit meiner ersten Studie mit dem Titel „SFRP2 Overexpression Induces an Osteoblast-like Phenotype in Prostate Cancer Cells“ (Paper I), die *in-vitro*-Experimente und RNA-Sequenzierungsberechnungen in R-Programmierung umfasst. Ziel ist es, die Rolle eines potenziellen Biomarkers, *SFRP2*, im Signaltranduktionsweg der Knochenmetastasierung bei Prostatakrebs zu untersuchen. Der Literatur zufolge spielt SFRP2 eine Rolle bei der Osteogenese und ist ein potenzieller Marker für die Prognose bei verschiedenen Krebsarten. Es ist bekannt, dass SFRP2 bei den meisten Krebsarten hypermethyliert ist, aber bisher wurde noch nicht untersucht, ob es mit der Knochenmetastasierung von Prostatakrebs in Verbindung steht. In dieser Arbeit haben wir gezeigt, dass die Überexpression von *SFRP2* die osteomimetischen Eigenschaften der Prostatakrebs-Zelllinie PC3 in einer knochenähnlichen Umgebung, die mit einer mit Kollagen 1 beschichteten Oberfläche nachgestellt wird, erhöht. Osteomimikry

ist eine trügerische Strategie von Krebszellen, um der Immunantwort bei Knochenmetastasen zu entgehen, indem sie osteoblastische Eigenschaften aufweisen. Diese Resultate bilden eine vielversprechende Grundlage/Basis für weiterführende Studien, die sich auf die Anwendung eines potentiellen Biomarkers fokussieren. Weitere Anwendungen dieses Biomarkers in der Diagnostik sind möglich, zum Beispiel um Knochenmetastasen bei Prostatakrebs in einem frühen Stadium zu erkennen.

Der zweite Teil meiner Dissertation befasst sich mit meiner gemeinsam verfassten Arbeit mit dem Titel "Hyaluronan Synthases' Expression and Activity Are Induced by Fluid Shear Stress in Bone Marrow-Derived Mesenchymal Stem Cells" (Paper II). Die Biomineralisierung des Knochens ist ein Schlüsselmechanismus bei der Knochenbildung, der die Aufrechterhaltung von Steifigkeit und Festigkeit gewährleistet. Das Gleichgewicht zwischen der Aktivität der knochenbildenden Osteoblasten und der knochenresorbierenden Osteoklasten ist für eine gesunde Knochenstruktur notwendig. Der Knochenumbau und die Mineralisierung werden durch mechanische Reize moduliert, indem Mechanotransduktionswege in Knochenzellen und MSCs im Knochenmark aktiviert werden. Ziel der Arbeit war es, die Wirkung von Flüssigkeitsscherkräften auf das Genexpressionsprofil und die Aktivität von Hyaluronsynthasen in aus Knochenmark stammenden MSCs zu untersuchen. Die RNA-Sequenzierung und die bioinformatische Analyse ergaben, dass Flüssigkeitsscherstress ausgeprägte transkriptomische Veränderungen hervorruft, die durch die Hochregulierung von Genen und biologischen Prozessen gekennzeichnet sind, die mit der Osteogenese und der Hyaluronan-Biosynthese in Verbindung stehen. Hyaluronan, ein nicht-verzweigendes Polysaccharid, ist an der Knochenentwicklung und Mineralisierung beteiligt und wird von MSCs im Knochenmark exprimiert. Wenn MSCs einer Scherbelastung ausgesetzt werden, wird die Expression von Hyaluronan-Synthase-Genen erhöht, insbesondere HAS1 und HAS2; sowie von Genen, die für ihre Rezeptoren kodieren, und diese Veränderungen der Genexpression sind mit einer erhöhten HAS-Aktivität verbunden. In unserer Studie konnte erstmals ein klarer Zusammenhang zwischen der Expression von HAS und der osteogenen Genexpression von aus Knochenmark stammenden MSC nachgewiesen werden, und es ist möglich, dass Hyaluronsynthase-Gene als Biomarker für MSCs mit osteogenem Potenzial identifiziert werden können.

Der dritte Teil meiner Arbeit basiert auf dem Artikel "Fusion of Normoxic- and Hypoxic-Preconditioned Myoblasts Leads to Increased Hypertrophy" (Paper III). Die Regeneration der Skelettmuskulatur findet in einer Umgebung statt, die unterschiedlichen Sauerstoffspannungen ausgesetzt ist. Ziel unserer Studie war es, die Auswirkungen einer

normoxischen/hypoxischen Vorbehandlung auf die Morphologie, Proliferation, Myogenese und das transkriptomische Profil von myoblastischen C2C12-Zellen zu untersuchen. Wir fanden heraus, dass eine verlängerte Exposition gegenüber Hypoxie (2 % Sauerstoff) zu einer Abrundung der Zellen führt und die Myoblastenfusion hemmt, aber keinen Einfluss auf die Proliferation der Myoblasten im Vergleich zu normoxischen Bedingungen (21 % Sauerstoff) hat. Als wir die gemischte Sauerstoffspannung einer *in vivo*-Verletzungssituation nachstellten, konnten wir interessanterweise beobachten, dass normoxische/hypoxische präkonditionierte C2C12 bei gemeinsamer Differenzierung eine signifikant erhöhte Myotubes-Größe, aber kleinere Bereiche und eine geringere Anzahl von Myotubes aufwiesen, was auf einen synergistischen Effekt der sauerstoffabhängigen Myoblasten-Subpopulationen auf die Myotube-Hypertrophie hindeutet. Das Transkriptom-Profiling dieser Myotubes, die sich von der Mischung aus normoxischen/hypoxischen vorkonditionierten Myoblasten unter Normoxie oder Hypoxie unterschieden, ergab zahlreiche zeitabhängig unterschiedlich exprimierte Gene. Eine hierarchische Clusteranalyse der 50 wichtigsten DEGs identifizierte Kandidatengene für die Kontrolle der myogenen Fusion bei verschiedenen Sauerstoffspannungen, darunter *Car9 (Carboxyanhydrase 9)*, ein mit Tumorhypoxie assoziiertes Gen, das unter hypoxischen Differenzierungsbedingungen am stärksten hochreguliert war. Somit haben wir eine Genexpressionskaskade identifiziert, die mit Hypoxie während der sauerstoffabhängigen Myogenese *in vitro* verbunden ist und die therapeutische Ziele für die Behandlung von hypoxiebedingten Skelettmuskelschäden *in vivo* darstellen könnte.

Das Hauptziel dieser Arbeit war die Kombination von *in-vitro*-Laborexperimenten mit Computeranalysen als Teil der translationalen Forschung. Insgesamt sollte durch eine Kombination aus Bioinformatik und experimentelle Forschung herausgefunden werden, welche potenziellen Marker für die Geweberegeneration gestört oder erforderlich sind.

5. Paper I

cells

IMPACT FACTOR 7.666

Indexed in: PubMed

Article

SFRP2 Overexpression Induces an Osteoblast-like Phenotype in Prostate Cancer Cells

Elif Akova Ölken, Attila Aszodi, Hanna Taipaleenmäki, Hiroaki Saito, Veronika Schönitzer, Michael Chaloupka, Maria Apfelbeck, Wolfgang Böcker and Maximilian Michael Saller

Special Issue
Molecular and Cellular Mechanisms of Cancers: Prostate Cancer 2022
Edited by
Dr. Claudio Festuccia

MDPI

https://doi.org/10.3390/cells11244081

cells

MDPI

Article

SFRP2 Overexpression Induces an Osteoblast-like Phenotype in Prostate Cancer Cells

Elif Akova Ölken [1], Attila Aszodi [1], Hanna Taipaleenmäki [2], Hiroaki Saito [2], Veronika Schönitzer [1], Michael Chaloupka [3], Maria Apfelbeck [3], Wolfgang Böcker [1] and Maximilian Michael Saller [1,*]

[1] Department of Orthopaedics and Trauma Surgery, Musculoskeletal University Center Munich (MUM), Ludwig-Maximilians-University (LMU) Hospital, Fraunhoferstraße 20, 82152 Planegg-Martinsried, Germany
[2] Institute of Musculoskeletal Medicine (IMM), Musculoskeletal University Center Munich (MUM), LMU Hospital, Fraunhoferstraße 20, 82152 Planegg-Martinsried, Germany
[3] Urologischen Klinik und Poliklinik, LMU Hospital, Marchioninistr 15, 81377 München, Germany
* Correspondence: maximilian.saller@med.uni-muenchen.de; Tel.: +49-89-4400-55486

Abstract: Prostate cancer bone metastasis is still one of the most fatal cancer diagnoses for men. Survival of the circulating prostate tumor cells and their adaptation strategy to survive in the bone niche is the key point to determining metastasis in early cancer stages. The promoter of *SFRP2* gene, encoding a WNT signaling modulator, is hypermethylated in many cancer types including prostate cancer. Moreover, SFRP2 can positively regulate osteogenic differentiation in vitro and in vivo. Here, we showed SFRP2 overexpression in the prostate cancer cell line PC3 induces an epithelial mesenchymal transition (EMT), increases the attachment, and modifies the transcriptome towards an osteoblast-like phenotype (osteomimicry) in a collagen 1-dependent manner. Our data reflect a novel molecular mechanism concerning how metastasizing prostate cancer cells might increase their chance to survive within bone tissue.

Keywords: SFRP2; osteomimicry; prostate cancer; PC3; bone metastasis; EMT; WNT signaling

Citation: Akova Ölken, E.; Aszodi, A.; Taipaleenmäki, H.; Saito, H.; Schönitzer, V.; Chaloupka, M.; Apfelbeck, M.; Böcker, W.; Saller, M.M. SFRP2 Overexpression Induces an Osteoblast-like Phenotype in Prostate Cancer Cells. *Cells* **2022**, *11*, 4081. https://doi.org/10.3390/cells11244081

Academic Editor: Claudio Festuccia

Received: 18 November 2022
Accepted: 14 December 2022
Published: 16 December 2022

1. Introduction

Prostate cancer is the second most abundant cancer type in males, and even with the high treatment success after early diagnosis, it is still the fifth cancer-related death cause worldwide [1]. In advanced prostate cancer (AdPCA), when cancer cells metastasize outside the primary location, the survival rate decreases dramatically due to currently unavailable therapeutic options and resistance to androgen depletion [2].

The most abundant metastatic site of AdPCA is bone, especially the spine, hip, and long bones [3]. Other cancer types, such as lung, breast, and kidney, also have a high potential to metastasize to bone at an advanced stage, but, unlike prostate cancer, these cancers cause bone resorption, whereas AdPCA can result in both bone-forming (osteoblastic) and bone-resorbing (osteolytic) metastasis [4]. However, the molecular pathways that underly prostate cancer bone metastasis and osteoblastic or osteolytic progression are still poorly elucidated.

Bone metastasis can be separated into early and late phases that are defined by specific time-dependent molecular pathways and interaction with local cells. In early metastasis, just after the cancer cells entered into and settled in the bone, colonization, survival, dormancy, and reactivation occur until the late metastasis stage, when the tumor starts to actively grow [5]. Only around 0.01% of circulating cancer cells can survive and adapt to the bone niche during the early bone metastasis stage [6]. In the late metastatic stage after the formation of bone macrometastasis, the survival rate of cancer patients drops dramatically, by almost 60% [7]. Therapeutically, it is therefore incredibly important to diagnose and intervene in bone metastases already at the early metastasis stage.

The PC3 cell line, derived from a grade IV bone metastatic prostatic adenocarcinoma, is an aggressive metastatic prostate cancer cell line [8]. Injection of PC3 cells into the murine tibiae leads to bone lesions [9], while silencing *Dickkopf-1* (*DKK1*), an inhibitor of the WNT (Wingless/Int) signaling, was found to allow PC3 cells to secrete osteoblast-related factors and increase alkaline phosphatase activity in bone marrow stromal cells [10]. Furthermore, injection of a *DKK1*-overexpressing prostate cancer cell line C4-2B reduces bone mineral density and, therewith, leads to the formation of osteoblastic lesions in a murine animal model [11]. Overall, the currently available data suggest that WNT signaling activity is involved in the balance between osteolytic and osteoblastic phenotypes in prostate cancer bone metastasis.

WNTs are secreted glycoproteins that bind to various cell surface receptors to modulate many cellular activities such as proliferation, differentiation, apoptosis, migration, invasion, and tissue homeostasis [12]. WNT signaling cascades are divided into the canonical WNT/ß-catenin pathway that is activated via the interaction of WNT with Frizzled receptors (FZDs) and LRP5/6 (low-density lipoprotein receptor-related protein 5/6), and the ß-catenin independent non-canonical pathways, such as WNT/Ca^{2+} signaling and WNT/PCP (planar cell polarity) signaling [13]. Aberrant WNT signaling is associated with the development of bone metastasis in prostate cancer [14]. Similar to other common cancer types, WNT signaling is continuously active in prostate cancer due to a downregulation of inhibitory WNT regulator genes, such as *Wnt Inhibitory Factor 1* (*WIF1*), *Dickkopf proteins* (*DKK1, DKK2, DKK3*), and *Secreted Frizzled Related Proteins* (*SFRP1, SFRP2, SFRP3, SFRP4*), usually caused by methylation of the respective promoter [15,16]. WIF1 and SFRPs can directly bind to WNT ligands, which, in turn, leads to a WNT signaling inhibition [15]. Moreover, SFRPs and DKKs bind competitively to receptors that are involved in WNT signaling. While DKKs can bind to the co-receptors of LRP5/6, SFRPs can bind to FZDs [16]. Despite the autocrine effect of these WNT signaling inhibitors on primary cancer cells, their paracrine effect on bone cells during metastasis could help to understand the molecular pathways underlying osteolytic or osteoblastic bone metastasis.

SFRP2 is a soluble extracellular protein that acts as a WNT signaling modulator. Although SFRP2 is known to prevent the binding of WNT ligands to their respective receptors [17], recent research has shown that it augments WNT16B and WNT3A to promote WNT signaling in advanced malignancies [18] and HEK293 cells [19], respectively. The modulatory activity of SFRP2 is still unclear and, therefore, represents a potential target for understanding its role in cancer progression. It is known that the *SFRP2* promoter is hypermethylated in primary prostate cancer, and, thus, *SFRP2* expression is silenced relative to adjacent prostate tissues [20]. This suggests that SFRP2 may act as a tumor suppressor in many cancer types, but recent studies have shown that SFRP2 could also act as a tumor promoter, depending on the cell type or cellular location [21,22]. Moreover, elevated serum levels of SFRP2 are associated with poor prognosis and metastasis in breast cancer patients, in which the *SFRP2* promoter is, similar to prostate cancer, hypermethylated in the primary cancer side [23].

Additionally, SFRP2 is the only negative regulator of WNT signaling that contributes to both bone morphogenesis (Gene Ontology: GO:0060349) and osteoblast differentiation (GO:0001649), and, thus, SFRP2 could be a potential regulator of bone metastasis, similar to *DKK1*. *Sfrp2*-deficient mice show poor osteogenic differentiation, whereas administration of recombinant SFRP2 restores the expression of the osteogenic markers *Runx2* and *Osx* in vitro [24]. Likewise, due to its interaction with the fibronectin–integrin complex, SFRP2 can increase cell adhesion, which is an essential prerequisite for cancer cells to survive in the metastatic bone niche [25]. These findings suggest that SFRP2 expression may play a key role in the osteotropic activity of cancer cells after leaving the primary location.

Prostate cancer cells must substantially adapt their transcriptional landscape in the metastatic bone target area to maintain their viability. This so called osteomimicry is a survival strategy of cancer cells in the bone during early metastasis and is characterized by the secretion of bone-related proteins to cope against immune system reactions [26]. AdPCA

cells acquire an osteoblast-like phenotype and secrete bone matrix proteins and osteoblast-related factors to mimic bone-related cells in the target niche [27]. After this dormancy step, depending on the secreted proteins, an increase or decrease in bone formation is induced. Therefore, SFRP2 promotes an osteoblastic phenotype in early metastasized prostate cancer cells and therewith promotes cell survival, or it additionally induces osteoblastic bone lesion in later stages due to an increase in osteoblastic differentiation. SFRP2 is a prospective target to detect poor prognosis of AdPCA.

Epithelial-mesenchymal transition (EMT) is another critical concept in the cellular plasticity of cancer cells during early metastasis. EMT allows cancer cells to survive during circulation until they reach their target tissue [28] by changing their morphology to a mesenchymal-like phenotype and altering biochemical pathways. The transformation of epithelial cancer cells into a mesenchymal cell phenotype increases their invasion potential into target tissues, including bone [29]. This fact underlines EMT as a potential marker for monitoring osteomimic features of cancer cells during early bone metastasis [30].

In this study, we found that overexpression of SFRP2 in the prostate cancer cell line PC3 increases the expression of osteoblast-like genes, when seeded on the most abundant bone extracellular matrix (ECM) structural protein, collagen 1 (COL1). Moreover, overexpression of SFRP2 alters the proliferation rate and morphology to a mesenchymal-like phenotype and increases the adhesion of PC3 cells when compared to a non-COL1-coated surface. These results emphasize that SFRP2 is a promising key element for prostate cancer cells to survive in the bone metastatic niche through osteomimicry during early bone metastasis.

2. Materials and Methods

2.1. Cell Line and Cell Culture Conditions

The PC3 cells, derived from bone metastasis of human prostate adenocarcinoma, were obtained from ATCC, USA. Cells were cultured for up to 10 passages in Dulbecco's Modified Eagle Medium + GlutaMax (Thermo Fisher, Waltham, MA, USA), with 10% fetal bovine serum (FBS, Sigma Aldrich, St. Louis, MI, USA) and 1% penicillin/streptomycin (Sigma Aldrich, USA) at 37 °C with 5% CO_2. The media were changed every 3 days. Due to the relatively low doubling time and the ability of cancer cells to grow on top of each other, the confluence was kept below 90% to avoid any disturbance of cell–surface interaction.

2.2. Generation of PC3 Cells Stably Overexpressing SFRP2

To understand the intrinsic and extrinsic effect of SFRP2 protein on prostate cancer cells, the coding sequence of the human *SFRP2* gene was stably expressed in PC3 cells by using a Sleeping Beauty transposon system. The Sleeping Beauty plasmid backbone pSBbi-RP (60513, Addgene, Watertown, MA, USA) [31] was modified in our laboratory by removing an EcoRI side with respective restriction enzymes and adding an extra multiple cloning sites (MCS) with the sequence for 6× His-Tag (HIS) (pSBbi-RP-deltaECO-HIS) by ligation. Initially, the human *SFRP2* coding sequence was digested from a pCMVS-PORT6 vector (6423, Horizon Discovery, Waterbeach, UK) with EcoRI and EcoRV (NEB, Ipswich, MA, USA), purified with NucleoSpin Gel and PCR Cleanup kit after gel electrophoresis (MN, Düren, Germany), and inserted into the pSBbi-RP-deltaECO-HIS backbone with the same restriction enzymes. After overnight ligation of the insert to the backbone at 4 °C, plasmids were inserted into *E.coli* DH5α by a heat shock transformation at 42 °C, and positive transformants were expanded in LB medium with ampicillin (Thermo Fisher, USA) overnight. To generate SFRP2 overexpressing ($PC3^{SFRP2}$) or control cells (PC3), 0.4 µg of the newly created plasmid, 0.9 µg transposase pCMV (CAT) T7-SB100 (24879, Addgene, Watertown, MA, USA), and 20 µL nucleofector solution (Amaxa™ Cell Line Nucleofector™ Kit V, Lonza, Basel, Switzerland) were added to 500,000 PC3 cells and electroporated with the 4D-Nucleofector™ Core Unit (program B 032, Lonza, Switzerland). Control PC3 cells were transfected with an empty pSBbi-RP-deltaECO-HIS backbone without the insert. After transfection, cells were treated with 2 µg/µL puromycin (Sigma Aldrich, St. Louis, MI, USA) for 14 days to kill non-stably transfected cells. For further

purification, cells were sorted according to their RFP expressions by fluorescent-activated cell sorting (FACS). The size and granularity of the RFP expressing PC3 and PC3^{SFRP2} cells were analyzed by forward and side scatter gating of the FACS results.

2.3. Surface Coating

Collagen 1 is the most abundant protein in the bone microenvironment and may, therefore, influence the response of prostate cancer cells. Therefore, we decided to mimic the bone microenvironment by coating the surface of all used cell culture-treated polystyrene (CCP) flasks or wells (Thermo Fisher, USA) and chambers (ibidi, Gräfelfing, Germany) with 20 µg/mL collagen 1, isolated from rat tails (Sigma-Aldrich, St. Louis, MI, USA) overnight at 4 °C and rinsing once with phosphate-buffered saline (PBS) before experiments. For all experiments, non-COL1-coated CCP flasks or wells served as controls and are referred to as CCP. In sum, we analyzed 4 different groups: CCP-PC3, CCP-PC3^{SFRP2}, COL1-PC3, and COL1-PC3^{SFRP2}.

2.4. Validation of SFPR2 Overexpression

To validate the overexpression of *SFRP2* at the transcriptional level, PC3 and PC3^{SFRP2} cells were seeded at a density of 8000 cells/cm^2 in COL1-coated and CCP T25 flasks. After the cells reached 90% confluency in about 3–4 days, total RNA was isolated with TRIzol (Invitrogen, Waltham, MA, USA) and purified with a Direct-Zol RNA Kit (Zymo Research, Irvine, CA, USA). cDNA was synthesized on PEQSTAR (PEQLAB, VWR, Radnor, PA, USA) using the Biozym cDNA Synthesis Kit (Biozym, Hessisch Oldendorf, Germany), with 1 µg of RNA and random hexamer primers, according to the manufacturer's protocol. qPCR was performed with specific FAM-labeled *SFRP2* primers (IDT, Coralville, USA) and Promega GoTaq qPCR kit (Promega, Madison, WI, USA), according to the manufacturer's protocol, with a LC96 LightCycler (Roche Applied Sciences, Penzberg, Germany). Human *HPRT* (IDT, Coralville, IA, USA) was used as a reference.

To validate the protein level of SFRP2 in PC3 cells, 15,000 cells/cm^2 were seeded in 8-well chamber slides (CCP: 8-well high µ-Slides, COL1: 8-well glass µ-Slides; both from ibidi, Gräfelfing, Germany). After 24 h, attached cells were rinsed with PBS, fixed with 4% PFA in PBS (Merck, Darmstadt, Germany) for 10 min at room temperature, and permeabilized with 1% Triton-X-100 (Sigma, USA). Immunocytochemistry (ICC) against SFRP2 was performed with a polyclonal rabbit@SFPR2 antibody (ab137560, Abcam, Cambridge, UK) and a goat@secondary antibody with conjugated Alexa Fluor 488 (ab150113, Abcam, Cambridge, MA, USA). Images were taken with an inverted epifluorescence microscope (AxioObserver, Zeiss, Jena, Germany).

2.5. Cell Proliferation, Metabolic Activity and Morphology

To analyze the consequence of SFRP2 overexpression on the proliferation of PC3 cells on COL1-coated and CCP surfaces, 2000 cells/cm^2 were seeded in T25 flasks and counted every 3–4 days with a hemocytometer. After counting, 2000 cells/cm^2 were re-seeded to the same flask, and the seed-count-cycle was repeated for up to 15 days. The population doubling time (*PDT*) and cumulative population doublings (*cumPD*) were calculated using the following formulas:

$$PDT(\bar{x}\ for\ days) = \frac{(Number\ of\ days\ passed\ between\ two\ passages\ x\ 24)\ x\ \log(2)}{\log(Number\ of\ counted\ cells) - \log(Initial\ number\ of\ cells\ seeded)}$$

$$cumPD\ (\bar{x}\ for\ days) = \frac{\ln \frac{(Number\ of\ counted\ cells)}{(Initial\ number\ of\ cells\ seeded)}}{\ln(2)}$$

Before each passaging, images of each experimental group were taken to analyze morphological differences. At least 100 cells per passage were analyzed for cell area and cell shape with ImageJ [32]. The cutoff for both area and aspect ratio is defined as 3 for better visualization in violin plots.

To analyze SFRP2-dependent changes in the metabolic activity of PC3 cells on CCP and COL1 surfaces, a WST-1 colorimetric assay was performed. Therefore, 10,000 cells/well were cultured overnight and afterwards incubated with the WST-1 Reagent (Roche Applied Sciences, Penzberg, Germany) in 1:10 final dilution in complete media for 4 h. The colorimetric change was measured on a Multiskan FC microplate reader (Thermo Fisher, USA) at 450 nm for formazan and 620 nm as reference.

To test the efficiency of a single PC3 or PC3^{SFRP2} cell to form colonies on CCP or COL1 surfaces, 400 cells/well were seeded in 6-well plates. After 10 days, newly formed colonies were fixed with 4% PFA in PBS and stained with 0.1% Crystal Violet in isopropanol (Sigma-Adrich, St. Louis, MI, USA). Colonies with at least 20 cells were counted, and colony forming unit (CFU) efficiency was calculated and normalized to CCP-PC3 cells.

2.6. Migration, Invasion and Attachment

To investigate if there is a relation between SFRP2 overexpression in PC3 cells and COL1 interaction, we analyzed the migration, invasion, and attachment characteristics. Random migration of PC3 and PC3^{SFRP2} on CCP and COL1 surfaces were observed with a time lapse microscope (Axiovert S100, Zeiss, Jena, Germany) at 37 °C 5% CO_2. Therefore, 5000 cells/well were seeded in 6-well plates, incubated overnight, and imaged every 15 min for 48 h. At least 100 cells per experiment were analyzed utilizing ImageJ and MTrackJ [33].

The invasion potential of PC3 or PC3^{SFRP2} through COL1-coated membranes was analyzed by a transwell assay with a membrane pore size of 12 µm (3403, Corning, Corning, NY, USA). Therefore, 50,000 cells/insert were seeded in media without FBS to the upper compartment. Media with 10% FBS in the lower compartment served as chemoattractants. After 6 h of incubation, cells were fixed with 4% PFA in PBS and stained with 0.01% DAPI in PBS. Images were taken on an inverted epifluorescence microscope (AxioObserver, Zeiss, Germany), and cells were automatically counted with the "find maxima" function of ImageJ.

To test the effect of SFRP2 overexpression on cell adhesion, 10,000 cells/well were seeded on COL1-coated or uncoated 96-well plates in serum-free medium and washed after 2 h of incubation with PBS. As a negative control, 1% BSA in PBS was used. The remaining adhered cells were stained with 0.1% crystal violet in methanol. The colorimetric measurement was performed on Multiskan FC Microplate Photometer (Thermo Fischer, Waltham, USA) at 570 nm.

2.7. Next Generation RNA Sequencing and Bioinformatics Analysis

To identify SFRP2-induced transcriptional changes in PC3 cells, 100,000 cells were seeded in T25 flasks, and RNA was isolated after 5 days, as described in Section 2.3., and RNA integrity was validated with Bioanalyzer (Agilent, Santa Clara, CA, USA). cDNA sequencing libraries were prepared with a SENSE mRNA-Seq Library Prep Kit V2 (Lexogen, Vienna, Austria). Sequencing was performed on a HiSeq1500 device (Illumina, San Diego, CA, USA) with a read length of 50 bp and a sequencing depth of approximately 12 million reads per sample.

Obtained FASTQ files were demultiplexed with sample-specific barcodes, and adaptor sequences were clipped before passing to the alignment. Reads were aligned to the homo sapiens reference genome (release GRCh38.101) using STAR (version 2.7.2b) [34].

Genes with less than 10 reads in all samples were filtered out, leaving 22,105 genes for further analysis. Gene expression was normalized with a variance stabilizing transformation (vst), which was further utilized for a principal component analysis (PCA).

Differentially expressed genes were calculated with the DESeq2 package (version 1.28.1) [35] in R (version 4.0.3). Significantly changed genes were determined by utilizing an adjusted p-value (p-adj) of <0.05 and a Log2FoldChange of ±2 as cut-offs and utilized for the MA-Plot. Gene set enrichment analysis (GSEA), utilizing significant changed genes without a Log2FoldChange cut-off (COL1-PC3 vs. COL1-PC3^{SFRP2}: 7174 significantly changed genes; CCP-PC3 vs. CCP-PC3^{SFRP2}: 88 significantly changed genes), was performed sep-

arately for each group with the clusterProfiler package (version 4.2.2) [36] to understand the match of significantly upregulated genes in each surface condition with gene ontology biological pathways.

By using the GO:0001649 osteoblast differentiation pathway gene set and our DESeq2 results without Log2FoldChange cut-offs, a matched gene set was created. Out of 158 genes in GO:0001649, 46 genes were found to be differentially expressed in between COL1-PC3 and COL1-PC3^{SFRP2}. These genes were used to create a heatmap and clustering analysis with normalized gene expressions, including all groups.

2.8. Statistical Analysis

All experiments were performed in triplicates and repeated at least three times. Statistical calculations were performed in R-Studio (version 4.1.0). After the verification of the Gaussian distribution and variance of the results, a two-way ANOVA was performed for two independent variables and their interactions. Significance of both the effect of surface coating and cell type and their interactions were calculated separately. Depending on the F-stat significance, multiple pairwise-comparison was performed with TukeyHSD (Tukey honest significant differences). Statistical significance was defined at a p-value of <0.05.

3. Results

3.1. Generation and Validation of PC3 Cells Stably Overexpressing SFRP2

As the *SFRP2* promoter is hypermethylated in many cancer cells, including PC3 cells, we created PC3 cells that stably overexpress SFRP2 by utilizing the Sleeping Beauty transposon system [37]. The unmodified bicistronic expression plasmid with coding sequences for red fluorescence protein (RFP/dTomato) and puromycin resistance was used for establishing stably transfected control cells (PC3), while the same plasmid with an insertion of the human coding sequence of human *SFRP2* was used to generate the *SFRP2* overexpressing cells (PC3^{SFRP2}, Figure 1A). After 14 days of puromycin selection, most cells stably expressed RFP (Figure 1B). To further enrich PC3 cells expressing high RFP and hence high *SFRP2*, FACS was performed (Figure 1B′), resulting in homogenous, bright RFP fluorescent cell populations (Figure 1B″).

To validate *SFRP2* overexpression on transcriptional and translational levels, we performed qPCR and immunocytochemistry (ICC) for PC3^{SFRP2} and PC3 cells seeded on COL1-coated and CCP surfaces. qPCR showed that *SFRP2* expression is more than 20-log2fold higher in PC3^{SFRP2} cells in comparison to control PC3 cells, independent of the cell culture surface (Figure 1C). Moreover, ICC revealed a clearly higher expression of SFRP2 protein in PC3^{SFRP2} cells in comparison to PC3 (Figure 1D,D′). In addition, these results specifically demonstrated that SFRP2 expression was not affected by different culturing methods in PC3^{SFRP2} cells.

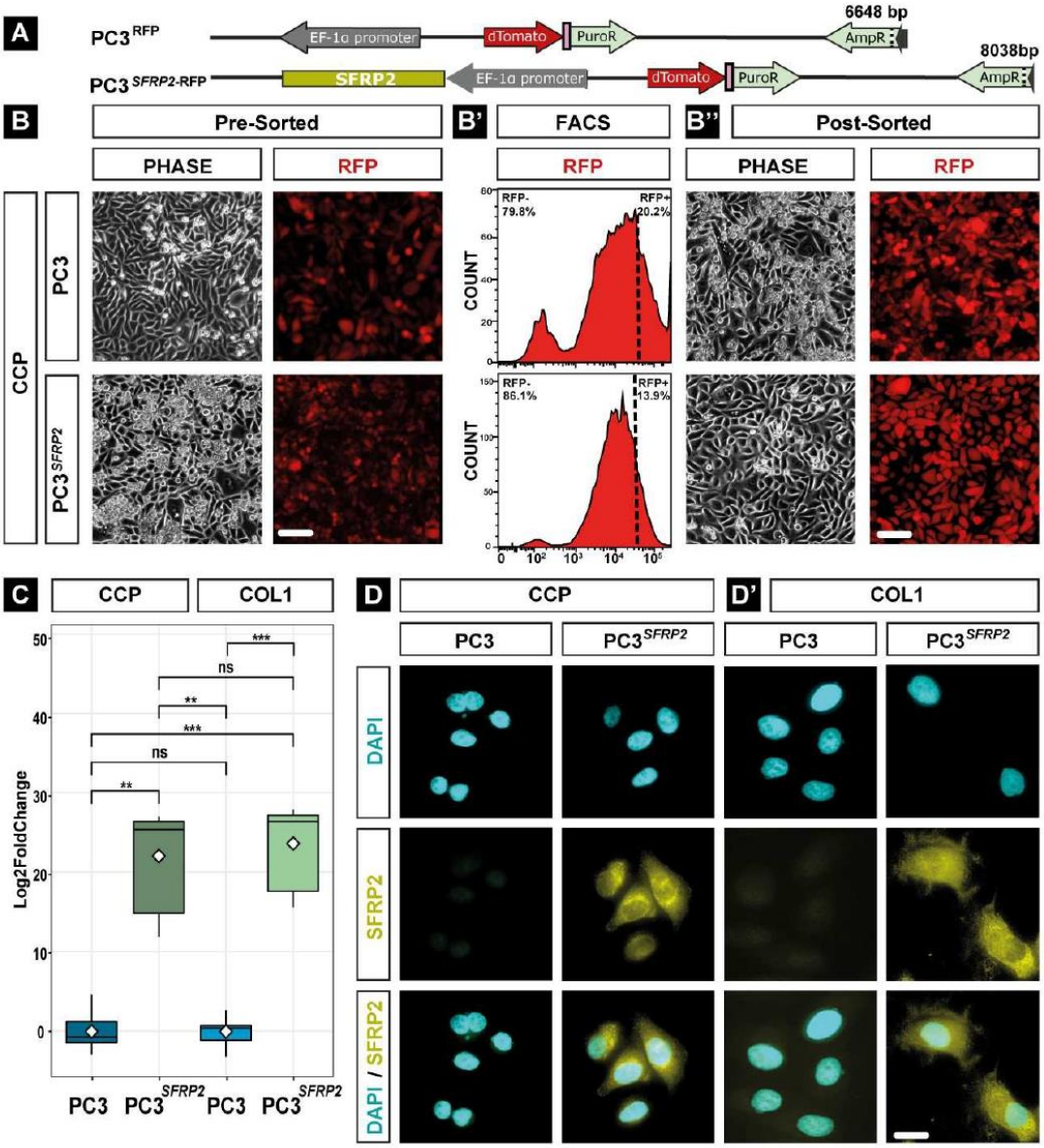

Figure 1. Generation and analysis of PC3 cells stably overexpressing SFRP2. The bicistronic expression plasmid contained either the coding sequences of *RFP* and puromycin for control cells ($PC3^{RFP}$) or an additional coding sequence for human *SFRP2* ($PC3^{SFRP2;\,RFP}$, **A**). Stably transfected cells were selected with puromycin for 14 days (**B**) and then enriched for high RFP fluorescence by FACS (**B′**), resulting in homogenous bright PC3 cell populations (**B′′**). qPCR validated a significantly higher *SFRP2* expression in $PC3^{SFRP2}$, when compared to PC3 cells, which was not affected by surface conditions (**C**). In addition, ICC against SFRP2 shows high expression of SFRP2 in the whole cytoplasm of $PC3^{SFRP2}$ cells compared to the controls, independent of the surface (**D**,**D′**). Significance level **: $p \leq 0.001$, ***: $p \leq 0.001$, ns: not significant. Scale bars: B/B′′: 100 µm, D/D′: 10 µm.

3.2. SFRP2 Overexpression Promotes a Higher Number of Differentially Expressed Genes in PC3 Cells on the COL1-Coated Surface Compared to the CCP Surface

To analyze the cell-intrinsic effect of SFRP2 overexpression in PC3 cells on both surfaces, we performed next generation RNA-sequencing. Interestingly, while just 17 genes were significantly differentially expressed in PC3 and PC3^{SFRP2} cells, when cultured on the CCP surface (Figure 2A, Table S1), culturing the cells on COL1 led to a significant increase of 453 differentially expressed genes (Figure 2A′). On the CCP surface, analysis of the gene ontology-related biological process of the upregulated genes in PC3^{SFRP2} was related to ER stress (Figure S1A). Yet, the downregulation of the type II collagen gene (*COL2A1*) in PC3^{SFRP2}, which is involved in cancer stemness in various cancer types [38], and the upregulation of *CDH15* (Cadherin 15) in PC3^{SFRP2}, which mediates intracellular adhesion [39], are promising predictors of the role of SFRP2 in cancer metastasis. When we compared gene expressions of PC3 and PC3^{SFRP2} cells that were seeded on COL1, PC3^{SFRP2} cells showed a significant COL1-dependent transcriptional adaptation, with 453 significantly differentially expressed genes (DEGs) (Figure 2A′, Table S2).

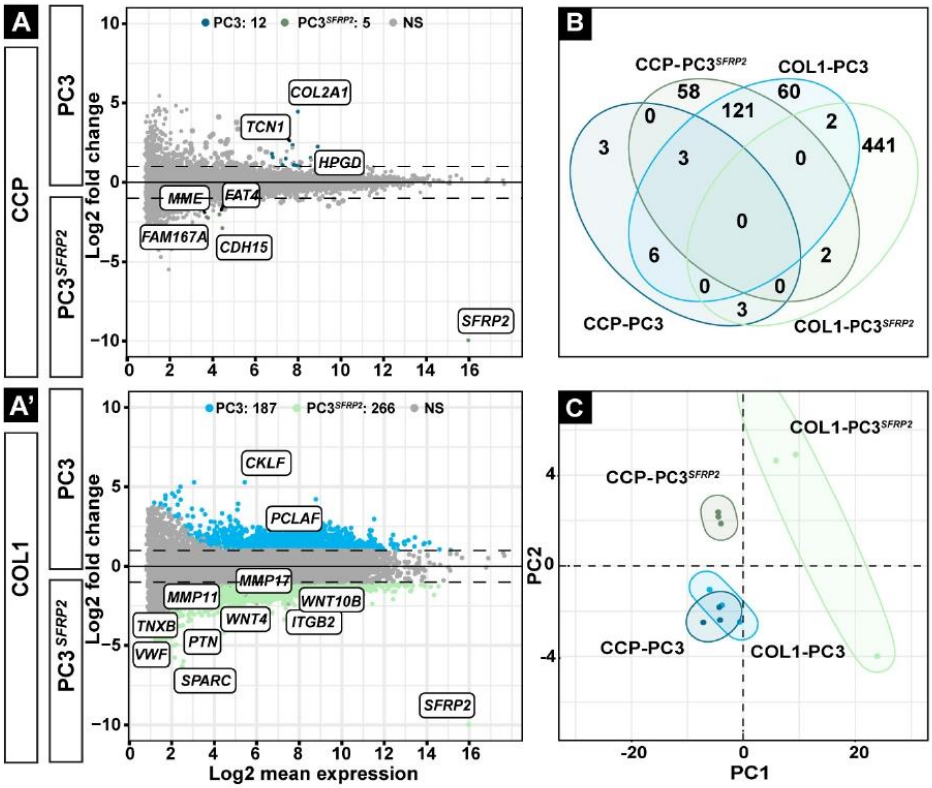

Figure 2. Differentially expressed gene (DEG) analysis of PC3 and PC3^{SFRP2} cells. Next-generation RNA sequencing was performed to uncover genes that are affected by SFRP2 overexpression and surface condition. MA plots show gene expression differences between PC3 and PC3^{SFRP2} on CCP (**A**) and COL1 (**A′**) surfaces. Genes that may influence osteomimicry were labelled in MA-plots. NS: not significant, blue: significantly upregulated in PC3, green: significantly upregulated in PC3^{SFRP2}. The Venn diagram illustrates the number of unique upregulated genes specific to each group (**B**). Principal component analysis (PCA) revealed a strong transcriptional response of PC3^{SFRP2} cells on COL1, when compared to PC3^{SFRP2} on CCP surface (**C**).

When we investigate the upregulated genes in COL1-PC3^{SFRP2} in detail, we discovered several genes that might contribute to the formation of osteomimicry. Members of the integrin (ITG) and matrix metalloproteinase (MMP) families mediate cell adhesion and invasion on or through extracellular matrices, respectively [40]. Interestingly, *ITGB2 (Integrin Subunit Beta 2)*, *MMP11 (Matrix Metallopeptidase 11)*, and *MMP17 (Matrix Metallopeptidase 11)* were significantly upregulated in COL1-PC3^{SFRP2} cells when compared to COL1-PC3. Moreover, increased expression of *TNXB* (*Tenascin XB*) causes an increase in cell adhesion [41], and *VWF* (*Von Willebrand Factor*) is a major platelet adhesion ligand [42] that contributes to the adhesion property of COL1-PC3^{SFRP2} cells. Similarly, upregulation of *PTN* (*Pleiotrophin/Osteoblast-Stimulating Factor 1*) and *SPARC* (*Secreted Protein Acidic and Cysteine Rich*), which represent biochemical markers for osteoblast-like cells [43,44], were also detected in COL1-PC3^{SFRP2} cells (Figure 2A′, Table S2).

As SFRP2 is a WNT signaling inhibitor, we specifically investigated the autocrine effect of SFRP2 on PC3 cells by WNT signaling-related gene set (GO:0016055). Interestingly, we did not observe a significant effect of SFRP2 overexpression on WNT signaling in PC3 when the cells were cultured on CCP surface (Table S1). *CTNNB1* encoding ß-catenin, which is an essential marker of canonical WNT signaling, was differentially expressed between PC3 and PC3^{SFRP2} on COL1-coated surface, but the Log2FoldChange was below the cut-off value $\pm |2|$ (Table S2). On the other hand, we found that WNT signaling-related genes such as *WNT4* and *WNT10B*, which are potential promoters of osteogenic differentiation [45,46], were significantly upregulated in COL1-PC3^{SFRP2} in comparison to COL1-PC3 (Figure 2A′, Table S2). In summary, differential gene expression analysis genes indicated the upregulation of some WNT signaling-related genes responsible in the osteogenic lineage in COL1-PC3^{SFRP2} cells when compared to COL1-PC3 cells.

PC3 cells cultured on CCP surface showed almost no COL1-dependent transcriptional adaptation when compared to PC3 on COL1 (Figure S1B, Table S3). In contrast, the expression of 451 genes were significantly changed in COL1-PC3^{SFRP2} cells in comparison to CCP-PC3^{SFRP2} cells (Figure S1B, Table S4).

Furthermore, by directly comparing DEGs in all groups using a Venn diagram, we observed that COL1-PC3^{SFRP2} cells have the highest number of significantly upregulated (Figure 2B) and downregulated (Figure S1C) genes when compared to all other groups. In addition, a principal component analysis (PCA) also showed that the surface induced only negligible transcriptional changes in PC3 cells, in contrast to PC3^{SFRP2} cells that were cultured on COL1, as COL1-PC3^{SFRP2} showed a clear shift of the PCA cluster in comparison to CCP-PC3^{SFRP2}.

3.3. SFRP2 Overexpression Leads to Osteotropic-like PC3 Cells on the COL1 Surface

To analyze the intrinsic effect of the 453 significant DEGs on the COL1 surface due to SFRP2 overexpression (Table S2), we first performed a gene ontology (GO) enrichment analysis to detect the corresponding biological process that may contribute to the metastasis process (Figure 3A). When we examined the top 20 significantly upregulated biological process in COL1-PC3 and COL1-PC3^{SFRP2}, we found that *SFRP2* overexpression causes a significant upregulation of genes that are associated with “Cell morphogenesis involved in differentiation”, indicating a possible EMT required for cancer metastasis, as well as with “Biological Adhesion” and “Cell Adhesion”, which may be required for osteotropic relocation of metastatic prostate cancer cells. The increase in “Taxis”- and “Locomotion”-related gene expression also supports the hypothesis that SFRP2 is involved in the relocation property of PC3 cells.

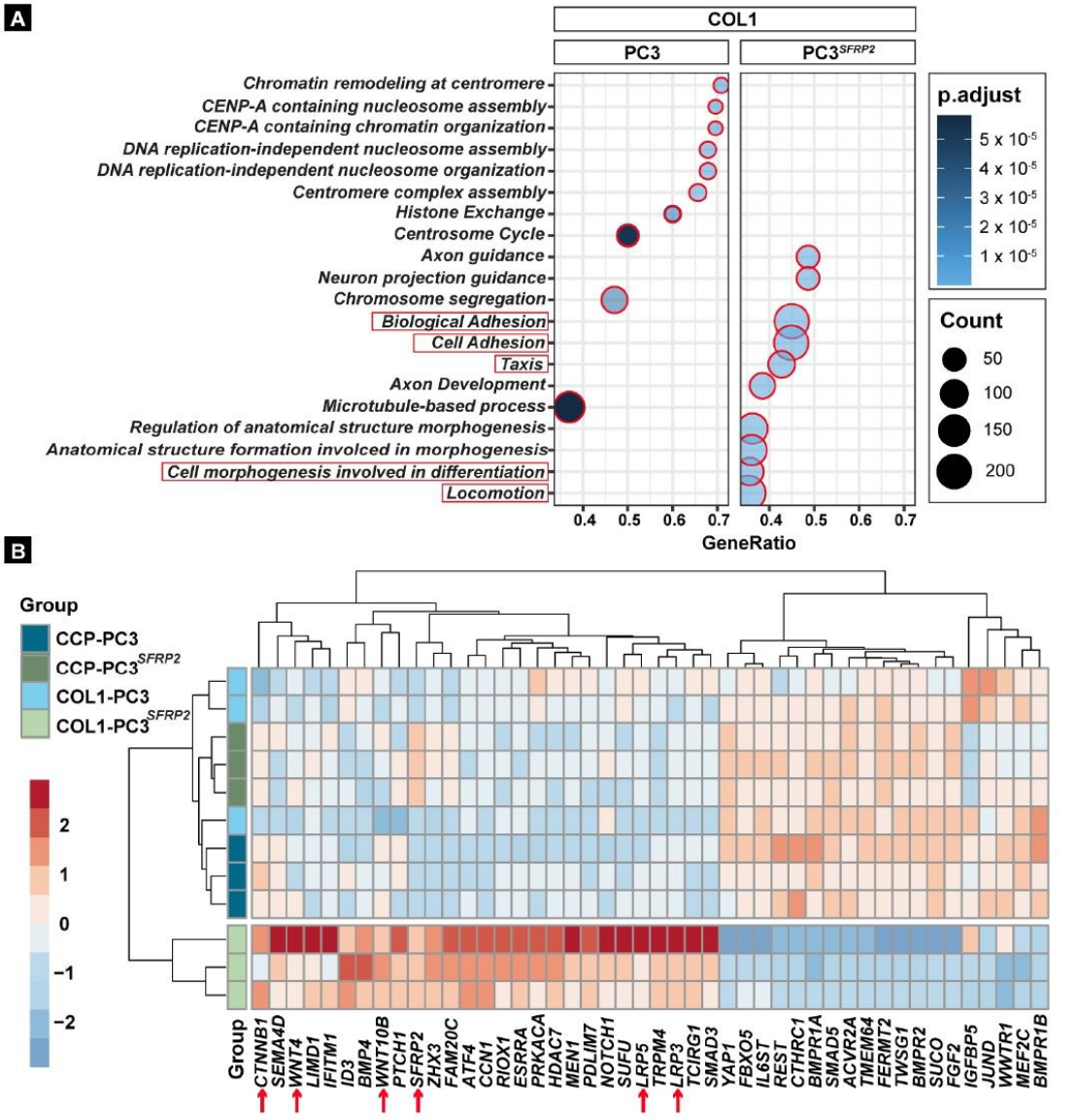

Figure 3. SFRP2 overexpression leads to osteotropic properties in PC3 cells on a COL1 surface. GO biological processes related to adhesion, taxis, and differentiation were significantly increased by SFRP2 overexpression compared to native PC3 cells when the cells were seeded on COL1 (**A**). Heatmap of osteoblast differentiation-related genes (GO:0001649) shows clear clustering of COL1-PC3^{SFRP2} from all other groups (**B**). Arrows indicate WNT signaling-related gene expression in osteoblast differentiation.

3.4. SFRP2 Overexpression Alters the Transcriptome of PC3 Cells towards an Osteoblast-like Phenotype on the COL1 Surface

Osteomimicry of metastatic cancer cells is defined by a molecular and phenotypic transition towards osteoblast-like cells in the bone environment. Therefore, we specifically evaluated genes that are involved in osteoblast differentiation (GO:0001649) within each experimental group. Interestingly, our analysis showed that, similar to the PCA (Figure 2C), COL1-PC3^{SFRP2} is characterized by a unique cluster of osteoblast differentiation-related genes, when compared to all other groups (Figure 3B). Specifically, even though SFRP2 is accepted as a negative regulator of WNT signaling [47], SFRP2 overexpression leads to a COL1-dependent increase in *WNT4* and *WNT10B*, as well as *CTNNB1* (ß-catenin) expression (Figure 3B). Besides the specific WNT proteins that can promote osteoblast differentiation, COL1-PC3^{SFRP2} cells also showed an increased expression of *BMP4* in comparison to all other groups, which is one of the most important osteoblastic lineage markers [48]. It is also known that prostate cancer cells secreting higher levels of BMP4 exhibit enhanced bone formation in vivo [49]. In addition, downregulation of the BMP receptors *BMPR1A*, *BMPR1B*, and *BMPPR2* in COL1-PC3^{SFRP2} suggests that the secreted BMPs might be not utilized by the cancer cells in an autocrine manner.

3.5. SFRP2 Overexpression Induces COL1-Dependent EMT in PC3 Cells

"Cell morphogenesis involved in differentiation" (GO:0010770) is defined as a change in cell size and shape due to the differentiation process [50,51]. EMT is a crucial morphology-altering step for all primary cancer cells in early metastasis [52]. As our GO analysis results indicated that SFRP2 significantly increases the expression of cell morphogenesis-related genes in PC3^{SFRP2} cells cultured on a COL1 surface (Figure 3A), we evaluated SFRP2-dependent changes of cell area and aspect ratio of PC3 and PC3^{SFRP2} cells on both surfaces in vitro.

PC3 and PC3^{SFRP2} cells did not show any differences in volume (Figure 4A, FSC-A) or granularity (Figure 4A, SSC-A) in suspension. However, while PC3 cells that were cultured on a CCP surface revealed the typical epithelial morphology, CCP-PC3^{SFRP2} showed a more roundish morphology (Figure 4B). In contrast, we observed that both cell types adopted an elongated cell morphology and increased cell area when cultured on COL1 (Figure 4B'). COL1 surface significantly increases the cell area in both cell types in a SFRP2-independent manner (Figure 4C). Intriguingly, COL1-PC3^{SFRP2} displayed significant cell elongation when compared to COL1-PC3 controls (Figure 4D). Furthermore, culturing PC3^{SFRP2} cell on COL1 led to a significant increase in cellular elongation in comparison to CCP-PC3^{SFRP2}.

This significant increase in the aspect ratio of PC3^{SFRP2} cells in comparison to native PC3 cells suggested that phenotypical EMT only occurs on the COL1 surface in a SFRP2-dependent manner (Figure 4D). To strengthen this finding on a transcriptional level, we matched the genes that are significantly upregulated in COL1-PC3^{SFRP2} and CCP-PC3^{SFRP2} cells with hallmark gene sets for EMT (Figure 4E and Figure S1D) and identified that 29 genes were upregulated related to Hallmark: EMT in COL1-PC3^{SFRP2}, including *FBLN1*, *FBLN2*, and *TGFB1*, when compared to CCP-PC3^{SFRP2} (Table S5). Taken together, high expression of SFRP2 in PC3 cells positively regulates essential EMT-related genes and therewith promotes cell elongation in a COL1-dependent manner.

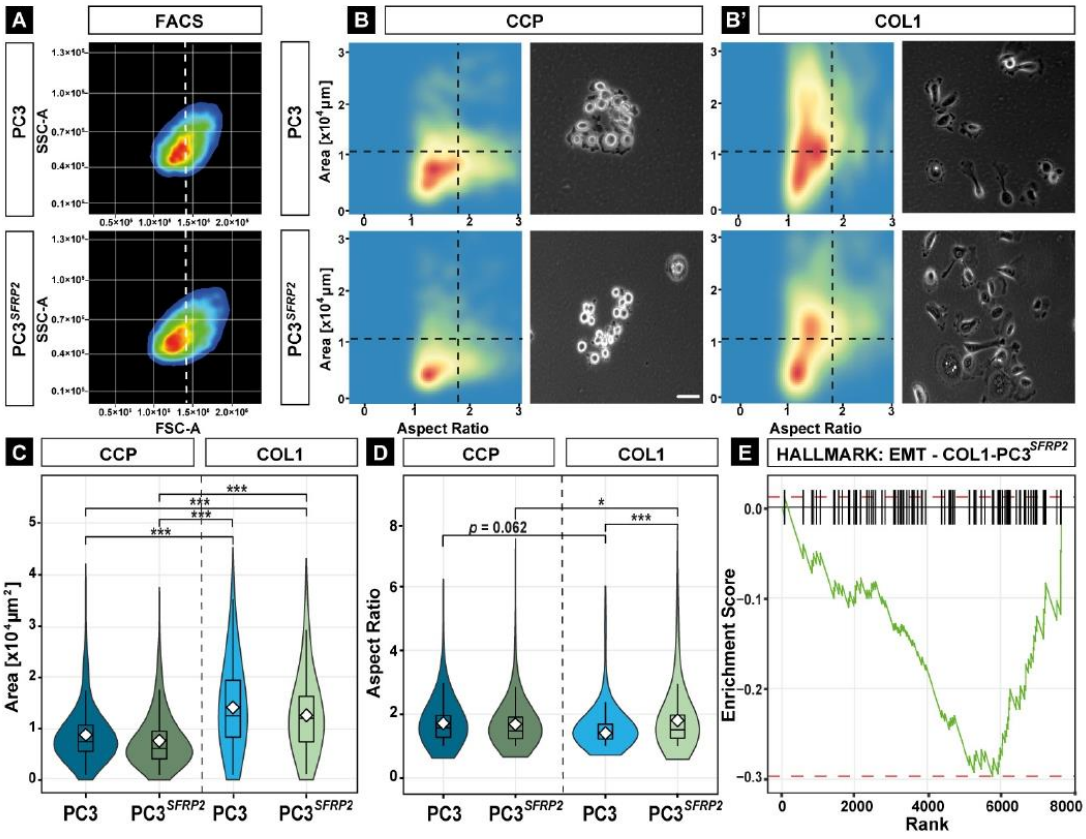

Figure 4. SFRP2 overexpression induces COL1-dependent EMT in PC3 cells. No morphological differences between PC3 and PC3^{SFRP2} were observed in FACS analysis when cells were in suspension (**A**). On the CCP surface, PC3 cells are epithelial-like, while PC3^{SFRP2} cells are more roundish (**B**). The COL1 surface induces an increase in cell size and elongation in both PC3 and PC3^{SFRP2} (**B'**). Quantification of the cell morphology reveals that COL1 significantly increases cell size in PC3^{SFRP2} cells (**C**) and elongation in COL1-PC3^{SFRP2} cells (**D**). RNAseq analysis revealed that COL1-PC3^{SFRP2} exhibited significant upregulation of the EMT pathway-related hallmark gene set when compared to CCP-PC3^{SFRP2}. COL1-PC3^{SFRP2} enrichment score < 0, CCP-PC3^{SFRP2} enrichment score > 0 (**E**). * $p \leq 0.05$; *** $p \leq 0.001$. Scale bar: 200 µm.

3.6. SFRP2 Overexpression Impedes the Reduction of Proliferation of PC3 Cells on COL1

Besides EMT, increased proliferation and metabolism inside the bone metastatic site, without being recognized by immune cells, is an additional crucial adaptation of cancer cells in early metastasis [53,54]. Therefore, proliferation was assessed by a cumulative population doubling, as well as a colony formation (CFU) assay.

Interestingly, while COL1-PC3 cells proliferate significantly slower, when compared to CCP-PC3 cells, the proliferation of PC3^{SFRP2} cells was not changed when seeded on COL1 (Figure 5A,B).

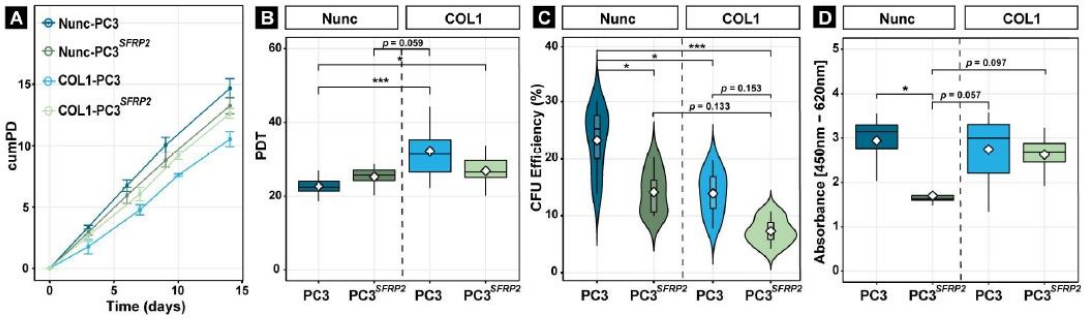

Figure 5. SFRP2 overexpression suppresses the reduced proliferation of PC3 cells on the COL1 surface. Cumulative population doubling (*cumPD*) (**A**) and population doubling time (*PDT*) (**B**) revealed that culturing PC3 cells on a COL1-coated surface reduced their proliferation in comparison to PC3^{SFRP2}. COL1, and SFRP2 mutually significantly reduced CFU efficiency of PC3 cells (**C**). Metabolic activity is significantly reduced in PC3^{SFRP2} cells on the CCP surface compared to native PC3. However, this significant difference is no longer observed when the cells are cultured on COL1 surface (**D**). Significance levels: * equals $p \leq 0.05$; *** equals $p \leq 0.001$.

Similarly, the COL1 surface significantly reduced the CFU efficiency in each group when compared to CCP-PC3 (Figure 5C). Interestingly, the lowest CFU efficiency was observed in COL1-PC3^{SFRP2}, which also supported potential EMT on COL1, as EMT causes loss of intercellular adhesion [55].

Moreover, the lower CFU efficiency, but similar proliferation rate between PC3 and PC3^{SFRP2} in each condition, was accompanied with a strong reduction of cellular metabolism in NCCPunc-PC3^{SFRP2} cells compared to CCP-PC3. However, the difference was no longer significant when cells were cultured on the COL1 surface.

3.7. SFRP2 Overexpression Enhances COL1-Dependent Migration, Invasion, and Metabolic Activity of PC3 Cells

After cancer cells leave the primary site, their biochemical adaption to migrate, invade, and adhere to the target side are crucial to complete early metastasis. The secreted proteins might help us to define the migration of cancer cells and the location of metastasis [56]. Our GO pathways analysis (Figure 3A) shows that SFRP2 overexpression enhances cell adhesion, taxis, and locomotion of PC3 cells when cultured on COL1 surface. These findings suggest that SFRP2 may contribute to the osteotropism of metastatic prostate cancer cells. To validate our bioinformatics analysis, we investigated random migration, invasion through a COL1 matrix, and adherence of PC3 and PC3^{SFRP2} cells on COL1 and CCP surfaces.

Interestingly, random migration assay demonstrated that the velocity of PC3 and PC3^{SFRP2} cells was not significantly different on the same surface, but COL1-PC3 cells had a significantly faster random migration when compared to CCP surface (Figure 6A). In contrast, when cells had to migrate through a COL1 matrix, we counted significantly more PC3^{SFRP2} cells in the lower compartment in comparison to PC3 cells (Figure 6B). Evaluation of cell attachment revealed that significantly more PC3^{SFRP2} cells adhered after 2 h on CCP when compared to CCP-PC3. However, this effect was not significant between COL1-PC3 and COL1-PC3^{SFRP2} (Figure 6C).

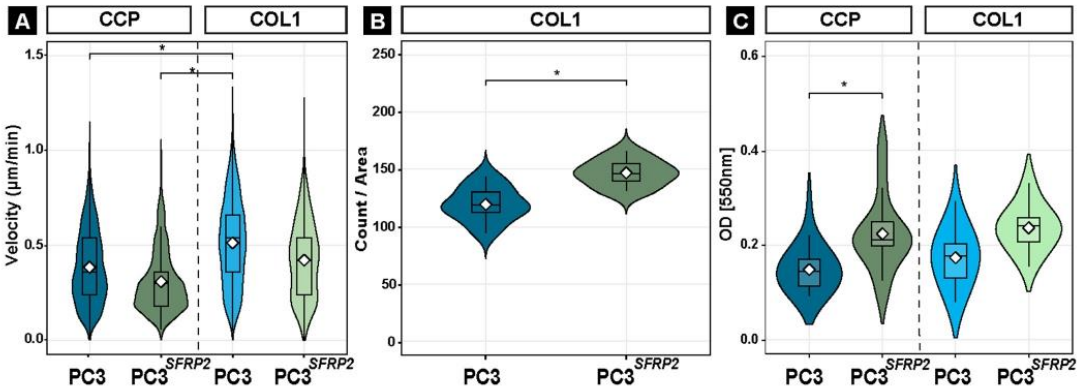

Figure 6. SFRP2 overexpression increases the osteotropic-like properties of PC3 cells on the COL1 surface. COL1-coating increases the random migration velocity of PC3 cells significantly, whereas overexpression of SFRP2 did not lead to such a significant increase in motility (**A**). Cellular invasion through a COL1 matrix shows that *SFRP2* overexpression significantly increases the invasion of the PC3 cells (**B**). Cell attachment assay shows an increase in attachment with *SFRP2* overexpression in PC3 cells cultured on both surfaces yet increase on COL1 is not significant. (**C**). Significance level: * equals $p \leq 0.05$.

4. Discussion

This manuscript attempts to provide new information on mechanisms in the process of prostate cancer bone metastasis. After prostate cancer cells leave the primary site, demethylation of the *SFRP2* promoter likely drives cancer cells towards bone to eventually metastasize. Osteomimicry is a key element of cancer cell survival during early metastasis [57], and SFRP2 may be one of the crucial molecular players that modulates cancer cells and their environment to increase their adaptation to evade the immune response (Figure 7). In this study, we aimed to find a potential solution to intervene in the process of metastasis before aggressive late metastasis, when the balance of bone formation and resorption is disturbed, and additional biochemical mechanisms are involved [58]. Evasion of osteomimicry property of cancer cells by inhibiting SFRP2 is a possible mechanism to suppress bone metastasis. Moreover, SFRP2 might be a potential molecular candidate to detect bone metastasis in prostate cancer patients before fatal outcomes develop.

Our observations suggested that SFRP2 alters the transcriptome and therewith alters cancer- and bone-related biological properties of PC3 cells when seeded on the bone environment-mimicking Collagen 1 surface. The results of differential gene expression analysis and in vitro experiments implicate that SFRP2 is one of the key elements leading to the adaptation of cancer cells in the metastatic bone microenvironment (Figure 7). Collagen 1-driven phenotypical change in $PC3^{SFRP2}$ cells towards a mesenchymal cell may help to understand the unclear mechanisms of osteomimicry. The great similarities between metastatic prostate cancer cells and osteoblasts support tumor cell survival in the bone microenvironment [53]. Deciphering such bone adaptation mechanisms of prostate cancer cells may result in the identification of novel therapeutic targets. The isolation of a specific, highly aggressive cancer cell subpopulations could contribute to the understanding of the entire metastatic pathway. In particular, the identification of molecular markers that cause EMT [58] and support osteomimicry of primary tumor cells may be a promising approach to interfere with early prostate cancer metastasis.

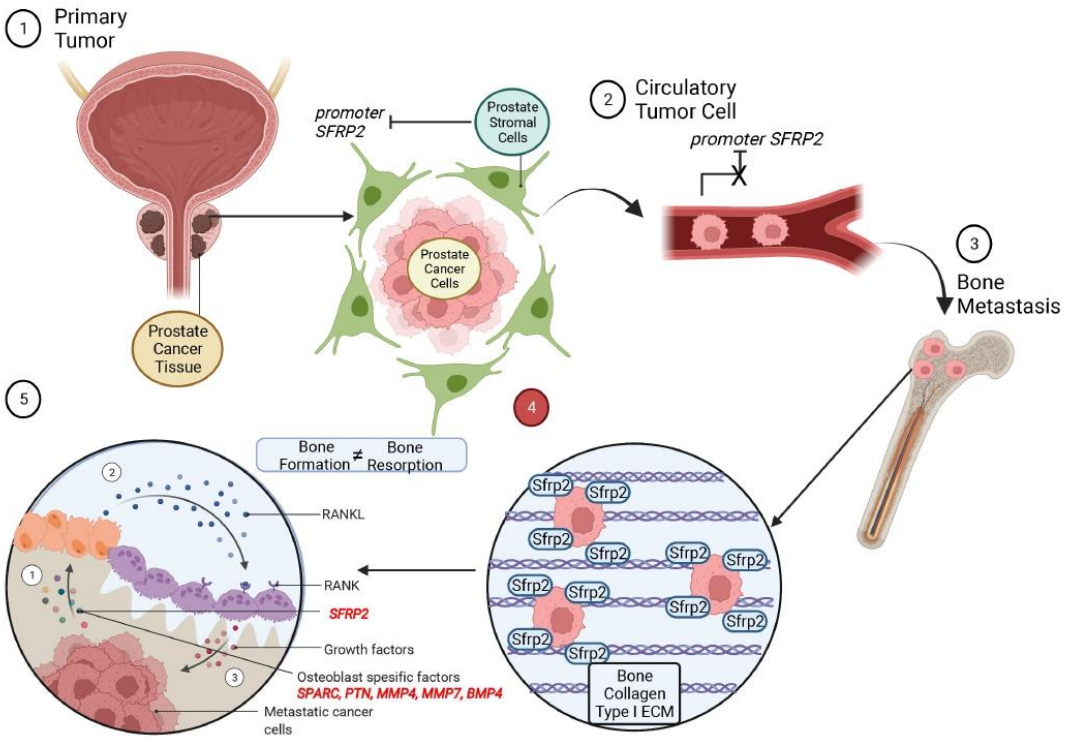

Figure 7. Visual representation of the potential effect of SFRP2 on prostate cancer cells during bone metastasis. After prostate cancer cells enter the circulation, SFRP2 expression leads them to attach and invade bone. PC3^{SFRP2} cells start to secrete osteoblast-specific factors for osteomimicry and disturb the balance between bone formation and resorption. Created with BioRender.com (accessed on 14 June 2022, adapted from "Metastasis to Bone Disrupts Bone Homeostasis").

By analyzing significantly differentially expressed genes between COL1-PC3 and COL1-PC3^{SFPR2} cells, we found the up-regulation of the *Osteonectin* (*SPARC*) gene, which encodes an abundant non-collagenous protein of bone ECM [59] in COL1-PC3^{SFPR2} cells. Prostate cancer cells are known to secrete a high level of SPARC protein when they are in the dormant stage of early bone metastasis [60]. The secretion of additional bone-related proteins in the bone microenvironment may allow cancer cells to settle, adapt, and survive more easily during metastatic progression. In accordance, COL1-PC3^{SFPR2} cells had a high expression of *Pleiotrophin* (*Osteoblast Specific Factor-1*, *PTN*), which is considered as a poor prognosis marker in prostate cancer patients with bone metastasis [61], but it is generally known as a secreted growth factor produced by osteoblasts during early osteogenic differentiation and angiogenesis [62].

For the survival of the cells during metastasis extravasation and colonization, the cancer cells must regain their adhesion properties to the ECM after leaving the circulation, and the secretion of specific adhesion molecules could guide cancer cells towards the target site. Therefore, upregulation of adhesion-related genes might be a possible indication of osteotropism, which may be triggered by the demethylation of the *SFRP2* gene. Increased expression of *TNXB* (*Tenascin XB*) and *VWF* (*Von Willebrand Factor*) are both accepted as promising bone metastasis-related markers [63] (Figure 2A′, Table S2) It is known that *TNXB* deficiency also causes significant bone loss in mice due to increase in osteoclasts [41], thus, the upregulation of *TNXB* triggered by SFRP2 overexpression in our in vitro study may also lead to reduced osteoclastogenesis in vivo, therefore further increasing bone formation

(Table S2). Furthermore, it was previously shown that *MMP11* upregulation is correlated to a poor prognosis of prostate cancer, and it is highly expressed in bone metastasis [64]. Furthermore, *Osteopontin* (*OPN*), a crucial ECM protein in the bone metastasis process [65], is a substrate of MMP17 [66]. Taken together, the increased expression of genes that are associated with bone formation in COL1-PC3^{SFRP2} underlines osteomimicry in early and late metastatic stages.

While several studies suggest a role of SFRP2 in WNT signaling, our gene expression data showed that SFRP2 overexpression did not cause a reduction of WNT signaling, neither on CCP nor COL1-coated surfaces, yet it increases WNT related ligands expression as *WNT4* and *WNT10B*.

As our data indicate that SFRP2 causes a molecular and phenotypical switch of PC3 cancer cells towards more osteoblast-like cells, these novel findings may help to monitor the osteotropic activity of metastatic prostate cancer cells in all phases of bone metastasis. After cancer cells enter the circulation to metastasize, osteotropic activity of prostate cancer cells could be detected by elevated serum SFRP2 levels in patients, similar to breast cancer patients with a poor prognosis [23]. Therefore, the regular analysis of SFRP2 serum levels after the first diagnosis of prostate cancer can be a solution to identify potential metastasizes in an early stage. However, further experiments will be needed to demonstrate demethylation of *SFRP2* in primary and metastatic cancer tissues and to confirm elevated SFRP2 serum levels to detect the type and location of the early bone metastasis of prostate cancers. Furthermore, besides SFRP2 function to upregulate osteoblast-related gene expression, its effect on osteogenic differentiation must be verified by in vitro mesenchymal stem cell differentiation assays to understand the influence of SFRP2 in late bone metastasis.

Supplementary Materials: The following supporting information can be downloaded at: https://www.mdpi.com/article/10.3390/cells11244081/s1, Figure S1: Differential Gene Expression Analysis; Table S1: DEG Gene List of CCP-PC3 and CCP-PC3^{SFRP2}; Table S2: DEG Gene List of COL1-PC3 and COL1-PC3^{SFRP2}; Table S3: DEG-Gene List of CCP-PC3 and COL1-PC3; Table S4: DEG Gene List of CCP-PC3^{SFRP2} and COL1-PC3^{SFRP2}; Table S5: Hallmark: EMT COL1-PC3^{SFRP2} and CCP-PC3^{SFRP2}.

Author Contributions: Conceptualization, E.A.Ö. and M.M.S.; methodology, E.A.Ö., H.T., H.S. and M.M.S.; software, E.A.Ö.; validation, E.A.Ö., H.T., H.S., A.A., V.S. and M.M.S.; formal analysis, E.A.Ö. and M.M.S.; investigation, E.A.Ö.; resources, H.T., H.S., A.A., M.C., M.A., W.B., V.S. and M.M.S.; data curation, E.A.Ö. and M.M.S.; writing—original draft preparation, E.A.Ö. and M.M.S.; writing—review and editing, E.A.Ö., H.T., H.S., A.A., V.S. and M.M.S.; visualization, E.A.Ö. and M.M.S.; supervision, M.M.S. All authors have read and agreed to the published version of the manuscript.

Funding: The study is supported by "Bayerischen Forschungsstiftung" under the "Forschungsverbund Tumordiagnostik für individualisierte Therapie (FORTiTher)" project (AZ-1365-18).

Institutional Review Board Statement: Not applicable.

Informed Consent Statement: Not applicable.

Data Availability Statement: Gene expression data are deposited at https://www.ncbi.nlm.nih.gov/geo/query/acc.cgi?acc=GSE217979, accessed on 18 November 2022. All in vitro data are available from the corresponding author upon reasonable request.

Acknowledgments: We thank Martina Burggraf, Heidrun Grondinger, and Zsuzsanna Farkas for their technical assistance.

Conflicts of Interest: The authors declare no conflict of interest.

References

1. Rawla, P. Epidemiology of Prostate Cancer. *World J. Oncol.* **2019**, *10*, 63–89. [CrossRef] [PubMed]
2. Lin, S.-C.; Yu-Lee, L.-Y.; Lin, S.-H. Osteoblastic Factors in Prostate Cancer Bone Metastasis. *Curr. Osteoporos. Rep.* **2018**, *16*, 642–647. [CrossRef] [PubMed]
3. Gandaglia, G.; Abdollah, F.; Schiffmann, J.; Trudeau, V.; Shariat, S.F.; Kim, S.P.; Perrotte, P.; Montorsi, F.; Briganti, A.; Trinh, Q.-D.; et al. Distribution of metastatic sites in patients with prostate cancer: A population-based analysis. *Prostate* **2014**, *74*, 210–216. [CrossRef]
4. Keller, E.T.; Brown, J. Prostate cancer bone metastases promote both osteolytic and osteoblastic activity. *J. Cell. Biochem.* **2004**, *91*, 718–729. [CrossRef]
5. Croucher, P.I.; McDonald, M.M.; Martin, T.J. Bone metastasis: The importance of the neighbourhood. *Nat. Rev. Cancer* **2016**, *16*, 373–386. [CrossRef]
6. Ban, J.; Fock, V.; Aryee, D.N.T.; Kovar, H. Mechanisms, Diagnosis and Treatment of Bone Metastases. *Cells* **2021**, *10*, 2944. [CrossRef] [PubMed]
7. Liu, D.; Kuai, Y.; Zhu, R.; Zhou, C.; Tao, Y.; Han, W.; Chen, Q. Prognosis of prostate cancer and bone metastasis pattern of patients: A SEER-based study and a local hospital based study from China. *Sci. Rep.* **2020**, *10*, 9104. [CrossRef]
8. Marchetti, C. Calcium signaling in prostate cancer cells of increasing malignancy. *Biomol. Concepts* **2022**, *13*, 156–163. [CrossRef]
9. Fradet, A.; Sorel, H.; Depalle, B.; Serre, C.M.; Farlay, D.; Turtoi, A.; Bellahcène, A.; Follet, H.; Castronovo, V.; Clézardin, P.; et al. A New Murine Model of Osteoblastic/Osteolytic Lesions from Human Androgen-Resistant Prostate Cancer. *PLoS ONE* **2013**, *8*, e75092. [CrossRef] [PubMed]
10. Butler, J.S.; Queally, J.M.; Devitt, B.M.; Murray, D.W.; Doran, P.P.; O'Byrne, J.M. Silencing Dkk1 expression rescues dexamethasone-induced suppression of primary human osteoblast differentiation. *BMC Musculoskelet. Disord.* **2010**, *11*, 210. [CrossRef]
11. Hall, C.L.; Bafico, A.; Dai, J.; Aaronson, S.A.; Keller, E.T. Prostate Cancer Cells Promote Osteoblastic Bone Metastases through Wnts. *Cancer Res.* **2005**, *65*, 7554–7560. [CrossRef] [PubMed]
12. Zhang, Y.; Wang, X. Targeting the Wnt/β-catenin signaling pathway in cancer. *J. Hematol. Oncol.* **2020**, *13*, 165. [CrossRef]
13. Patel, S.; Alam, A.; Pant, R.; Chattopadhyay, S. Wnt Signaling and Its Significance Within the Tumor Microenvironment: Novel Therapeutic Insights. *Front. Immunol.* **2019**, *10*, 2872. [CrossRef] [PubMed]
14. Wang, Y.; Singhal, U.; Qiao, Y.; Kasputis, T.; Chung, J.-S.; Zhao, H.; Chammaa, F.; Belardo, J.A.; Roth, T.M.; Zhang, H.; et al. Wnt Signaling Drives Prostate Cancer Bone Metastatic Tropism and Invasion. *Transl. Oncol.* **2020**, *13*, 100747. [CrossRef] [PubMed]
15. Agostino, M.; Pohl, S.-G. Wnt Binding Affinity Prediction for Putative Frizzled-Type Cysteine-Rich Domains. *Int. J. Mol. Sci.* **2019**, *20*, 4168. [CrossRef]
16. Gã¶tze, S.; Wolter, M.; Reifenberger, G.; Mã¼Ller, O.; Sievers, S. Frequent promoter hypermethylation of Wnt pathway inhibitor genes in malignant astrocytic gliomas. *Int. J. Cancer* **2010**, *126*, 2584–2593. [CrossRef]
17. Rogan, M.R.; Patterson, L.L.; Byerly, C.D.; Luo, T.; Paessler, S.; Veljkovic, V.; Quade, B.; McBride, J.W. Ehrlichia chaffeensis TRP120 Is a Wnt Ligand Mimetic That Interacts with Wnt Receptors and Contains a Novel Repetitive Short Linear Motif That Activates Wnt Signaling. *mSphere* **2021**, *6*, e00216-21. [CrossRef]
18. Sun, Y.; Zhu, D.; Chen, F.; Qian, M.; Wei, H.; Chen, W.; Xu, J. SFRP2 augments WNT16B signaling to promote therapeutic resistance in the damaged tumor microenvironment. *Oncogene* **2016**, *35*, 4321–4334. [CrossRef]
19. von Marschall, Z.; Fisher, L.W. Secreted Frizzled-related protein-2 (sFRP2) augments canonical Wnt3a-induced signaling. *Biochem. Biophys. Res. Commun.* **2010**, *400*, 299–304. [CrossRef]
20. Perry, A.S.; O'Hurley, G.; Raheem, O.A.; Brennan, K.; Wong, S.; O'Grady, A.; Kennedy, A.-M.; Marignol, L.; Murphy, T.; Sullivan, L.; et al. Gene expression and epigenetic discovery screen reveal methylation of SFRP2 in prostate cancer. *Int. J. Cancer* **2013**, *132*, 1771–1780. [CrossRef]
21. Lee, J.-L.; Lin, C.-T.; Chueh, L.-L.; Chang, C.-J. Autocrine/Paracrine Secreted Frizzled-related Protein 2 Induces Cellular Resistance to Apoptosis. *J. Biol. Chem.* **2004**, *279*, 14602–14609. [CrossRef] [PubMed]
22. Murillo-Garzón, V.; Kypta, R. WNT signalling in prostate cancer. *Nat. Rev. Urol.* **2017**, *14*, 683–696. [CrossRef] [PubMed]
23. Huang, C.; Ye, Z.; Wan, J.; Liang, J.; Liu, M.; Xu, X.; Li, L. Secreted Frizzled-Related Protein 2 Is Associated with Disease Progression and Poor Prognosis in Breast Cancer. *Dis. Markers* **2019**, *2019*, 6149381. [CrossRef]
24. de Castro, L.F.; Sworder, B.J.; Mui, B.; Futrega, K.; Berendsen, A.; Phillips, M.D.; Burbach, N.J.; Cherman, N.; Kuznetsov, S.; Gabet, Y.; et al. Secreted frizzled related-protein 2 (Sfrp2) deficiency decreases adult skeletal stem cell function in mice. *Bone Res.* **2021**, *9*, 49. [CrossRef] [PubMed]
25. van Loon, K.; Huijbers, E.J.M.; Griffioen, A.W. Secreted frizzled-related protein 2: A key player in noncanonical Wnt signaling and tumor angiogenesis. *Cancer Metastasis Rev.* **2021**, *40*, 191–203. [CrossRef]
26. Schild, T.; Low, V.; Blenis, J.; Gomes, A.P. Unique Metabolic Adaptations Dictate Distal Organ-Specific Metastatic Colonization. *Cancer Cell* **2018**, *33*, 347–354. [CrossRef]
27. Furesi, G.; Rauner, M.; Hofbauer, L.C. Emerging Players in Prostate Cancer–Bone Niche Communication. *Trends Cancer* **2021**, *7*, 112–121. [CrossRef]
28. Jadaan, D.Y.; Jadaan, M.M.; McCabe, J.P. Cellular Plasticity in Prostate Cancer Bone Metastasis. *Prostate Cancer* **2015**, *2015*, 651580. [CrossRef]

29. Gao, D.; Zhang, X.H.F.; Thompson, E.W.; Mittal, V. EMT process in bone metastasis. In *Bone Sarcomas and Bone Metastases-From Bench to Bedside*; Academic Press: Cambridge, MA, USA, 2022; pp. 359–370.
30. Monteran, L.; Ershaid, N.; Sabah, I.; Fahoum, I.; Zait, Y.; Shani, O.; Cohen, N.; Eldar-Boock, A.; Satchi-Fainaro, R.; Erez, N. Bone metastasis is associated with acquisition of mesenchymal phenotype and immune suppression in a model of spontaneous breast cancer metastasis. *Sci. Rep.* **2020**, *10*, 13838. [CrossRef]
31. Ivics, Z.; Izsvák, Z. Nonviral Gene Delivery with the *Sleeping Beauty* Transposon System. *Hum. Gene Ther.* **2011**, *22*, 1043–1051. [CrossRef]
32. Schneider, C.A.; Rasband, W.S.; Eliceiri, K.W. NIH Image to ImageJ: 25 Years of image analysis. *Nat. Methods* **2012**, *9*, 671–675. [CrossRef] [PubMed]
33. Meijering, E.; Dzyubachyk, O.; Smal, I. Methods for Cell and Particle Tracking. *Methods Enzymol.* **2012**, *504*, 183–200. [CrossRef]
34. Dobin, A.; Davis, C.A.; Schlesinger, F.; Drenkow, J.; Zaleski, C.; Jha, S.; Batut, P.; Chaisson, M.; Gingeras, T.R. STAR: Ultrafast universal RNA-seq aligner. *Bioinformatics* **2013**, *29*, 15–21. [CrossRef] [PubMed]
35. Love, M.I.; Huber, W.; Anders, S. Moderated estimation of fold change and dispersion for RNA-seq data with DESeq2. *Genome Biol.* **2014**, *15*, 550. [CrossRef]
36. Yu, G.; Wang, L.-G.; Han, Y.; He, Q.-Y. clusterProfiler: An R Package for Comparing Biological Themes Among Gene Clusters. *OMICS J. Integr. Biol.* **2012**, *16*, 284–287. [CrossRef] [PubMed]
37. Kowarz, E.; Löscher, D.; Marschalek, R. Optimized Sleeping Beauty transposons rapidly generate stable transgenic cell lines. *Biotechnol. J.* **2015**, *10*, 647–653. [CrossRef] [PubMed]
38. Talluri, B.; Amar, K.; Saul, M.; Shireen, T.; Konjufca, V.; Ma, J.; Ha, T.; Chowdhury, F. COL2A1 Is a Novel Biomarker of Melanoma Tumor Repopulating Cells. *Biomedicines* **2020**, *8*, 360. [CrossRef]
39. Donalies, M.; Cramer, M.; Ringwald, M.; Starzinski-Powitz, A. Expression of M-cadherin, a member of the cadherin multigene family, correlates with differentiation of skeletal muscle cells. *Proc. Natl. Acad. Sci. USA* **1991**, *88*, 8024–8028. [CrossRef]
40. Yue, J.; Zhang, K.; Chen, J. Role of Integrins in Regulating Proteases to Mediate Extracellular Matrix Remodeling. *Cancer Microenviron.* **2012**, *5*, 275–283. [CrossRef]
41. Kajitani, N.; Yamada, T.; Kawakami, K.; Matsumoto, K.-I. TNX deficiency results in bone loss due to an increase in multinucleated osteoclasts. *Biochem. Biophys. Res. Commun.* **2019**, *512*, 659–664. [CrossRef]
42. Yang, A.-J.; Wang, M.; Wang, Y.; Cai, W.; Li, Q.; Zhao, T.-T.; Zhang, L.-H.; Houck, K.; Chen, X.; Jin, Y.-L.; et al. Cancer cell-derived von Willebrand factor enhanced metastasis of gastric adenocarcinoma. *Oncogenesis* **2018**, *7*, 12. [CrossRef] [PubMed]
43. Lamprou, M.; Kaspiris, A.; Panagiotopoulos, E.; Giannoudis, P.V.; Papadimitriou, E. The role of pleiotrophin in bone repair. *Injury* **2014**, *45*, 1816–1823. [CrossRef] [PubMed]
44. Baird, A.; Lindsay, T.; Everett, A.; Iyemere, V.; Paterson, Y.Z.; McClellan, A.; Henson, F.M.D.; Guest, D.J. Osteoblast differentiation of equine induced pluripotent stem cells. *Biol. Open* **2018**, *7*, bio033514. [CrossRef] [PubMed]
45. Zhang, Q.; Pan, Y.; Ji, J.; Xu, Y.; Zhang, Q.; Qin, L. Roles and action mechanisms of WNT4 in cell differentiation and human diseases: A review. *Cell Death Discov.* **2021**, *7*, 287. [CrossRef]
46. Bennett, C.N.; Longo, K.A.; Wright, W.S.; Suva, L.J.; Lane, T.F.; Hankenson, K.D.; MacDougald, O.A. Regulation of osteoblastogenesis and bone mass by Wnt10b. *Proc. Natl. Acad. Sci. USA* **2005**, *102*, 3324–3329. [CrossRef]
47. Liu, J.; Xiao, Q.; Xiao, J.; Niu, C.; Li, Y.; Zhang, X.; Zhou, Z.; Shu, G.; Yin, G. Wnt/β-catenin signalling: Function, biological mechanisms, and therapeutic opportunities. *Signal Transduct. Target. Ther.* **2022**, *7*, 3. [CrossRef]
48. Chang, S.-F.; Chang, T.-K.; Peng, H.-H.; Yeh, Y.-T.; Lee, D.-Y.; Yeh, C.-R.; Zhou, J.; Cheng, C.-K.; Chang, C.A.; Chiu, J.-J. BMP-4 Induction of Arrest and Differentiation of Osteoblast-Like Cells via $p21^{CIP1}$ and $p27^{KIP1}$ Regulation. *Mol. Endocrinol.* **2009**, *23*, 1827–1838. [CrossRef]
49. Lee, Y.-C.; Cheng, C.-J.; Bilen, M.A.; Lu, J.-F.; Satcher, R.L.; Yu-Lee, L.-Y.; Gallick, G.E.; Maity, S.N.; Lin, S.-H. BMP4 Promotes Prostate Tumor Growth in Bone through Osteogenesis. *Cancer Res.* **2011**, *71*, 5194–5203. [CrossRef]
50. Ashburner, M.; Ball, C.A.; Blake, J.A.; Botstein, D.; Butler, H.; Cherry, J.M.; Davis, A.P.; Dolinski, K.; Dwight, S.S.; Eppig, J.T.; et al. Gene ontology: Tool for the unification of biology. *Nat. Genet.* **2000**, *25*, 25–29. [CrossRef]
51. The Gene Ontology Consortium. The Gene Ontology resource: Enriching a GOld mine. *Nucleic Acids Res.* **2021**, *49*, D325–D334. [CrossRef]
52. Vergara, D.; Simeone, P.; Franck, J.; Trerotola, M.; Giudetti, A.; Capobianco, L.; Tinelli, A.; Bellomo, C.; Fournier, I.; Gaballo, A.; et al. Translating epithelial mesenchymal transition markers into the clinic: Novel insights from proteomics. *EuPA Open Proteom.* **2016**, *10*, 31–41. [CrossRef] [PubMed]
53. Teti, A. Osteomimicry how tumor cells try to deceive the bone. *Front. Biosci.* **2010**, *2*, 907–915. [CrossRef] [PubMed]
54. Yeh, A.C.; Ramaswamy, S. Mechanisms of Cancer Cell Dormancy—Another Hallmark of Cancer? *Cancer Res.* **2015**, *75*, 5014–5022. [CrossRef]
55. Le Bras, G.F.; Taubenslag, K.J.; Andl, C.D. The regulation of cell-cell adhesion during epithelial-mesenchymal transition, motility and tumor progression. *Cell Adhes. Migr.* **2012**, *6*, 365–373. [CrossRef]
56. Lau, W.M.; Weber, K.L.; Doucet, M.; Chou, Y.-T.; Brady, K.; Kowalski, J.; Tsai, H.-L.; Yang, J.; Kominsky, S.L. Identification of prospective factors promoting osteotropism in breast cancer: A potential role for CITED2. *Int. J. Cancer* **2010**, *126*, 876–884. [CrossRef] [PubMed]

57. Cox, R.F.; Jenkinson, A.; Pohl, K.; O'Brien, F.J.; Morgan, M.P. Osteomimicry of Mammary Adenocarcinoma Cells In Vitro; Increased Expression of Bone Matrix Proteins and Proliferation within a 3D Collagen Environment. *PLoS ONE* **2012**, *7*, e41679. [CrossRef]
58. Jin, J.-K.; Dayyani, F.; Gallick, G.E. Steps in prostate cancer progression that lead to bone metastasis. *Int. J. Cancer* **2011**, *128*, 2545–2561. [CrossRef]
59. Rosset, E.M.; Bradshaw, A.D. SPARC/osteonectin in mineralized tissue. *Matrix Biol.* **2016**, *52–54*, 78–87. [CrossRef]
60. Sharma, S.; Xing, F.; Liu, Y.; Wu, K.; Said, N.; Pochampally, R.; Shiozawa, Y.; Lin, H.-K.; Balaji, K.; Watabe, K. Secreted Protein Acidic and Rich in Cysteine (SPARC) Mediates Metastatic Dormancy of Prostate Cancer in Bone. *J. Biol. Chem.* **2016**, *291*, 19351–19363. [CrossRef]
61. Liu, S.; Shen, M.; Hsu, E.-C.; Zhang, C.A.; Garcia-Marques, F.; Nolley, R.; Koul, K.; Rice, M.A.; Aslan, M.; Pitteri, S.J.; et al. Discovery of PTN as a serum-based biomarker of pro-metastatic prostate cancer. *Br. J. Cancer* **2021**, *124*, 896–900. [CrossRef]
62. Tare, R.S.; Oreffo, R.O.C.; Clarke, N.M.P.; Roach, H.I. Pleiotrophin/Osteoblast-Stimulating Factor 1: Dissecting Its Diverse Functions in Bone Formation. *J. Bone Miner. Res.* **2002**, *17*, 2009–2020. [CrossRef] [PubMed]
63. Vashisht, S.; Bagler, G. An Approach for the Identification of Targets Specific to Bone Metastasis Using Cancer Genes Interactome and Gene Ontology Analysis. *PLoS ONE* **2012**, *7*, e49401. [CrossRef] [PubMed]
64. Zhang, X.; Huang, S.; Guo, J.; Zhou, L.; You, L.; Zhang, T.; Zhao, Y. Insights into the distinct roles of MMP-11 in tumor biology and future therapeutics (Review). *Int. J. Oncol.* **2016**, *48*, 1783–1793. [CrossRef] [PubMed]
65. Pang, X.; Gong, K.; Zhang, X.; Wu, S.; Cui, Y.; Qian, B.-Z. Osteopontin as a multifaceted driver of bone metastasis and drug resistance. *Pharmacol. Res.* **2019**, *144*, 235–244. [CrossRef] [PubMed]
66. Papke, C.L.; Yamashiro, Y.; Yanagisawa, H. MMP17/MT4-MMP and Thoracic Aortic Aneurysms. *Circ. Res.* **2015**, *117*, 109–112. [CrossRef]

6. Paper II

International Journal of *Molecular Sciences*

IMPACT FACTOR 6.208

Indexed in: PubMed

Article

Hyaluronan Synthases' Expression and Activity Are Induced by Fluid Shear Stress in Bone Marrow-Derived Mesenchymal Stem Cells

Sebastian Reiprich, Elif Akova, Attila Aszódi and Veronika Schönitzer

Special Issue
Mechanobiology in Cells and Tissues
Edited by
Prof. Dr. Sabata Martino

MDPI

https://doi.org/10.3390/ijms22063123

International Journal of
Molecular Sciences

MDPI

Article

Hyaluronan Synthases' Expression and Activity Are Induced by Fluid Shear Stress in Bone Marrow-Derived Mesenchymal Stem Cells

Sebastian Reiprich, Elif Akova, Attila Aszódi and Veronika Schönitzer *

Experimental Surgery and Regenerative Medicine (ExperiMed), Department of General, Trauma and Reconstructive Surgery, Munich University Hospital, Ludwig-Maximilians-University, 80336 Munich, Germany; Sebastian.Reiprich@med.uni-muenchen.de (S.R.); Elif.Akova@med.uni-muenchen.de (E.A.); Attila.Aszodi@med.uni-muenchen.de (A.A.)
* Correspondence: Veronika.Schoenitzer@med.uni-muenchen.de; Tel.: +49-89-4400-53147

Abstract: During biomineralization, the cells generating the biominerals must be able to sense the external physical stimuli exerted by the growing mineralized tissue and change their intracellular protein composition according to these stimuli. In molluscan shell, the myosin-chitin synthases have been suggested to be the link for this communication between cells and the biomaterial. Hyaluronan synthases (HAS) belong to the same enzyme family as chitin synthases. Their product hyaluronan (HA) occurs in the bone and is supposed to have a regulatory function during bone regeneration. We hypothesize that HASes' expression and activity are controlled by fluid-induced mechanotransduction as it is known for molluscan chitin synthases. In this study, bone marrow-derived human mesenchymal stem cells (hMSCs) were exposed to fluid shear stress of 10 Pa. The RNA transcriptome was analyzed by RNA sequencing (RNAseq). HA concentrations in the supernatants were measured by ELISA. The cellular structure of hMSCs and HAS2-overexpressing hMSCs was investigated after treatment with shear stress using confocal microscopy. Fluid shear stress upregulated the expression of genes that encode proteins belonging to the HA biosynthesis and bone mineralization pathways. The HAS activity appeared to be induced. Knowledge about the regulation mechanism governing HAS expression, trafficking, enzymatic activation and quality of the HA product in hMSCs is essential to understand the biological role of HA in the bone microenvironment.

Keywords: mesenchymal stem cells; mechanotransduction; osteogenic differentiation; biomineralization; hyaluronan synthases

Citation: Reiprich, S.; Akova, E.; Aszódi, A.; Schönitzer, V. Hyaluronan Synthases' Expression and Activity Are Induced by Fluid Shear Stress in Bone Marrow-Derived Mesenchymal Stem Cells. *Int. J. Mol. Sci.* **2021**, *22*, 3123. https://doi.org/10.3390/ijms22063123

Academic Editor: Sabata Martino

Received: 4 March 2021
Accepted: 16 March 2021
Published: 18 March 2021

1. Introduction

Biomineralization is defined as a process by which living organisms control the formation of hierarchically structured minerals. In animals, the ability to produce biominerals evolved around 550 million years ago [1]. Interestingly, biomineralization arose independently multiple times in various phyla through the attachment of amorphous precursor nanoparticles [2,3], implicating that the chemical, physical and molecular mechanisms responsible for mineralization are developed by convergent evolution. The extra- and intracellular processes must be fine-tuned inside specialized cells generating mineral deposits such as epithelial mantle cells in molluscs or osteoblasts in the bone.

During the evolution of biomineralization, an intricate set of mechanisms which convert mechanical stimuli into biochemical cascades, termed mechanotransduction, has been developed as a general machinery for the regulation of biomaterial designs [4]. The phenomenon of mechanotransduction is an integral part of the general process of skeletal adaptation to mechanical loads as described by Wolff's law [5]. Bone is a dynamic tissue and its mineral density, along with chemical signals, changes in response to the applied forces on the bone. Mechanically induced bone remodeling, the physiological balance

between bone formation and bone resorption, is primarily attributed to osteocytes and osteoblasts; however, other cells in the bone marrow such as multipotent mesenchymal stem cells (MSCs) are also mechanically sensitive [6]. It has been shown that various types of fluid shear stress (steady, pulsatile, oscillatory) facilitate MSC osteogenic differentiation in two-dimensional (2D) in vitro culture systems in a range of 0.1–2 Pa [7]. In vivo, numerical poroelastic modeling predicted that mechanical loading-induced interstitial fluid movement through the lacunar-canalicular network of the bone osteoid generates a fluid shear stress between 0.8 and 3 Pa [8,9]. However, volumetric- and time-averaged shear stress calculations upon cyclic loading in porcine trabecular bone marrow, where MSCs reside, ranged from 2.14 to 15.57 Pa [10].

Mechanotransduction also plays a regulatory role in the formation of molluscan shell. In general, an organic matrix is necessary for the nucleating minerals and crystals. Chitin, a homo-polymer of β- (1-4) linked N-acetylglucosamine molecules, is the main part of this matrix and fulfills an important function in the formation and functionality of mollusc larval shells [11,12]. The molluscan myosin-chitin synthases, which are responsible for the production of chitin, are unique transmembrane enzymes with an N-terminal myosin motor domain and highly conserved regions of charged amino acids. The complexity of the enzymatic structure indicates that the myosin-chitin synthases coordinate the intracellular processes of the shell-forming epithelial cells and the extracellular mineralization events via mechanical signal transduction [4,13,14].

Hyaluronan (HA), just like chitin, is a linear polysaccharide, which consists of alternating residues of β-D-(1-4)-N-acetylglucosamine and β-D-(1-3)-glucuronic acid. HA plays important roles in skeletal biology, influencing processes such as migration and condensation of skeletogenic progenitor cells, limb development, joint cavity formation and longitudinal bone growth [15,16]. HA is synthesized by adult human MSCs (hMSCs) [17,18], osteoclast-like cells [19,20], osteoblasts [21] and osteocyte-like cells [22,23] and is a main component of the bone marrow. However, its precise function in the bone remodeling process is not yet known [24]. Furthermore, HA may act as a regulator of mineralization, although it does not change the rate of crystal growth [25]. HA binds hydroxyapatite in calcified cartilage and bone. HA of high molecular weight (>500—~2000 kDa) stimulates proliferation and mineralization in rat osteoblasts, while HA of low molecular weight (<8 kDa) increases only proliferation [26]. Due to its abundant negative charges, HA might be able to bind calcium in high concentration to induce crystallization. HA could also have a function in mineralization initiation by space capture and/or matrix organization [27,28]. HA is produced by hyaluronan synthases (HAS) which belong to the glycosyltransferases 2-family together with chitin synthases and cellulose synthases. The three known mammalian HAS isoforms (HAS1, HAS2 and HAS3) are plasma membrane glycosyltransferases sharing 55–70% structural identity. The isoenzymes have seven membrane-spanning domains and a large cytoplasmic region with the active enzyme and substrate binding sites. HAS isoforms differ in the molecular size of their product: HAS1 and HAS2 polymerize HA chains of around 2×10^6 Da, whereas HAS3 produces shorter chains of 1×10^5 Da to 1×10^6 Da. Human bone marrow-derived MSCs express all three HAS isoforms and the HA receptor CD44.

The question arises as to whether HA plays a similar regulatory role in bone formation to chitin in molluscan shell formation. However, the processes in the bone might be more complicated, since bone remodels in a way unlike molluscan shell. In this study, we applied fluid shear stress to bone marrow-derived hMSCs as mechanical stimuli and analyzed the complete set of RNA transcripts and the activity of HASes in hMSCs. In some bone diseases, the HA content in the bone or HAS expression in hMSCs is changed [18,29,30]. Understanding the regulatory mechanisms of HAS in hMSCs will provide therapeutic starting points for an improved fracture healing in patients suffering from one of these bone diseases.

2. Results

2.1. Cell Morphology of hMSCs after Exposure to Fluid Shear Stress

To induce mechanotransduction via fluid shear stress in hMSCs obtained from the bone marrow of four healthy donors (hMSC-2, hMSC-15, hMSC-19 and hMSC-20), cells were cultured on fibronectin-coated channel slides which were connected to a medium-containing tubing system driven by a peristaltic pump. As a control, hMSCs were cultured on fibronectin-coated 24-well plates under static conditions. The whole system, except the pump itself, as well as the control cells were kept in a humidified incubator at 37 °C and 5% CO_2 (Figure 1A). Cells after seeding were allowed to adhere for 6.5 h before shear stress of 10 Pa (100 dyn/cm^2) was applied for a duration of 20 h. This pressure level matches the range of volumetric mean marrow shear stress in porcine femurs of 7.1 ± 6.2 Pa during stress relaxation and 9.6 ± 6.9 Pa during cyclic loading as demonstrated by Metzger et al. [10]. Differences in shape and alignment between control and shear stress-exposed hMSCs were clearly visible under phase-contrast microscopy. In comparison to the cuboidal shape of the static cells, the hMSCs upon shear stress had a longer, more spindle-like morphology and aligned along the flow direction (Figure 1B). There was no difference between hMSCs obtained from different donors.

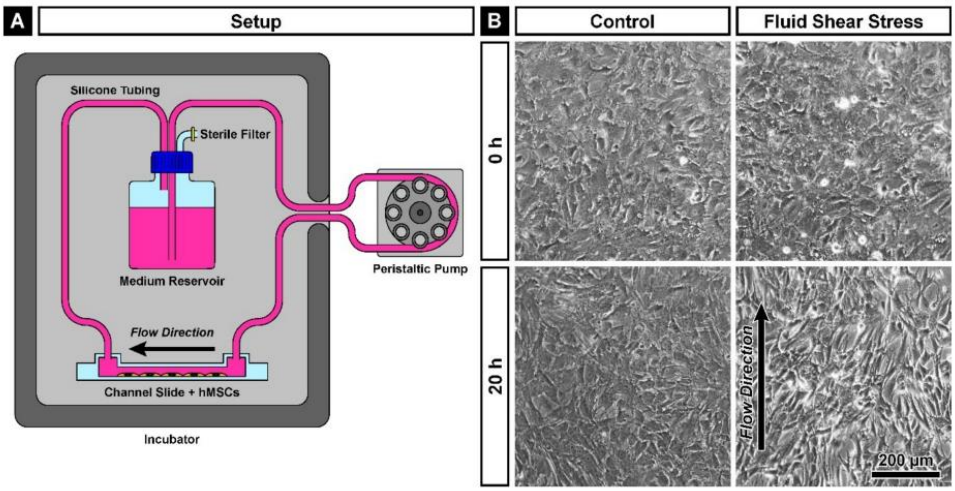

Figure 1. Exposure of human mesenchymal stem cells (hMSCs) to fluid shear stress. (**A**) Schematic drawing of the experimental setup. All components besides the peristaltic pump were kept in a humidified incubator at 37 °C and 5% CO_2. (**B**) Phase-contrast microscopy of hMSC-2. After 20 h of shear stress, an arrangement of the cells along the flow direction (arrow) is visible. Note the spindle-like shape of the cells after the shear stress.

2.2. Transcriptional Changes in hMSCs Exposed to Shear Stress

To assess the impact of shear stress on gene expression, we performed next-generation RNA sequencing of the hMSC transcriptome obtained from four different donors. Principal component analysis (PCA) showed a clear segmentation according to the applied fluid flow along PC1 (Figure 2A). Although the expression profiles of the donors along PC2 were different, these discrepancies remained comparable despite the application of fluid shear stress. For further analysis of the gene expression response to fluid flow, we investigated the significantly up- and downregulated genes in shear stress-exposed versus control hMSCs. The genes were filtered by a minimum of ten reads to exclude lower expression and the remaining mapped genes were considered as significantly changed with an adjusted *p*-value smaller than 0.05. As biological relevant changes in gene expression, we defined a $\log_2$-fold change smaller than -2 or higher than 2. This resulted in 683 significantly downregulated and 624 significantly upregulated genes (Figure 2B).

A graphical presentation of the 25 most upregulated and the 25 most downregulated genes is depicted in the heat map (Figure 2C), while the volcano plot (Figure D) shows all genes with more than ten reads with cut-off lines for significance and biological relevance. In the volcano plot, the top 25 upregulated and top 25 downregulated genes are indicated in blue color. Among the prominent upregulated genes, we found *Wnt1*, *Wnt16* and *BMP2*, which are known to be involved in bone remodeling and to induce bone formation [31–33]; *TNFSF14*, which participates in the cellular response to a mechanical stimulus [34,35]; *PTGS2*, which is a regulator of bone metabolism [36] and upregulated upon shear stress in MSCs [37]; *CLDN4*, which is important for calcium-independent cell adhesion activity at tight junctions [38]; and *XIRP1*, which prevents actin depolymerization [39]. Distinguished downregulated genes were *LDB2*, which regulates cell migration [40]; *C3AR1*, which is involved in chemotaxis of mesenchymal stem cells [41]; *CDH10*, which encodes for a calcium-dependent cell adhesion protein [42]; and *MKI67*, *DLGAP5* and *NUF2*, which play roles in the cell cycle and cell proliferation [43–45].

In order to elucidate the function of HA in hMSCs treated with shear stress, we highlighted significantly changed genes of the hyaluronan biosynthetic pathway (GO:0030213) and the significantly changed HA receptors *CD44*, *HMMR*, *ICAM1* and *LAYN* with red color in the volcano plot (Figure 2D). The expression levels of *LAYN* and *HMMR* are decreased, indicating a potential inhibition of cell migration. The HA receptor layilin interacts with actin filaments and might promote cell migration; however, its exact biological function is not known yet [46]. The hyaluronan-mediated motility receptor, HMMR, is responsible for cell motility [47]. Interestingly, there is a clear tendency for upregulation of the hyaluronan synthase genes *HAS1* and *HAS2* and the hyaluronan receptors *ICAM1*, *IL1B* and *PDGFB* with a $\log_2$-fold change higher than 2. *ICAM-1* encodes for an Ig-like cell adhesion molecule, which mediates cell–cell adhesion or serves as a receptor for extracellular HA [48]. At the transcriptional level, the expression of hyaluronan synthases is regulated by numerous growth factors and cytokines, e.g., PDGF-BB [49] and IL1-β [50].

Altogether, in our experimental setup, hMSCs responded to fluid shear stress by increasing the expression of genes involved in bone formation, cell adhesion to the surface, cell–cell adhesion and hyaluronan biosynthesis. On the contrary, expression of genes associated with proliferation, the cell cycle and migration was diminished upon exposure to fluid flow.

2.3. Fluid Shear Stress Regulated Biological Pathways in hMSCs

To further investigate the response of hMSCs upon mechanical stimulation with fluid shear stress, we performed Gene Ontology (GO) enrichment analysis of the 624 upregulated genes. Figure 3 shows a selection of differentially regulated biological processes involved in the positive regulation of the skeletal system development, biomineralization and HA biosynthesis. The enrichment score was calculated by dividing the sample frequency by the background frequency of genes annotated to a certain GO term. As a kind of control for a reaction to the mechanical stimulus, the GO term of "cellular response to fluid shear stress" was also significantly overrepresented.

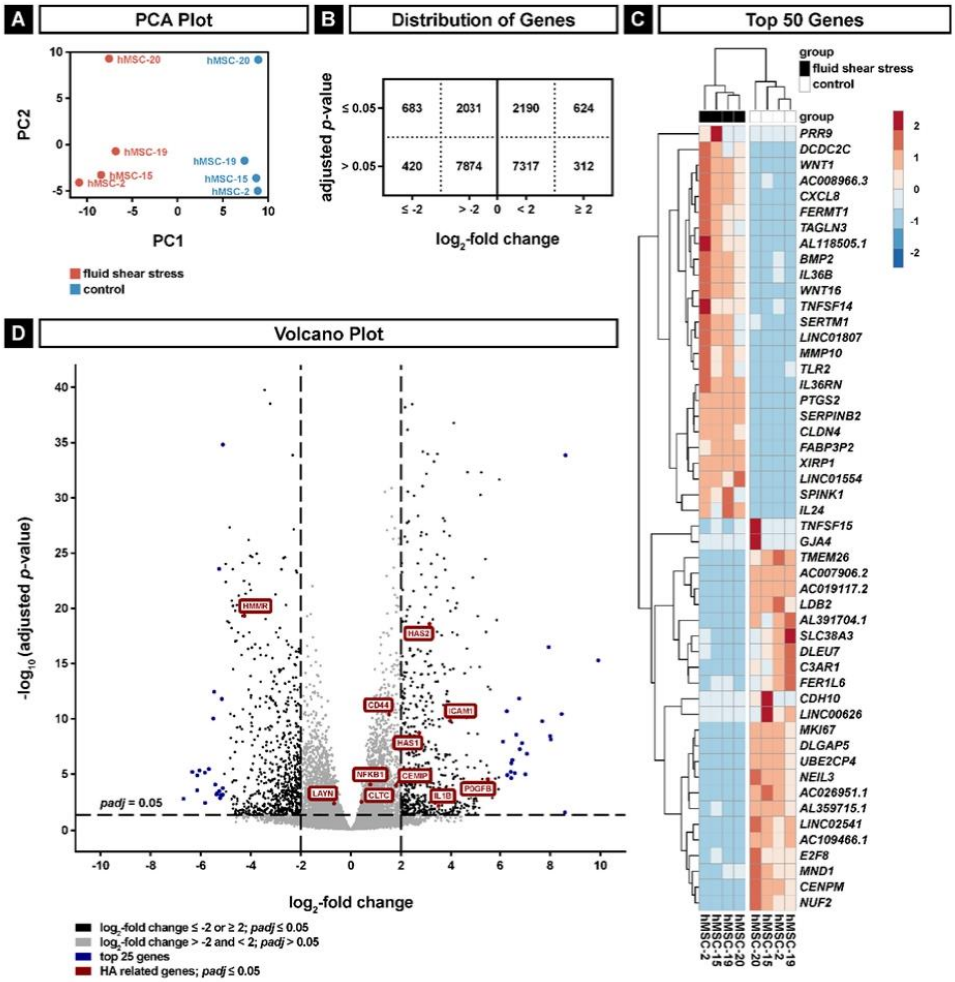

Figure 2. Next-generation RNA sequencing analyses of hMSCs exposed to fluid shear stress. (**A**) Principal component analysis (PCA) for fluid shear stress (PC1) and donors (PC2). (**B**) Distribution of genes with more than ten reads; genes are grouped according to significance (adjusted $p \leq 0.05$) and $\log_2$-fold change (≤ -2 or ≥ 2). (**C**) Heatmap of the 50 most significantly regulated genes with the highest and lowest $\log_2$-fold changes. (**D**) Volcano plot of genes with more than ten reads. Dashed lines show thresholds for significance ($p \leq 0.05$) and $\log_2$-fold change (≤ -2 or ≥ 2). The top significantly regulated genes with the highest and lowest $\log_2$-fold change are shown in blue; the significantly changed genes of the hyaluronan biosynthetic pathway (GO:0030213) and the significantly changed hyaluronan (HA) receptors *CD44*, *HMMR*, *ICAM1* and *LAYN* are shown in red.

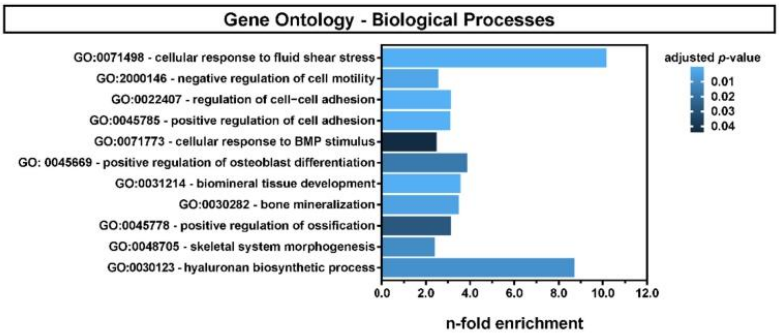

Figure 3. Gene set enrichment analysis of the 624 upregulated genes (adjusted $p \leq 0.05$; $\log_2$-fold change ≥ 2). Overrepresented biological processes are involved in the morphogenesis of the skeletal system, biomineralization, HA biosynthesis and the response to fluid shear stress.

In detail, the genes which contribute to the "cellular response to fluid shear stress" (GO:0071498) showed a clear cluster of nine significantly upregulated genes (*HAS2*, *KLF2*, *KLF4*, *MEF2C*, *MTSS1*, *PTGS2*, *SRC*, *SREBF2*, *TFPI2*), six genes without changes (*ASS1*, *CA2*, *HDAC3*, *MAPK7*, *PKD2*, *PTK2B*) and three significantly downregulated genes (*MAP2K5*, *NFE2L2*, *SOCS5*) in hMSCs. Thus, we observed a clear tendency for a positive response to fluid shear stress. Although we found donor-dependent differences in the expression levels of the individual genes, all donors showed a reaction to the mechanical stimulus in the expression of the majority of genes with minor individual differences (Figure 4A). None of the downregulated genes had a $\log_2$-fold change (LFC) value smaller than -2, but *HAS2*, *KLF2*, *KLF4*, *MTSS1*, *PTGS2* and *TFPI2* exhibited a significant LFC value higher than 2 (Figure 4B).

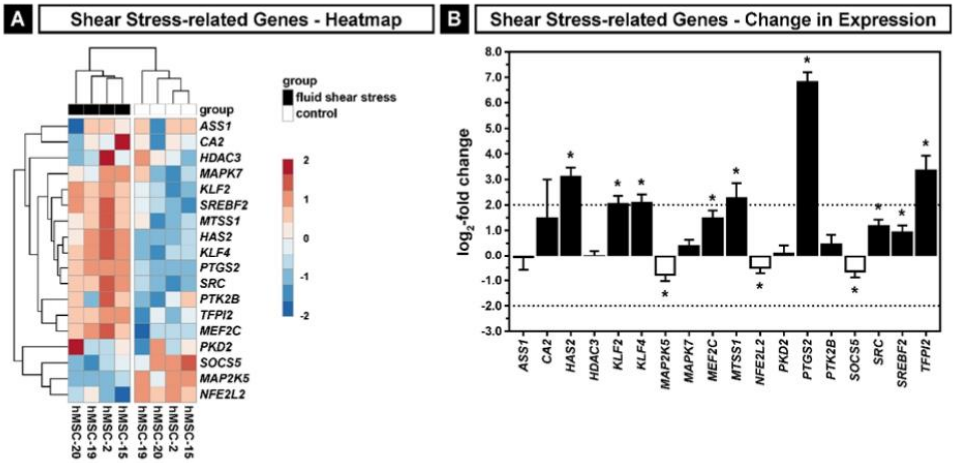

Figure 4. Cellular response to fluid shear stress (GO:0071498) in hMSCs. (**A**) Heatmap of the gene set. (**B**) Change in expression of the gene set. Black bars show upregulation of expression induced by fluid shear stress; white bars show downregulation; dashed lines indicate the thresholds for the $\log_2$-fold change of ≤ -2 and ≥ 2; asterisks indicate an adjusted $p \leq 0.05$. Error bars represent SE.

In particular, the upregulation of *PTGS2* is a well-known marker for shear stress in hMSCs [37]. The transcription factor KLF4 regulates membranous and endochondral ossification during skeletal development [51]. *HAS2* belongs to the known genes which are induced by high shear stress, as it was demonstrated that the expression of HAS2 is

increased by pulsatile, arterial-like shear stress, but not by lower shear stress in human umbilical vein endothelial cells [52].

Mechanotransduction is known to be important for the regulation of osteogenic differentiation of MSCs [53]; therefore, we took a closer look at the bone-related genes contributing to the overrepresented pathways shown in Figure 3 (GO:0071773, GO:0045669, GO:0031214, GO:0030282 and GO:0045778). Our analysis revealed 24 significantly upregulated genes (Figure 5A,B) with a $\log_2$-fold change higher than 2. Bone morphogenetic protein (BMP) signaling is essential in bone formation and represented here by *BMP2*, *BMP6* and the receptor *BMPR1B*, which are involved in bone remodeling and osteoblast differentiation [33]. BMP2-induced osteogenesis is enhanced by the presence of IL6 in vitro and in vivo [54]. We also observed an upregulation of three genes (*DMP1*, *IBSP* and *SPP1*) coding for non-collagenous bone matrix proteins of the small integrin-binding ligand, the N-linked glycoprotein family [55], which are important for bone mineralization [56]. *WNT1* and *WNT10B* are also part of the significantly upregulated genes in these bone-related pathways, both involved in the generation and function of osteoblasts [31,57]. The gene set also contains the aforementioned *PTGS2* and *SOX11*, which are involved in early osteoblast differentiation [58]. We also detected an upregulation of *ODAPH*, which participates in the enamel mineralization of teeth [59], and *PTHLH*, a gene important for bone integrity [60]. The upregulation of these bone-related genes showed only a slight donor-to-donor variability (Figure 5A).

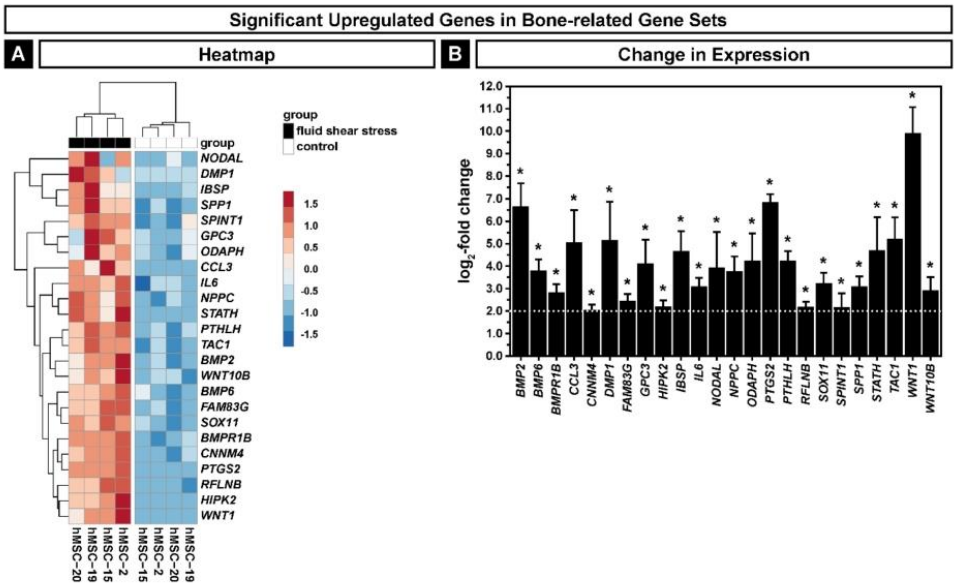

Figure 5. Significantly upregulated bone-related genes in hMSCs exposed to fluid shear stress. (**A**) Heatmap of the genes. (**B**) Change in expression of the genes. The dashed line indicates the threshold for the $\log_2$-fold change of ≥ 2; asterisks indicate an adjusted $p \leq 0.05$. Error bars represent SE.

To obtain a better understanding about the expression changes of the HA-related genes induced by the exposure to fluid shear stress, we selected the gene set of the hyaluronan biosynthetic process (GO:0030213) and the genes encoding for five HA receptors (*CD44*, *HMMR*, *ICAM1*, *LAYN* and *LYVE1*). Plotted as a heatmap, we found a group of nine significantly upregulated genes (*CD44*, *CEMIP*, *CLTC*, *HAS1*, *HAS2*, *ICAM1*, *IL1B*, *NFKB1*, *PDGFB*), seven genes with insignificant changes in expression (*ABCC5*, *AP2A1*, *EGF*, *HAS3*, *HYAL1*, *LYVE1*, *SMPD3*, *TGFB1*) and two genes showing a significant downregulation with an overall tendency to a positive LFC (Figure 6A). Whilst *HAS1*, *HAS2*, *ICAM1*, *IL1B* and

PDGFB showed a significant LFC higher than 2, the expression of *HAS3* was not changed significantly. Only *HMMR* was significantly downregulated with an LFC smaller than −2 (Figure 6B). CD44, the best known HA receptor, is involved in several intracellular signaling pathways regulating cell–cell and cell–substrate adhesion, proliferation, motility, migration, nuclear signaling and HA endocytosis and degradation [61].

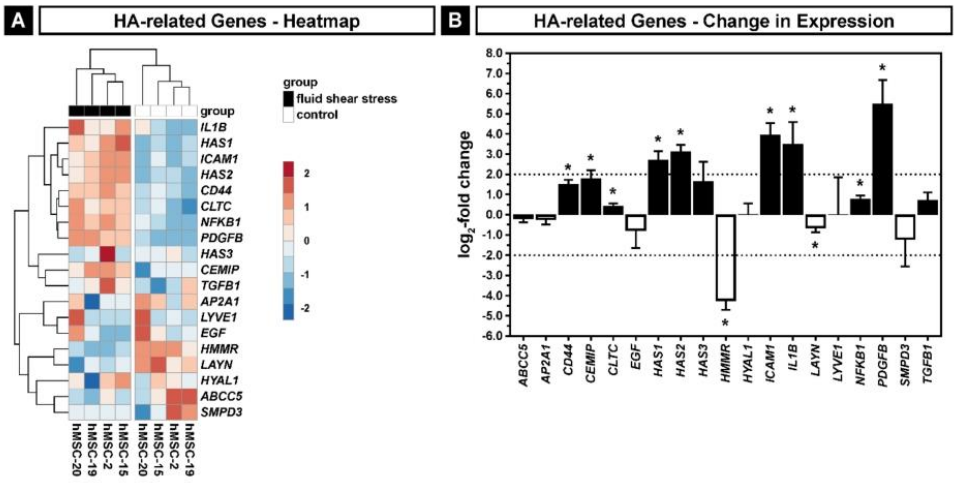

Figure 6. Hyaluronan biosynthetic process (GO:0030213) and five HA receptors (*CD44*, *HMMR*, *ICAM1*, *LAYN* and *LYVE1*) in hMSCs exposed to fluid shear stress. (**A**) Heatmap of the gene set. (**B**) Change in expression of the gene set. Black bars show an upregulation of expression by fluid shear stress; white bars show downregulation; dashed lines indicate the thresholds for the $\log_2$-fold change of ≤ -2 and ≥ 2; asterisks indicate an adjusted $p \leq 0.05$. Error bars represent SE.

In summary, the bioinformatics analysis of the gene expression profiles of hMSCs upon shear stress demonstrates not only changes in the expression levels of the known gene set regulating the cellular response to fluid flow but also changes in the genes participating in bone development and HA synthesis. This might be an indication that the expression of HASes in MSCs is regulated by mechanical stimuli induced by fluid shear stress in the bone marrow microenvironment.

2.4. Impact of Fluid Shear Stress on the Activity of HAS

In order to investigate whether the applied shear stress regulates the transport and the localization of the hyaluronan synthases in the plasma membrane, we performed immunofluorescence staining with antibodies against HAS2 and the HA receptor CD44 to delineate the cell membrane. In addition, actin cytoskeletal structures were visualized by phalloidin staining. As control, we used the previously described HAS2-overexpressing immortalized hMSC cell line, SCP1-HAS2-eGFP, in which the HAS2 gene is under the control of the constitutive cytomegalovirus promoter [62]. We observed that the application of fluid shear stress induced morphological changes in both primary hMSCs and SCP1-HAS2-eGFP cells. In general, top-view confocal microscopy images indicated a reduced cell area (Figure 7A), whilst side-view images revealed an increased height of the cells exposed to shear stress compared with static controls (Figure 7B). Due to these morphological changes upon the treatment with shear stress, we were not able to investigate the localization of HAS2 in detail. Indicating the overexpression of HAS2, the SCP1-HAS2-eGFP cells exhibited a stronger fluorescence signal for HAS2 compared to the primary cells, which exhibited a clearer pattern of distribution around the nucleus (blue-colored signal). The red CD44 staining showed bright spots corresponding to microvillus-like protrusions, visible as F-actin (white)-containing spikes on the cell surface in the side view of the cells (Figure 7B).

The mean length of the protrusions in hMSCs (0.497 ± 0.098 µm) was significantly increased by the application of fluid shear stress (0.593 ± 0.079 µm), the overexpression of HAS2-eGFP (0.570 ± 0.084 µm) or a combination of both conditions (0.604 ± 0.086 µm) (Figure 7C). Under static conditions (control), the HAS2-eGFP-overexpressing cells displayed a significantly higher density of protrusions (0.392 ± 0.174 U/µm) compared to the primary hMSCs (0.182 ± 0.129 U/µm). Interestingly, fluid shear stress significantly increased the density of protrusions in hMSCs (0.545 ± 0.290 U/µm), but not in SCP1-HAS2-eGFP cells (0.510 ± 0.221 U/µm). A recent study by Koistinen et al. demonstrated that the formation of such protrusions in HAS3-overexpressing human breast adenocarcinoma cell line MCF-7 was triggered by active hyaluronan synthesis [63]. Since only HASes localized in the plasma membrane are active, our results also indicate that more HASes are transported to the plasma membrane because of the mechanical stimulation.

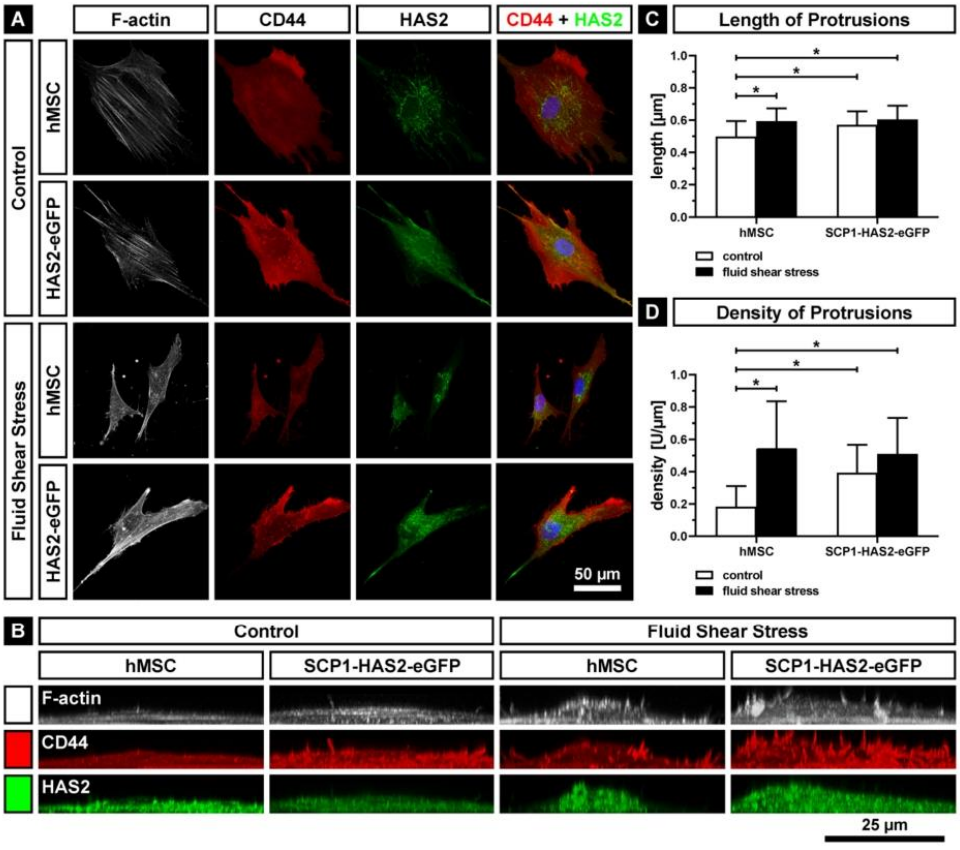

Figure 7. Formation of cell protrusions after the application of 20 h of fluid shear stress on primary hMSCs and HAS2-overexpressing immortalized hMSCs (SCP1-HAS2-eGFP). Cells were stained for confocal microscopy with phalloidin for F-actin (white); immunostained for CD44 (red) and HAS2 (green); and counterstained with DAPI for the nuclei (blue). (**A**) Z-stack maximum projection of fluid shear stress-stimulated and static (control) cells. (**B**) Y-stack maximum projection of shear stressed and control cells. Note the increased number of actin-containing membrane protrusions upon shear stress. (**C**) Length of protrusions. (**D**) Density of protrusions. Asterisks indicate a p-value < 0.05. Error bars represent SD.

Furthermore, we determined the amount of secreted HA in the supernatants of fluid shear stress-treated hMSCs compared to the static cultured hMSCs using a commercial HA-ELISA kit. In the static cultures, the basic activity levels ranged between 101.6 ± 38.0

and 322.3 ± 48.8 ng HA/1×10^4 cells among the donors. Consistent with this result, a donor-dependent variation of HAS activity has been previously reported [17]. Similarly, the HA levels in fluid flow-exposed hMSCs displayed a broad variance (130.5 ± 1.1 to 427.5 ± 89.4 ng HA/1×10^4 cells) (Figure 8A). Nevertheless, focusing on the single donors, three out of the four donors (hMSC-2, hMSC-15 and hMSC-20) showed an upregulation of their HA secretion (1.32 ± 0.28- to 2.07 ± 0.43-fold), whilst one (hMSC-19) exhibited a modest downregulation (0.84 ± 0.32-fold change) (Figure 8B) after exposure to fluid shear stress. The upregulation of HA secretion was significant in hMSC-2 and hMSC-15 ($p < 0.05$).

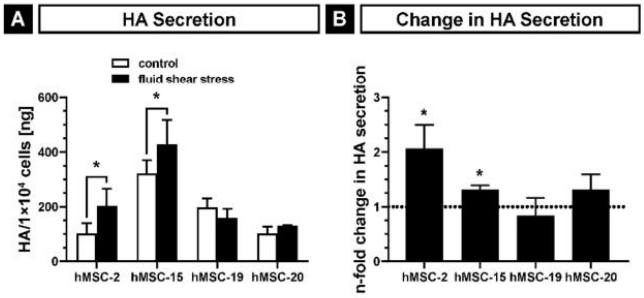

Figure 8. Hyaluronan synthase (HAS) activity in hMSCs cultured under fluid shear stress as determined by a hyaluronan ELISA assay-based quantification of secreted HA. (**A**) The graph shows the mean HA content per 1 × 10^4 cells in the supernatant after 20 h of incubation in culture medium with or without the application of fluid shear stress; (**B**) n-fold change in the HA secretion of each donor due to shear stress. Asterisks indicate a *p*-value < 0.05. Error bars represent SD.

Altogether, the increased number of microvillus-like protrusions and the slightly higher amount of secreted HA upon fluid shear stress indicate the mechanosensitivity of the HASes in hMSCs.

3. Discussion

Bone marrow-resident MSCs play an important role in bone formation and homeostasis. This function in vivo is mainly fulfilled by their osteogenic differentiation capacity through osteoprogenitor cells, pre-osteoblasts and mature osteoblasts. It has been previously reported that MSC differentiation into the osteogenic lineage in vitro can be induced by the application of different types of mechanical stimulations such as matrix strains and shear stress [64]. In vivo, bone cells and hMSCs are exposed to fluid shear stress due to the lacunae and canaliculi that serve as a channel system for fluids in the bone [65]. Fluid flow is generated by changes in blood pressure due to muscle contractions and due to mechanical loading and can reach pressure levels over 10 Pa in the bone marrow of mammals [10,66]. In hMSCs, the primary cilium is suspected to be the main sensor for the mechanoperception of fluid shear stress [37]. In the present study, we demonstrated that our experimental system drives a cellular and molecular response of hMSCs upon mechanical stimulation induced by steady fluid flow. We observed a clear morphological change from a cuboidal geometry to a more hydrodynamic, spindle-like shape. The changes in the gene expression level were proven by the enrichment of different gene sets linked to mechanoperception, such as the cellular response to fluid shear stress (GO:0071498), or by the upregulation of the expression of *PTGS2*, which is a well-known marker for the application of this stimulus in hMSCs [37]. Beside the direct response to the fluid flow-induced mechanical signals, gene sets that are linked indirectly to fluid shear stress also show an enrichment, particularly reactions to changed physical conditions via cell cycle arrest (GO:0007050), downregulation of motility (GO:2000146), upregulation of adhesion (GO:0045785) and changes in intercellular adhesions (GO:0022407).

Commitment towards the osteogenic lineage in hMSCs can be achieved via mechanotransduction [53], applying various types of physical stimuli such as tension [67], compression [68,69] and fluid shear stress [70]. Although a variety of mechanosensors have been described for different bone cells, e.g., integrins and cadherins/β-catenin in osteoblasts [71–74], the aforementioned mechanoperception by the primary cilium is the key player in hMSCs [37,75], resulting in an extensive upregulation of the expression levels of *PTGS2* and *BMP2*. Signal transduction of mechanically stimulated osteogenesis in hMSCs is mediated by MAP kinase pathways [76] and Wnt signaling [31,32]. *PTGS2*, *BMP2*, *WNT1* and *WNT16* are part of the 25 most upregulated genes in our dataset, whilst *BMP6*, *WNT10B* and *BMPR1B* were at least part of the 624 significantly upregulated genes as well as part of gene sets linked to osteogenesis. According to the literature, we observed enrichments in the cellular response to a BMP stimulus (GO:0071773) without the addition of these proteins, the upregulations of osteoblast differentiation (GO:0045669), biomineral tissue development (GO:0070169), bone mineralization (GO:0030501) and ossification (GO:0045778) and skeletal system morphogenesis (GO:0048705).

In bone marrow-derived hMSCs, all three HAS isoenzymes (HAS1, HAS2 and HAS3) are expressed, while HAS2 is the most abundant isoform and HAS3 has the lowest expression level [17,62]. The present study confirms these results by determination of the transcript expression levels of *HASes* in hMSCs obtained from different donors (see Supplementary Materials). We have also found that the differential expression levels of *HAS1* and *HAS2* were significantly upregulated in hMSCs upon shear stress. The lowest expressed isoform *HAS3* showed a positive tendency in only one donor. Previously, it was demonstrated that the expression of HAS2 is induced by pulsatile, arterial-like shear stress, but not by lower shear stress in human umbilical vein endothelial cells (hUVECs) [52]. To our knowledge, we confirmed, for the first time, that the expression of HAS1 and HAS2 is influenced by shear stress in hMSCs. In endothelial cells, HAS expression and HA production are regulated by KLF2-mediated glycolysis [77]. In our study, *KLF2* is significantly upregulated (Figure 4B), but we also observed an upregulation of cytokine mRNAs regulating HAS expression such as *PDGF-BB* and *IL1-β* (Figure 2D).

Our data strongly suggest that fluid shear stress not only upregulates the mRNA expression of HASes but it also increases their activities. On the one hand, the HA content in the supernatants of hMSCs cultured in the presence of shear stress was higher than in the supernatants of hMSCs cultured under static conditions (Figure 8). On the other hand, we observed the formation of microvillus-like spikes on the surface of the cells treated with shear stress (Figure 7). At first glance, these structures do not have any physical meaning since they are formed against the shear stress flow without adherence to the substratum. However, such structures are known to be induced by increased activity of HASes [63]. HAS2-overexpressing hMSCs, which have an increased HAS activity in comparison to non-transduced hMSCs [62], display a higher number of protrusions with and without shear stress. This indicates that the formation of the protrusions depends on the activity of HASes in our study. Since we were not able to build up the flow system under the confocal microscope, we could not monitor the microvilli-like structures in alive hMSCs. Although the fixation procedure disturbs the length and the density of the plasma membrane protrusions, they can be used for a comparative analysis as they still show the relative differences between the analyzed groups [63,78,79]. The length and density of the protrusions might also depend on the cell type. Our data suggest a reduced actin depolymerization due to the upregulation of *XIRP1*, an inhibitor of actin depolymerization. The consequence might be the increased attachment of the shear stress-induced cells as indicated by the negative regulation of cell motility (GO:2000146) and the positive regulation of cell adhesion (GO:0045785). However, there could also be a correlation with the increased formation of HAS-induced protrusions which are known to contain actin filaments in themselves and in their cortical bases [63]. We also observed actin filaments mainly in the bases of the protrusions (Figure 7).

The molluscan myosin-chitin synthases are assumed to be involved in the formation of actin-rich microvilli at the shell-forming interface [80]. As the chitin synthases might be localized in the tips of these microvilli, HASes and myosin 10 are located in the protrusions of HA-producing cells [63]. These arrangements of the glycosyltransferases could have consequences for transducing shear and adhesive forces between the mineralizing composite and the material forming cells [80].

The exact function of HA in hMSCs is not fully understood yet. HA might regulate their adhesive properties in the bone microenvironment [62], but it could also play a crucial role in the mineralization process of the bone. In this work, we demonstrated that the expression and activity of HASes are regulated by fluid shear stress in bone marrow-derived hMSCs, concomitant with the upregulated expression levels of genes related to their osteogenic potential. Taking into account that genetically diverse MSC subpopulations in the bone marrow likely experience various types of fluid shear stress with different magnitudes and durations, our study has an obvious limitation when interpreting the in vitro experimental data for the in vivo situation. Therefore, further studies are needed to elucidate the relevance of HA in the bone microenvironment.

4. Materials and Methods

4.1. Cell Isolation and Culture

Human MSCs were isolated from the bone marrow of femoral heads of four healthy male donors (49 to 87 years old) recruited at the Clinic for General, Trauma and Reconstructive Surgery of the Ludwig-Maximilians-University (LMU, Munich, Germany). The study was approved by the ethics committee of Ludwig-Maximilians-University, Munich (project code 19-177, 24 July 2019) and performed according to the Declaration of Helsinki. A written informed consent declaring that the eliminated tissue can be used for medical studies at the university hospital was signed by all donors. The cell isolation was performed by washing the bone graft material with DPBS (pH 7.4, Biochrom, Berlin, Germany). Afterwards, the bone material was incubated with 250 U/mL collagenase II (Worthington Biochemical Corp., Lakewood, NJ, USA) in DMEM (Life Technologies, Carlsbad, CA, USA) three times for 10 min each at 37 °C. Both suspensions were filtered with a 100-µm cell strainer to remove bone fragments. After centrifugation at 500× *g* for 5 min, the cell pellet was resuspended in a culture medium consisting of MEM α with nucleosides and GlutaMAX supplement (Life Technologies) containing 10% (*v*/*v*) fetal bovine serum (Sigma-Aldrich, St. Louis, MO, USA), and 1000 U/mL penicillin and 1000 µg/mL streptomycin (Biochrom) at 37 °C with 5% CO_2 and ~90% humidity. Nonadherent cells were removed by washing with DPBS for three times after the first three days in culture. Cells were passaged when reaching a confluence of ~80% and frozen at passage three in culture medium containing additional 20% (*v*/*v*) FBS and 10% (*v*/*v*) dimethyl sulfoxide (Applichem, Darmstadt, Germany) in liquid nitrogen. Aliquots were thawed and cultured five days in advance to the experiments, which were always performed with cells in passage four.

The generation and culture conditions of the HAS2-overexpressing immortalized hMSCs (SCP1-HAS2-eGFP) are described elsewhere [62].

4.2. Application of Fluid Shear Stress

To apply fluid shear stress as a stimulus of mechanotransduction in hMSCs, a setup for culture under flow conditions was created (Figure 1A). Therefore, a µ-Slide I 0.2 Luer ibiTreat (Ibidi, Planegg, Germany) was connected via a silicone tubing with 1.6 mm inner diameter (Ibidi) with a medium reservoir in a Nalgene cell culture medium bottle (Thermo Fisher Scientific, Waltham, MA, USA) containing 50 mL culture medium with two connectors and a pressure equalization set (0.22 µm sterile filter) on the GL45 lid (DWK Life Sciences, Wertheim, Germany) for medium circulation. Downstream of the reservoir and upstream of the channel slide, a PharMed Ismaprene pump tubing with 2.79 mm inner diameter (Ismatec, Wertheim, Germany) was inserted, to connect an IPC-8 peristaltic pump (Ismatec) to drive the medium flow. The pump was calibrated to create

a fluid shear stress of 10 Pa (100 dyn/cm^2) inside the channel slide according to the manufacturer's instructions to reach the level of volumetric mean marrow shear stress in porcine femurs [10]. All components beside the pump were kept under the cell culture conditions in the incubator and put there, altogether with the medium, 24 h in advance to the experiment. Beside the channel slides, 24-well plates (Nunc, Darmstadt, Germany) or 8-well chamber slide ibidiTreat (Ibidi) was used for the static control cells, which were all coated with 2 µg/cm^2 human plasma fibronectin (Millipore, Billerica, MA, USA) in DPBS for 1.5 h at 37 °C and washed with DPBS. The number of seeded cells was: 2.5×10^5 cells per channel slide; 1×10^5 cells per well of the plate; 5×10^4 cells per well of the chamber. After 6.5 h of adhesion, the medium was changed in the control wells and the channel slides were connected to the flow setup to apply shear stress for 20 h. Before and after the mechanical stimulation, images were taken from both conditions using an Axiovert 40 CFL microscope (Carl Zeiss, Oberkochen, Germany).

4.3. Next-Generation RNA Sequencing and Bioinformatics

The cells from all four donors were lysed in 200 µl Trizol (Life Technologies) per well (24-well plate)/channel slide. After RNA isolation by following a standardized protocol, RNA quality and quantity were measured using a BioAnalyzer (Agilent, Santa Clara, CA, USA). The libraries for sequencing were prepared with a SENSE mRNA-Seq Library Prep Kit V2 (Lexogen, Vienna, Austria) and sequenced on a HiSeq1500 device (Illumina, San Diego, CA, USA) with a read length of 50 bp and a sequencing depth of approximately 15 million reads per sample. The raw basecall (Bcl) files were demultiplexed with Illumina_Demultiplex. Transcriptomes were aligned to the human reference genome GRCh38.99 by using STAR (version 2.7.2b) [81] to obtain the reads per gene.

DESeq2 (version 1.26.0) [82] was used to analyze the results of RNA sequencing and the comparison of differentially expressed genes in between treatment methods run on R version 3.6.1. Low gene expressions were filtered through elimination of row counts by a cutoff of a minimum 10 reads per gene, which resulted in the remaining 21,451 genes. The data were normalized through variance-stabilizing transformation (vst), and for a principal component analysis (PCA), the vst data were transformed to $\log_2$. Differentially expressed genes were obtained through DESeq2 and insignificant genes were filtered by a 0.05 adjusted *p*-value cutoff. Log_2-fold changes (LFC) smaller than -2 or higher than 2 were defined as thresholds to identify biologically relevant results. From 21,451 genes, 624 were considered to be upregulated and 683 were downregulated after application of the fluid stress (Figure 2B).

Up- and downregulated genes in the DESeq2 results were analyzed for their Biological Process Gene Ontology Results (GO) by using clusterProfiler (v3.14.3) [83] with org.Hs.eg.db_3.10. The datasets of pathways of interest are involved in the skeletal system, biomineralization, HA biosynthesis and, to indicate the reaction to the mechanical stimulus, the response to fluid shear stress. The enrichment scores were calculated by dividing the sample frequency by the background frequency of genes annotated to a certain GO term. The sample frequency is the number of genes annotated to a certain GO term in the input list divided by the number of all genes in the input list (adjusted $p \leq 0.05$; $\log_2$-fold change $\geq$2; part of the background set provided by clusterProfiler). The background frequency is the number of all genes annotated to a GO term divided by the number of genes of the entire background set provided by clusterProfiler.

The expression of HA-related genes, a subset consisting of the hyaluronan biosynthetic process (GO:0030213) and five HA receptors (*CD44*, *HMMR*, *ICAM1*, *LAYN* and *LYVE1*) obtained from the DESeq2 results was analyzed concerning the LFC and adjusted *p*-values. In a similar manner, the change in expression levels in the subset of genes corresponding to the cellular response to fluid shear stress (GO:0071498) was used to verify mechanotransduction.

4.4. Immunostaining, Confocal Microscopy and Quantification of Protrusions

Fluorescence staining of primary hMSCs and SCP1-HAS3-eGFP cells was performed to analyze the morphological changes at the molecular level after the application of fluid shear stress. Therefore, 1×10^3 cells were seeded in 300 µl culture medium per well of a fibronectin-coated 8-well chamber slide as static control, and 2.5×10^5 or 1.25×10^4 cells on two fibronectin-coated channel slides. The complete experimental procedure was performed as described above: the two µ-slides were connected in a row, with the higher cell density upstream. The staining was performed on the slide with the lower cell density. After 20 h in the experimental setup, the cells were washed with DPBS and fixed for 10 min at room temperature with 4% (*w/v*) paraformaldehyde in DPBS, followed by a permeabilization step with 0.1% (*v/v*) Triton X100 (Sigma-Aldrich) in DPBS per well/channel. After an additional washing step with DPBS, the cells were blocked with 1% (*w/v*) BSA (Sigma-Aldrich) in DPBS for 1 h at room temperature. Following this, a rabbit anti-HAS2 antibody (1:100, orb157430, Biorbyt, Cambridge, UK) and a mouse anti-CD44 antibody (1:400, #3570, Cell Signaling Technology, Cambridge, UK) were diluted in 1% BSA in DPBS. The fixed cells were incubated over night at 4 °C in primary solution. Afterwards, the wells were washed with 1% BSA in DPBS. As secondary antibodies, a goat anti-rabbit Alexa Fluor 488 conjugate (4 µg/mL, A10036, Thermo Fisher Scientific), a donkey anti-mouse Alexa Fluor 546 conjugate (4 µg/mL, A11008, Thermo Fisher Scientific) and a phalloidin Alexa Fluor 647 conjugate (1:50, A22287, Thermo Fisher Scientific) diluted in 1% BSA in DPBS were added for 1 h at room temperature. The cells were washed with DPBS before the nuclei were counterstained for 2 min with 4,6-diamidino-2-phenylindole (DAPI) and washed a final time with DPBS. Finally, the stained cells were kept in DPBS to perform confocal microscopy using a Leica SP8 AOBS WLL, a HC PL APO 63×/1.30 GLYC CORR CS2 objective and Lightning deconvolution software applying 1.28× zoom (all from Leica Microsystems, Wetzlar, Germany). Quantification of protrusions and the definition of density (ratio of detected protrusions to cell edge length) were performed as described elsewhere [78] using the FiloQuant plugin [84] for the FIJI software [85]. Therefore, the single image analysis tool was used in combination with manual outlining of the cell edges on y-stack maximum projection images based on the CD44 staining. For quantification, 30 to 48 cells per group (hMSC-2, hMSC-15 and SCP2-HAS2-eGFP) were analyzed. The statistical analysis was performed using the GraphPad Prism software (GraphPad Software, San Diego, CA, USA) to perform a Kruskall–Wallis test with Dunn's multiple comparison test. A p-value less than 0.05 was considered as statistically significant.

4.5. HA-ELISA

HAS activity was analyzed by measuring the HA content in the supernatant of the cells cultured with fluid shear stress and cells cultured in 8-well slides as static control. As substrate, 10 mM N-acetyl-D-glucosamine (Sigma-Aldrich) was added to the standard culture medium for 20 h during the experiment. Afterwards, the supernatant was collected. As described above, the cells were washed, fixed and stained with a phalloidin Alexa Fluor 488 conjugate (1:400, A12379, Thermo Fisher Scientific) diluted in DPBS for 1 h at room temperature. After washing in DPBS, the nuclei were counterstained with DAPI. Finally, mosaic pictures of the whole growth area were taken using an AxioObserver Z1 (Carl Zeiss). The cells were counted using the FIJI software [85]. The quantification of the HA content in the supernatant was performed using the commercial enzyme-linked immunosorbent assay (ELISA) TECO Human Hyaluronic Acid Test TE1017-2 Kit (TECOmedical, Bünde, Germany) according to the manufacturer's instructions. The absorbance was determined with a photometric plate reader MultiscanFC (Thermo Fisher Scientific). Two wells per experiment were measured, and the whole experiment was performed three times per donor. The statistical analysis was performed using the GraphPad Prism software (GraphPad Software, San Diego, CA, USA) to test for Gaussian distribution and to perform a paired t-test. A p-value less than 0.05 was considered as statistically significant.

Supplementary Materials: A list with the LFC, *padj* and transcripts per million for all above mentioned genes and a figure showing the individual changes of vst values can be found at https://www.mdpi.com/1422-0067/22/6/3123/s1.

Author Contributions: Study conception and design, S.R., A.A. and V.S.; methodology and investigation, S.R. and V.S.; validation, formal analysis, S.R., E.A. and V.S.; resources, A.A.; writing—original draft preparation, S.R., E.A. and V.S.; writing—review and editing, S.R., A.A. and V.S.; supervision, A.A. and V.S.; project administration, S.R. and V.S.; funding acquisition, V.S. All authors have read and agreed to the published version of the manuscript.

Funding: This research was supported by the Faculty of Medicine, LMU (FöFoLE, 785) to V.S. and by the German Research Foundation to V.S. (SCHO 1664/1-1).

Institutional Review Board Statement: The study was conducted according to the guidelines of the Declaration of Helsinki, and approved by the Ethics Committee of Ludwig-Maximilians-University, Munich (project code 19-177, 24 July 2019).

Informed Consent Statement: Informed consent, declaring that any surplus tissue can be used for medical studies at the university hospital, was obtained from all subjects involved in the study.

Data Availability Statement: All raw sequencing data are available upon request and approval of the local ethics committee.

Acknowledgments: V.S. thanks Ingrid Weiss for her enthusiasm and valuable discussions. V.S. and S.R. thank Heidrun Grondinger for technical assistance.

Conflicts of Interest: The authors declare no conflict of interest.

Abbreviations

BMP	Bone morphogenetic protein
CMV	cytomegalovirus
HA	hyaluronan
HAS	hyaluronan synthases
hMSCs	human mesenchymal stem cells
hUVECs	human umbilical vein endothelial cells
LFC	$\log_2$-fold change
min	minutes
Padj	adjusted *p*-value
RNAseq	RNA sequencing
SD	standard deviation
SE	standard error

References

1. Lowenstam, H.A.; Weiner, S. *On Biomineralization*; Oxford University Press: New York, NY, USA, 1989.
2. Gilbert, P.; Porter, S.M.; Sun, C.Y.; Xiao, S.; Gibson, B.M.; Shenkar, N.; Knoll, A.H. Biomineralization by particle attachment in early animals. *Proc. Natl. Acad. Sci. USA* **2019**, *116*, 17659–17665. [CrossRef]
3. Mahamid, J.; Aichmayer, B.; Shimoni, E.; Ziblat, R.; Li, C.; Siegel, S.; Paris, O.; Fratzl, P.; Weiner, S.; Addadi, L. Mapping amorphous calcium phosphate transformation into crystalline mineral from the cell to the bone in zebrafish fin rays. *Proc. Natl. Acad. Sci. USA* **2010**, *107*, 6316–6321. [CrossRef] [PubMed]
4. Weiss, I.M. Species-specific shells: Chitin synthases and cell mechanics in molluscs. *Z. Kristallogr.* **2012**, *227*, 723–738. [CrossRef]
5. Wolff, J. Das Gesetz der Transformation der Knochen. *Hirschwald Berl. Ger.* **1893**, *19*, 1222–1224. [CrossRef]
6. Da Silva Madaleno, C.; Jatzlau, J.; Knaus, P. BMP signalling in a mechanical context—Implications for bone biology. *Bone* **2020**, *137*, 115416. [CrossRef]
7. Yourek, G.; McCormick, S.M.; Mao, J.J.; Reilly, G.C. Shear stress induces osteogenic differentiation of human mesenchymal stem cells. *Regen Med.* **2010**, *5*, 713–724. [CrossRef] [PubMed]
8. McCoy, R.J.; O'Brien, F.J. Influence of shear stress in perfusion bioreactor cultures for the development of three-dimensional bone tissue constructs: A review. *Tissue Eng. Part B Rev.* **2010**, *16*, 587–601. [CrossRef]
9. Weinbaum, S.; Cowin, S.C.; Zeng, Y. A model for the excitation of osteocytes by mechanical loading-induced bone fluid shear stresses. *J. Biomech.* **1994**, *27*, 339–360. [CrossRef]
10. Metzger, T.A.; Schwaner, S.A.; LaNeve, A.J.; Kreipke, T.C.; Niebur, G.L. Pressure and shear stress in trabecular bone marrow during whole bone loading. *J. Biomech.* **2015**, *48*, 3035–3043. [CrossRef]

11. Weiss, I.M.; Schonitzer, V. The distribution of chitin in larval shells of the bivalve mollusk *Mytilus galloprovincialis*. *J. Struct. Biol.* **2006**, *153*, 264–277. [CrossRef]
12. Schonitzer, V.; Weiss, I.M. The structure of mollusc larval shells formed in the presence of the chitin synthase inhibitor Nikkomycin Z. *BMC Struct. Biol.* **2007**, *7*, 71. [CrossRef] [PubMed]
13. Weiss, I.M.; Schonitzer, V.; Eichner, N.; Sumper, M. The chitin synthase involved in marine bivalve mollusk shell formation contains a myosin domain. *FEBS Lett.* **2006**, *580*, 1846–1852. [CrossRef] [PubMed]
14. Weiss, I.M.; Luke, F.; Eichner, N.; Guth, C.; Clausen-Schaumann, H. On the function of chitin synthase extracellular domains in biomineralization. *J. Struct. Biol.* **2013**, *183*, 216–225. [CrossRef] [PubMed]
15. Bastow, E.R.; Byers, S.; Golub, S.B.; Clarkin, C.E.; Pitsillides, A.A.; Fosang, A.J. Hyaluronan synthesis and degradation in cartilage and bone. *Cell Mol. Life Sci.* **2008**, *65*, 395–413. [CrossRef]
16. Astachov, L.; Vago, R.; Aviv, M.; Nevo, Z. Hyaluronan and mesenchymal stem cells: From germ layer to cartilage and bone. *Front. Biosci* **2011**, *16*, 261–276. [CrossRef]
17. Qu, C.; Rilla, K.; Tammi, R.; Tammi, M.; Kroger, H.; Lammi, M.J. Extensive CD44-dependent hyaluronan coats on human bone marrow-derived mesenchymal stem cells produced by hyaluronan synthases HAS1, HAS2 and HAS3. *Int. J. Biochem. Cell Biol.* **2014**, *48*, 45–54. [CrossRef]
18. Calabro, A.; Oken, M.M.; Hascall, V.C.; Masellis, A.M. Characterization of hyaluronan synthase expression and hyaluronan synthesis in bone marrow mesenchymal progenitor cells: Predominant expression of HAS1 mRNA and up-regulated hyaluronan synthesis in bone marrow cells derived from multiple myeloma patients. *Blood* **2002**, *100*, 2578–2585. [CrossRef] [PubMed]
19. Wong, G.L. Basal activities and hormone responsiveness of osteoclast-like and osteoblast-like bone cells are regulated by glucocorticoids. *J. Biol. Chem.* **1979**, *254*, 6337–6340. [CrossRef]
20. Wong, G.L.; Luben, R.A.; Cohn, D.V. 1,25-dihydroxycholecalciferol and parathormone: Effects on isolated osteoclast-like and osteoblast-like cells. *Science* **1977**, *197*, 663–665. [CrossRef] [PubMed]
21. Adams, J.R.; Sander, G.; Byers, S. Expression of hyaluronan synthases and hyaluronidases in the MG63 osteoblast cell line. *Matrix Biol.* **2006**, *25*, 40–46. [CrossRef]
22. Chopra, R.K.; Li, Z.M.; Vickery, S.; Anastassiades, T. Newly synthesized proteoglycans secreted by sequentially derived populations of cells from new-born rat calvaria: Effects of transforming growth factor-beta and matrigenin activity. *Cell Differ. Dev.* **1990**, *32*, 47–59. [CrossRef]
23. Luben, R.A.; Wong, G.L.; Cohn, D.V. Biochemical characterization with parathormone and calcitonin of isolated bone cells: Provisional identification of osteoclasts and osteoblasts. *Endocrinology* **1976**, *99*, 526–534. [CrossRef] [PubMed]
24. Salbach, J.; Rachner, T.D.; Rauner, M.; Hempel, U.; Anderegg, U.; Franz, S.; Simon, J.C.; Hofbauer, L.C. Regenerative potential of glycosaminoglycans for skin and bone. *J. Mol. Med.* **2012**, *90*, 625–635. [CrossRef]
25. Boskey, A.L.; Dick, B.L. Hyaluronan interactions with hydroxyapatite do not alter in vitro hydroxyapatite crystal proliferation and growth. *Matrix* **1991**, *11*, 442–446. [CrossRef]
26. Huang, L.; Cheng, Y.Y.; Koo, P.L.; Lee, K.M.; Qin, L.; Cheng, J.C.; Kumta, S.M. The effect of hyaluronan on osteoblast proliferation and differentiation in rat calvarial-derived cell cultures. *J. Biomed. Mater. Res. A* **2003**, *66*, 880–884. [CrossRef]
27. Knudson, C.B.; Knudson, W. Hyaluronan-binding proteins in development, tissue homeostasis, and disease. *FASEB J.* **1993**, *7*, 1233–1241. [CrossRef] [PubMed]
28. Fisher, L.W. *The Nature of the Proteoglycans of Bone*; EBESCO Media: Birmingham, AL, USA, 1985.
29. Oohira, A.; Nogami, H. Elevated accumulation of hyaluronate in the tubular bones of osteogenesis imperfecta. *Bone* **1989**, *10*, 409–413. [CrossRef]
30. Benisch, P.; Schilling, T.; Klein-Hitpass, L.; Frey, S.P.; Seefried, L.; Raaijmakers, N.; Krug, M.; Regensburger, M.; Zeck, S.; Schinke, T.; et al. The transcriptional profile of mesenchymal stem cell populations in primary osteoporosis is distinct and shows overexpression of osteogenic inhibitors. *PLoS ONE* **2012**, *7*, e45142.
31. Joeng, K.S.; Lee, Y.C.; Lim, J.; Chen, Y.; Jiang, M.M.; Munivez, E.; Ambrose, C.; Lee, B.H. Osteocyte-specific WNT1 regulates osteoblast function during bone homeostasis. *J. Clin. Investig.* **2017**, *127*, 2678–2688. [CrossRef]
32. Moverare-Skrtic, S.; Henning, P.; Liu, X.; Nagano, K.; Saito, H.; Borjesson, A.E.; Sjogren, K.; Windahl, S.H.; Farman, H.; Kindlund, B.; et al. Osteoblast-derived WNT16 represses osteoclastogenesis and prevents cortical bone fragility fractures. *Nat. Med.* **2014**, *20*, 1279–1288. [CrossRef] [PubMed]
33. Tsuji, K.; Bandyopadhyay, A.; Harfe, B.D.; Cox, K.; Kakar, S.; Gerstenfeld, L.; Einhorn, T.; Tabin, C.J.; Rosen, V. BMP2 activity, although dispensable for bone formation, is required for the initiation of fracture healing. *Nat. Genet.* **2006**, *38*, 1424–1429. [CrossRef] [PubMed]
34. Kilic, A.; Ameli, A.; Park, J.A.; Kho, A.T.; Tantisira, K.; Santolini, M.; Cheng, F.; Mitchel, J.A.; McGill, M.; O'Sullivan, M.J.; et al. Mechanical forces induce an asthma gene signature in healthy airway epithelial cells. *Sci. Rep.* **2020**, *10*, 966. [CrossRef]
35. Natarajan, M.; Aravindan, N.; Sprague, E.A.; Mohan, S. Hemodynamic Flow-Induced Mechanotransduction Signaling Influences the Radiation Response of the Vascular Endothelium. *Radiat. Res.* **2016**, *186*, 175–188. [CrossRef]
36. Blackwell, K.A.; Raisz, L.G.; Pilbeam, C.C. Prostaglandins in bone: Bad cop, good cop? *Trends Endocrinol. Metab.* **2010**, *21*, 294–301. [CrossRef]
37. Hoey, D.A.; Tormey, S.; Ramcharan, S.; O'Brien, F.J.; Jacobs, C.R. Primary cilia-mediated mechanotransduction in human mesenchymal stem cells. *Stem Cells* **2012**, *30*, 2561–2570. [CrossRef] [PubMed]

38. Kubota, K.; Furuse, M.; Sasaki, H.; Sonoda, N.; Fujita, K.; Nagafuchi, A.; Tsukita, S. Ca(2+)-independent cell-adhesion activity of claudins, a family of integral membrane proteins localized at tight junctions. *Curr. Biol.* **1999**, *9*, 1035–1038. [CrossRef]
39. Pacholsky, D.; Vakeel, P.; Himmel, M.; Lowe, T.; Stradal, T.; Rottner, K.; Furst, D.O.; van der Ven, P.F. Xin repeats define a novel actin-binding motif. *J. Cell Sci.* **2004**, *117 (Pt 22)*, 5257–5268. [CrossRef]
40. Storbeck, C.J.; Wagner, S.; O'Reilly, P.; McKay, M.; Parks, R.J.; Westphal, H.; Sabourin, L.A. The Ldb1 and Ldb2 transcriptional cofactors interact with the Ste20-like kinase SLK and regulate cell migration. *Mol. Biol. Cell* **2009**, *20*, 4174–4182. [CrossRef] [PubMed]
41. Schraufstatter, I.U.; Discipio, R.G.; Zhao, M.; Khaldoyanidi, S.K. C3a and C5a are chemotactic factors for human mesenchymal stem cells, which cause prolonged ERK1/2 phosphorylation. *J. Immunol.* **2009**, *182*, 3827–3836. [CrossRef] [PubMed]
42. Shimoyama, Y.; Tsujimoto, G.; Kitajima, M.; Natori, M. Identification of three human type-II classic cadherins and frequent heterophilic interactions between different subclasses of type-II classic cadherins. *Biochem. J.* **2000**, *349 Pt 1*, 159–167. [CrossRef]
43. Gerdes, J.; Lemke, H.; Baisch, H.; Wacker, H.H.; Schwab, U.; Stein, H. Cell cycle analysis of a cell proliferation-associated human nuclear antigen defined by the monoclonal antibody Ki-67. *J. Immunol.* **1984**, *133*, 1710–1715. [PubMed]
44. Bassal, S.; Nomura, N.; Venter, D.; Brand, K.; McKay, M.J.; van der Spek, P.J. Characterization of a novel human cell-cycle-regulated homologue of Drosophila dlg1. *Genomics* **2001**, *77*, 5–7. [CrossRef]
45. Hori, T.; Haraguchi, T.; Hiraoka, Y.; Kimura, H.; Fukagawa, T. Dynamic behavior of Nuf2-Hec1 complex that localizes to the centrosome and centromere and is essential for mitotic progression in vertebrate cells. *J. Cell Sci.* **2003**, *116 Pt 16*, 3347–3362. [CrossRef]
46. Bono, P.; Cordero, E.; Johnson, K.; Borowsky, M.; Ramesh, V.; Jacks, T.; Hynes, R.O. Layilin, a cell surface hyaluronan receptor, interacts with merlin and radixin. *Exp. Cell Res.* **2005**, *308*, 177–187. [CrossRef]
47. Hardwick, C.; Hoare, K.; Owens, R.; Hohn, H.P.; Hook, M.; Moore, D.; Cripps, V.; Austen, L.; Nance, D.M.; Turley, E.A. Molecular cloning of a novel hyaluronan receptor that mediates tumor cell motility. *J. Cell Biol.* **1992**, *117*, 1343–1350. [CrossRef] [PubMed]
48. McCourt, P.A.; Ek, B.; Forsberg, N.; Gustafson, S. Intercellular adhesion molecule-1 is a cell surface receptor for hyaluronan. *J. Biol. Chem.* **1994**, *269*, 30081–30084. [CrossRef]
49. Li, L.; Asteriou, T.; Bernert, B.; Heldin, C.H.; Heldin, P. Growth factor regulation of hyaluronan synthesis and degradation in human dermal fibroblasts: Importance of hyaluronan for the mitogenic response of PDGF-BB. *Biochem. J.* **2007**, *404*, 327–336. [CrossRef] [PubMed]
50. Selbi, W.; de la Motte, C.; Hascall, V.; Phillips, A. BMP-7 modulates hyaluronan-mediated proximal tubular cell-monocyte interaction. *J. Am. Soc. Nephrol.* **2004**, *15*, 1199–1211. [CrossRef] [PubMed]
51. Michikami, I.; Fukushi, T.; Tanaka, M.; Egusa, H.; Maeda, Y.; Ooshima, T.; Wakisaka, S.; Abe, M. Kruppel-like factor 4 regulates membranous and endochondral ossification. *Exp. Cell Res.* **2012**, *318*, 311–325. [CrossRef]
52. Maroski, J.; Vorderwulbecke, B.J.; Fiedorowicz, K.; Da Silva-Azevedo, L.; Siegel, G.; Marki, A.; Pries, A.R.; Zakrzewicz, A. Shear stress increases endothelial hyaluronan synthase 2 and hyaluronan synthesis especially in regard to an atheroprotective flow profile. *Exp. Physiol.* **2011**, *96*, 977–986. [CrossRef] [PubMed]
53. Stewart, S.; Darwood, A.; Masouros, S.; Higgins, C.; Ramasamy, A. Mechanotransduction in osteogenesis. *Bone Jt. Res.* **2020**, *9*, 1–14. [CrossRef] [PubMed]
54. Huang, R.L.; Sun, Y.; Ho, C.K.; Liu, K.; Tang, Q.Q.; Xie, Y.; Li, Q. IL-6 potentiates BMP-2-induced osteogenesis and adipogenesis via two different BMPR1A-mediated pathways. *Cell Death Dis.* **2018**, *9*, 144. [CrossRef]
55. Fisher, L.W.; Fedarko, N.S. Six genes expressed in bones and teeth encode the current members of the SIBLING family of proteins. *Connect. Tissue Res.* **2003**, *44* (Suppl. 1), 33–40. [CrossRef]
56. Ling, Y.; Rios, H.F.; Myers, E.R.; Lu, Y.; Feng, J.Q.; Boskey, A.L. DMP1 depletion decreases bone mineralization in vivo: An FTIR imaging analysis. *J. Bone Min. Res.* **2005**, *20*, 2169–2177. [CrossRef]
57. Bennett, C.N.; Longo, K.A.; Wright, W.S.; Suva, L.J.; Lane, T.F.; Hankenson, K.D.; MacDougald, O.A. Regulation of osteoblastogenesis and bone mass by Wnt10b. *Proc. Natl. Acad. Sci. USA* **2005**, *102*, 3324–3329. [CrossRef]
58. Gadi, J.; Jung, S.H.; Lee, M.J.; Jami, A.; Ruthala, K.; Kim, K.M.; Cho, N.H.; Jung, H.S.; Kim, C.H.; Lim, S.K. The transcription factor protein Sox11 enhances early osteoblast differentiation by facilitating proliferation and the survival of mesenchymal and osteoblast progenitors. *J. Biol. Chem.* **2013**, *288*, 25400–25413. [CrossRef] [PubMed]
59. Parry, D.A.; Brookes, S.J.; Logan, C.V.; Poulter, J.A.; El-Sayed, W.; Al-Bahlani, S.; Al Harasi, S.; Sayed, J.; Raif el, M.; Shore, R.C.; et al. Mutations in C4orf26, encoding a peptide with in vitro hydroxyapatite crystal nucleation and growth activity, cause amelogenesis imperfecta. *Am. J. Hum. Genet.* **2012**, *91*, 565–571. [CrossRef]
60. Amizuka, N.; Karaplis, A.C.; Henderson, J.E.; Warshawsky, H.; Lipman, M.L.; Matsuki, Y.; Ejiri, S.; Tanaka, M.; Izumi, N.; Ozawa, H.; et al. Haploinsufficiency of parathyroid hormone-related peptide (PTHrP) results in abnormal postnatal bone development. *Dev. Biol.* **1996**, *175*, 166–176. [CrossRef]
61. Entwistle, J.; Hall, C.L.; Turley, E.A. HA receptors: Regulators of signalling to the cytoskeleton. *J. Cell Biochem.* **1996**, *61*, 569–577. [CrossRef]
62. Reiprich, S.; Hofbauer, E.; Kiderlen, S.; Clausen-Schaumann, H.; Bocker, W.; Aszodi, A.; Schonitzer, V. Adhesive Properties of the Hyaluronan Pericellular Coat in Hyaluronan Synthases Overexpressing Mesenchymal Stem Cells. *Int. J. Mol. Sci.* **2020**, *21*, 3827. [CrossRef] [PubMed]

63. Koistinen, V.; Karna, R.; Koistinen, A.; Arjonen, A.; Tammi, M.; Rilla, K. Cell protrusions induced by hyaluronan synthase 3 (HAS3) resemble mesothelial microvilli and share cytoskeletal features of filopodia. *Exp. Cell Res.* **2015**, *337*, 179–191. [CrossRef]
64. You, J.; Yellowley, C.E.; Donahue, H.J.; Zhang, Y.; Chen, Q.; Jacobs, C.R. Substrate deformation levels associated with routine physical activity are less stimulatory to bone cells relative to loading-induced oscillatory fluid flow. *J. Biomech. Eng.* **2000**, *122*, 387–393. [CrossRef] [PubMed]
65. Burger, E.H.; Klein-Nulend, J. Mechanotransduction in bone-role of the lacuno-canalicular network. *FASEB J.* **1999**, *13*, S101–S112. [CrossRef]
66. Knothe Tate, M.L.; Steck, R.; Forwood, M.R.; Niederer, P. In vivo demonstration of load-induced fluid flow in the rat tibia and its potential implications for processes associated with functional adaptation. *J. Exp. Biol.* **2000**, *203 Pt 18*, 2737–2745.
67. Haasper, C.; Jagodzinski, M.; Drescher, M.; Meller, R.; Wehmeier, M.; Krettek, C.; Hesse, E. Cyclic strain induces FosB and initiates osteogenic differentiation of mesenchymal cells. *Exp. Toxicol. Pathol.* **2008**, *59*, 355–363. [CrossRef] [PubMed]
68. Jagodzinski, M.; Breitbart, A.; Wehmeier, M.; Hesse, E.; Haasper, C.; Krettek, C.; Zeichen, J.; Hankemeier, S. Influence of perfusion and cyclic compression on proliferation and differentiation of bone marrow stromal cells in 3-dimensional culture. *J. Biomech.* **2008**, *41*, 1885–1891. [CrossRef] [PubMed]
69. Haudenschild, A.K.; Hsieh, A.H.; Kapila, S.; Lotz, J.C. Pressure and distortion regulate human mesenchymal stem cell gene expression. *Ann. Biomed. Eng.* **2009**, *37*, 492–502. [CrossRef]
70. Li, Y.J.; Batra, N.N.; You, L.; Meier, S.C.; Coe, I.A.; Yellowley, C.E.; Jacobs, C.R. Oscillatory fluid flow affects human marrow stromal cell proliferation and differentiation. *J. Orthop. Res.* **2004**, *22*, 1283–1289. [CrossRef]
71. Zimmerman, D.; Jin, F.; Leboy, P.; Hardy, S.; Damsky, C. Impaired bone formation in transgenic mice resulting from altered integrin function in osteoblasts. *Dev. Biol.* **2000**, *220*, 2–15. [CrossRef]
72. Kapur, S.; Baylink, D.J.; Lau, K.H. Fluid flow shear stress stimulates human osteoblast proliferation and differentiation through multiple interacting and competing signal transduction pathways. *Bone* **2003**, *32*, 241–251. [CrossRef]
73. Norvell, S.M.; Alvarez, M.; Bidwell, J.P.; Pavalko, F.M. Fluid shear stress induces beta-catenin signaling in osteoblasts. *Calcif. Tissue Int.* **2004**, *75*, 396–404. [CrossRef]
74. Arnsdorf, E.J.; Tummala, P.; Jacobs, C.R. Non-canonical Wnt signaling and N-cadherin related beta-catenin signaling play a role in mechanically induced osteogenic cell fate. *PLoS ONE* **2009**, *4*, e5388. [CrossRef]
75. Chen, J.C.; Hoey, D.A.; Chua, M.; Bellon, R.; Jacobs, C.R. Mechanical signals promote osteogenic fate through a primary cilia-mediated mechanism. *FASEB J.* **2016**, *30*, 1504–1511. [CrossRef] [PubMed]
76. Glossop, J.R.; Cartmell, S.H. Effect of fluid flow-induced shear stress on human mesenchymal stem cells: Differential gene expression of IL1B and MAP3K8 in MAPK signaling. *Gene Exp. Patterns* **2009**, *9*, 381–388. [CrossRef]
77. Wang, G.; Kostidis, S.; Tiemeier, G.L.; Sol, W.; de Vries, M.R.; Giera, M.; Carmeliet, P.; van den Berg, B.M.; Rabelink, T.J. Shear Stress Regulation of Endothelial Glycocalyx Structure Is Determined by Glucobiosynthesis. *Arter. Thromb. Vasc. Biol.* **2020**, *40*, 350–364. [CrossRef] [PubMed]
78. Kyykallio, H.; Oikari, S.; Bueno Alvez, M.; Gallardo Dodd, C.J.; Capra, J.; Rilla, K. The Density and Length of Filopodia Associate with the Activity of Hyaluronan Synthesis in Tumor Cells. *Cancers* **2020**, *12*, 1908. [CrossRef] [PubMed]
79. Rilla, K.; Tiihonen, R.; Kultti, A.; Tammi, M.; Tammi, R. Pericellular hyaluronan coat visualized in live cells with a fluorescent probe is scaffolded by plasma membrane protrusions. *J. Histochem. Cytochem.* **2008**, *56*, 901–910. [CrossRef] [PubMed]
80. Weiss, I.M. *Mineral-Chitin Composites in Molluscs in Extracellular Sugar-Based Biopolymers Matrices*; Cohen, E., Merzendorfer, H., Eds.; Springer: Cham, Switzerland, 2019; pp. 57–93.
81. Dobin, A.; Davis, C.A.; Schlesinger, F.; Drenkow, J.; Zaleski, C.; Jha, S.; Batut, P.; Chaisson, M.; Gingeras, T.R. STAR: Ultrafast universal RNA-seq aligner. *Bioinformatics* **2013**, *29*, 15–21. [CrossRef]
82. Love, M.I.; Huber, W.; Anders, S. Moderated estimation of fold change and dispersion for RNA-seq data with DESeq2. *Genome Biol.* **2014**, *15*, 550. [CrossRef]
83. Yu, G.; Wang, L.G.; Han, Y.; He, Q.Y. clusterProfiler: An R package for comparing biological themes among gene clusters. *OMICS* **2012**, *16*, 284–287. [CrossRef] [PubMed]
84. Jacquemet, G.; Paatero, I.; Carisey, A.F.; Padzik, A.; Orange, J.S.; Hamidi, H.; Ivaska, J. FiloQuant reveals increased filopodia density during breast cancer progression. *J. Cell Biol.* **2017**, *216*, 3387–3403. [CrossRef] [PubMed]
85. Schindelin, J.; Arganda-Carreras, I.; Frise, E.; Kaynig, V.; Longair, M.; Pietzsch, T.; Preibisch, S.; Rueden, C.; Saalfeld, S.; Schmid, B.; et al. Fiji: An open-source platform for biological-image analysis. *Nat. Methods* **2012**, *9*, 676–682. [CrossRef] [PubMed]

7. Paper III

Article

Fusion of Normoxic- and Hypoxic-Preconditioned Myoblasts Leads to Increased Hypertrophy

Tamara Pircher, Henning Wackerhage, Elif Akova, Wolfgang Böcker, Attila Aszodi and Maximilian M. Saller

Special Issue
100th Anniversary of Nobel Prize in Physiology or Medicine 1922: Metabolism in Muscle
Edited by
Dr. Valentina Di Felice

https://doi.org/10.3390/cells11061059

cells

MDPI

Article

Fusion of Normoxic- and Hypoxic-Preconditioned Myoblasts Leads to Increased Hypertrophy

Tamara Pircher [1], Henning Wackerhage [2], Elif Akova [1], Wolfgang Böcker [1], Attila Aszodi [1] and Maximilian M. Saller [1,*]

[1] Department of Orthopaedics and Trauma Surgery, Musculoskeletal University Center Munich (MUM), Ludwig-Maximilians-University (LMU), Fraunhoferstraße 20, 82152 Planegg-Martinsried, Germany; tamara.pircher@med.uni-muenchen.de (T.P.); elif.akova@med.uni-muenchen.de (E.A.); wolfgang.boecker@med.uni-muenchen.de (W.B.); attila.aszodi@med.uni-muenchen.de (A.A.)

[2] Faculty of Sport and Health Sciences, Technical University of Munich, Georg-Brauchle-Ring 60, 80992 Munich, Germany; henning.wackerhage@tum.de

* Correspondence: maximilian.saller@med.uni-muenchen.de; Tel.: +49-89-4400-55486

Abstract: Injuries, high altitude, and endurance exercise lead to hypoxic conditions in skeletal muscle and sometimes to hypoxia-induced local tissue damage. Thus, regenerative myoblasts/satellite cells are exposed to different levels and durations of partial oxygen pressure depending on the spatial distance from the blood vessels. To date, it is unclear how hypoxia affects myoblasts proliferation, differentiation, and particularly fusion with normoxic myoblasts. To study this, we investigated how 21% and 2% oxygen affects C2C12 myoblast morphology, proliferation, and myogenic differentiation and evaluated the fusion of normoxic- or hypoxic-preconditioned C2C12 cells in 21% or 2% oxygen in vitro. Out data show that the long-term hypoxic culture condition does not affect the proliferation of C2C12 cells but leads to rounder cells and reduced myotube formation when compared with myoblasts exposed to normoxia. However, when normoxic- and hypoxic-preconditioned myoblasts were differentiated together, the resultant myotubes were significantly larger than the control myotubes. Whole transcriptome sequencing analysis revealed several novel candidate genes that are differentially regulated during the differentiation under normoxia and hypoxia in mixed culture conditions and may thus be involved in the increase in myotube size. Taken together, oxygen-dependent adaption and interaction of myoblasts may represent a novel approach for the development of innovative therapeutic targets.

Keywords: C2C12; myoblasts; myotube; fusion; myogenic differentiation; hypoxia; oxygen

Citation: Pircher, T.; Wackerhage, H.; Akova, E.; Böcker, W.; Aszodi, A.; Saller, M.M. Fusion of Normoxic- and Hypoxic-Preconditioned Myoblasts Leads to Increased Hypertrophy. *Cells* **2022**, *11*, 1059. https://doi.org/10.3390/cells11061059

Academic Editor: Valentina Di Felice

Received: 23 February 2022
Accepted: 19 March 2022
Published: 21 March 2022

1. Introduction

Since the great oxidation event about 2.4 billion years ago, oxygen has become essential for most forms of life. To date, most organisms not only utilize oxygen for ATP resynthesis through oxidative phosphorylation but also sense oxygen levels and respond to hypoxia with adaptations mediated by signal transduction proteins such as hypoxia-induced factors.

In muscle tissues, and specifically in skeletal muscles, oxygen regulates functions such as proliferation, differentiation, and metabolic activity. Physiologically, hypoxia in skeletal muscle cells occurs during embryogenesis or muscle regeneration after injury. Moreover, satellite cells are located in hypoxic niches between the sarcolemma and the basal membrane, which have been shown to be essential for embryogenesis and injury-induced regeneration [1,2].

Other forms of physiological hypoxia are high altitude and exercise [3]. Exposure to altitude leads to hypoxic adaption and increased oxygen capacity in the blood—for example, by promoting erythropoietin (EPO) expression [4]—while hypoxic exposure of populations for thousands of years has resulted in the selection of mutants of genes such as *EPAS1* (Endothelial PAS Domain Protein 1) in Tibetans and other people [5].

Hypoxia can also be caused by pathological defects such as arteriosclerosis or muscle injury. Extreme muscle trauma is the most common injury seen in trauma centers and the morbidity is highly associated with ischemia, often resulting in permanent disability or even amputation [6,7]. After 6 h of ischemia, muscle is severely damaged, with outcomes ranging from loss of muscle function to necrosis [8]. During ischemia, first, phosphocreatine and glycogen decrease; lactate then increases; and eventually, ATP declines, leading to rigor mortis [8].

Immediately after reversible ischemic injury, satellite-cell-mediated regeneration is initiated [9,10]; the physiological function of satellite cells (SCs) relies on blood flow and oxygen [11]. To date, many studies have analyzed skeletal muscle regeneration only at fixed oxygen partial pressures. In real life, however, SCs and myoblasts are likely to be exposed to spatiotemporally different levels of oxygen depending on how close they are to functioning, oxygen-delivering blood vessels. Later, myoblasts that were exposed to different levels of oxygen will differentiate into myotubes at higher or lower oxygen partial pressures, depending on the regeneration and function of the vasculature. To date, it is not known how such variations of oxygen partial pressure affect myoblast proliferation and their differentiation into myotubes. In particular, we do not understand how mixed populations of normoxic- and hypoxic-conditioned myoblasts differentiate into myotubes at different oxygen levels.

Given this gap in our knowledge, we investigated the effects of 21% normoxia and 2% hypoxia on C2C12 myoblast proliferation and differentiation into myotubes at 21% normoxia or 2% hypoxia. We also analyzed how the mixing of normoxic- and hypoxic-conditioned myoblasts affects myogenic differentiation and transcription. Our data show that long-term hypoxia does not affect myoblast proliferation. Instead, it influences their differentiation into myotubes, with the greatest differences observed when mixed cultures differentiate. Hypoxia drives a unique gene expression program that includes high expression of *Car9* (carbonic anhydrase 9), a known target of hypoxia-related transcription factors.

2. Materials and Methods

2.1. Cell Culture Conditions

C2C12 immortalized mouse myoblasts (Sigma Aldrich, USA) were cultured up to 15 passages in growth medium (GM) composed of Dulbecco's Modified Eagle Medium (DMEM) with GlutaMAX I (Thermo Fisher, USA), 10% fetal bovine serum (FBS, Sigma Aldrich, St. Louis, MI, USA), and 40 IU/mL penicillin/streptomycin (Biochrom, Berlin, Germany) at 37 °C with 5% CO_2/21% O_2 (normoxia) or 5% CO_2/2% O_2 (hypoxia). The medium was changed at least twice per week, if not stated otherwise, and cell confluence was kept below 50% to avoid spontaneous fusion of C2C12 cells.

2.2. Cell Proliferation and Morphology

To evaluate potential changes in cell proliferation due to continuous low oxygen concentration, we quantified cumulative population doublings (cumPD) and population doubling time (PDT) over 28 days. Therefore, 50,000 cells were seeded in T25 cell culture flasks and counted every 3 or 4 days, respectively. To assess oxygen-related differences in cell morphology, phase contrast images were taken 24 h after cell counting and the cell area, as well as the aspect ratio (AR), of at least 250 cells over all passages was quantified with ImageJ [12].

2.3. Generation of Stably Fluorescent C2C12 Cells

To analyze the interaction between hypoxic and normoxic cultured cells, we stably inserted the coding sequence for the green or red fluorescent protein (GFP or RFP) into C2C12 myoblasts. Therefore, 0.4 µL of sleeping beauty transposon plasmids (GFP: pSBbiGP; RFP: psBbiRP) [13], 0.9 µg transposase (pCMV(CAT)T7-SB100) [14], and 20 µL nucleofector solution (Amaxa™ Cell Line Nucleofactor™ Kit V, Lonza, Basel, Switzerland) were added to 500,000 cells and electroporated with the 4D-Nucleofector™ Core Unit (program B

032, Lonza, Basel, Switzerland). After nucleofection, cells were seeded in 6-well plates, selected with 2 µg/mL puromycin (Thermo Fisher, Waltham, MA, USA) for 10 days under normoxic condition and then sorted for high fluorescence (FACSAriaFusion, BD, Franklin Lakes, NJ, USA). For all further experiments, $C2C12^{GFP}$ were exclusively cultured at 21% O_2, while $C2C12^{RFP}$ were cultured at 2% O_2.

2.4. Myoblast Fusion Assay

To observe fusion of cells that were cultured at different oxygen concentrations, 6-well plates were seeded with 450,000 cells/well with only $C2C12^{GFP}$ or $C2C12^{RFP}$ or a combination of both (225,000 cells/well of $C2C12^{GFP}$ and $C2C12^{RFP}$) and incubated in 21% or 2% O_2. After 6 days of proliferation in GM, myogenic differentiation was induced by switching to the differentiation medium (DM) consisting of DMEM supplemented with 2% horse serum (HS, Sigma Aldrich, St. Louis, MI, USA) and 40 IU/mL penicillin/streptomycin. After 4 days of myogenic differentiation, the cells were fixed in 4% paraformaldehyde (PFA) in phosphate-buffered saline (PBS) for 15 min at room temperature, washed three times in PBS, and the newly formed myotubes were visualized by immunocytochemistry using an antibody against myosin heavy chain 1E (MYH1E, clone MF20, obtained from the Developmental Studies Hybridoma Bank developed under the auspices of the NICHD and maintained by The University of Iowa, Department of Biological Sciences, Iowa City, IA, USA 52242). Therefore, fixed cells were blocked with blocking solution (0.5% Triton X-100 and 10% horse serum in PBS) for 1 h at room temperature and incubated overnight at 4 °C with the primary antibody (1:50 in blocking solution). Afterwards, cells were washed three times with PBS at room temperature and incubated with appropriate fluorophore-conjugated secondary donkey anti-mouse antibodies (1:500 in blocking solution, Thermo Fisher, Waltham, MA, USA) for 1 h at room temperature. Finally, cells were washed twice in PBS, counterstained with 4′,6-diamidine-2′-phenylindole dihydrochloride (DAPI), washed once with PBS, and mounted with Fluoroshield (Abcam, Cambridge, UK). Large overview images covering an area of slightly over 0.75 cm^2 were acquired with an epifluorescence microscope (AxioObserver, Zeiss, Jena, Germany).

To quantify differences in C2C12 fusion, the relative number of myotubes (MT: MT^{GFP}, MT^{RFP}, or $MT^{GFP+RFP}$) were quantified with ImageJ (NIH, USA). Therefore, GFP and RFP image channels were converted to 8-bit grayscale, noise was reduced with a 2-pixel median filter, and a manually determined threshold including all fused cells was applied. Afterwards, the MYH1E image channel was also converted to 8-bit grayscale and merged with the newly created GFP and the RFP image channels using the image calculator, thereby only overlapping cells within both images present in the final composite (GFP and MYH1E-channel image; RFP and MHY1E-channel image). Finally, both composites were merged into one colored image using channel merger of ImageJ and counted manually with the ImageJ cell counter.

Absolute areas of GFP^+, RFP^+, and RFP^+/GFP^+ pixels in the $MYH1E^+$ area were determined with a custom python script (Python 3.7.6) using the following libraries tools: numpy (for matrix processing), scikit-image (for standard image processing algorithm implementations), and matplotlib (for visualization).

All images were read into memory and single-pixel calculation was used to detect cells. Furthermore, the images were treated in the same way as in ImageJ, and the merged image was subtracted from the composites (GFP and MYH1E-channel image; RFP and MHY1E-channel image) to maintain the area for MT^{GFP} and MT^{RFP} without inclusion of $MT^{GFP+RFP}$.

2.5. mRNA-Sequencing and Bioinformatic Analysis

To identify candidate genes that are differentially regulated, C2C12 cells were differentiated as described above and lysed with Trizol (Invitrogen, Waltham, MA, USA) after 24, 72, 96, or 144 h. RNA was isolated with Direct-zol™ (Zymo-Research, Irvine, CA, USA) and RNA integrity was validated with a Bioanalyzer (Agilent, Santa Clara, CA, USA).

RNA-sequencing libraries were generated using the SENSE mRNA-Seq Library Prep Kit V2 (Lexogen, Vienna, Austria) according to the manufacturer's protocol. Sequencing was performed on a HiSeq1500 device (Illumina, San Diego, CA, USA) with a read length of 50 bp and a sequencing depth of approximately 6 million reads per sample.

FASTQ files were demultiplexed by the sample-specific barcodes used for generation of each library. Reads were aligned to the *Mus musculus* genome (release GRCh38.99) using STAR (version 2.7.2b). Genes with less than 10 reads were filtered out in all samples, leaving 22,105 genes for further analysis. Normalization was performed through variance stabilizing transformation (vst) for Principal Component Analysis (PCA) and the most differentially expressed genes were selected for further clustering. Differential gene expression was analyzed by the DESeq2 package (version 1.28.1) in R software (version 4.0.3) with an adjusted *p*-value (*p*-adj) of <0.05 and a Log2FoldChange of ±2 cut-off for each condition and each time point. Venn diagram was created using significantly different expressed genes with a *p*-adj value of <0.05. Gene set enrichment analysis (GSEA) was performed at each time point through the Molecular Signatures Database (MSigDB) R package (version 7.0) using org.Mm.eg.db (version 3.11.4) and mouse_H_v5 hallmark gene set.

2.6. Statistical Analysis

Morphology and proliferation experiments were carried out three times in triplicates and C2C12 fusion experiments were carried out four times in triplicates. Statistical significance was calculated after determination of a Gaussian distribution using either a one-way ANOVA or a *t*-test with appropriate posthoc tests in R (version 4.1.0). Statistical significance was assumed at a *p*-value of $\leq$0.05. Data were represented as either the mean and the standard deviation (SD) or the median with quartiles.

3. Results

3.1. Prolonged Hypoxic Exposure Affects the Morphology of C2C12 Myoblasts but Does Not Change Their Proliferation

To evaluate whether long-term hypoxia affects cell morphology, C2C12 myoblasts were exposed to 2% oxygen for 4 weeks. Prolonged hypoxia altered the morphology of C2C12 myoblasts, as shown in Figure 1B, compared with C2C12 in normoxia (Figure 1A). Hypoxic cells had the same area (Figure 1A',B',C), but their aspect ratio was 16% smaller ($p \leq 0.05$) compared to myoblasts cultured under normoxia (Figure 1D).

To determine the effect of long-term 2% hypoxia on proliferation, we quantified the cumulative population doubling and the population doubling time of C2C12 myoblasts over 28 days. Although the cumulative population doubling of hypoxic cultured C2C12 was 6.5% lower compared with normoxic cells (Figure 1E), the mean population doubling time was not significantly different (Figure 1F), suggesting that long-term hypoxia does not affect proliferation.

3.2. Long-Term Hypoxia Inhibits Myoblast Fusion In Vitro

Next, we investigated whether long-term hypoxia affects myogenic differentiation. We found that 2% hypoxia inhibited the formation of myotubes, when compared with normoxic myoblasts (Figure 2A). Specifically, the area of myotubes was 71.1% smaller ($p \leq 0.001$; Figure 2B) and the relative number of myotubes was 56.0% lower ($p \leq 0.05$; Figure 2C) in hypoxia than in normoxia.

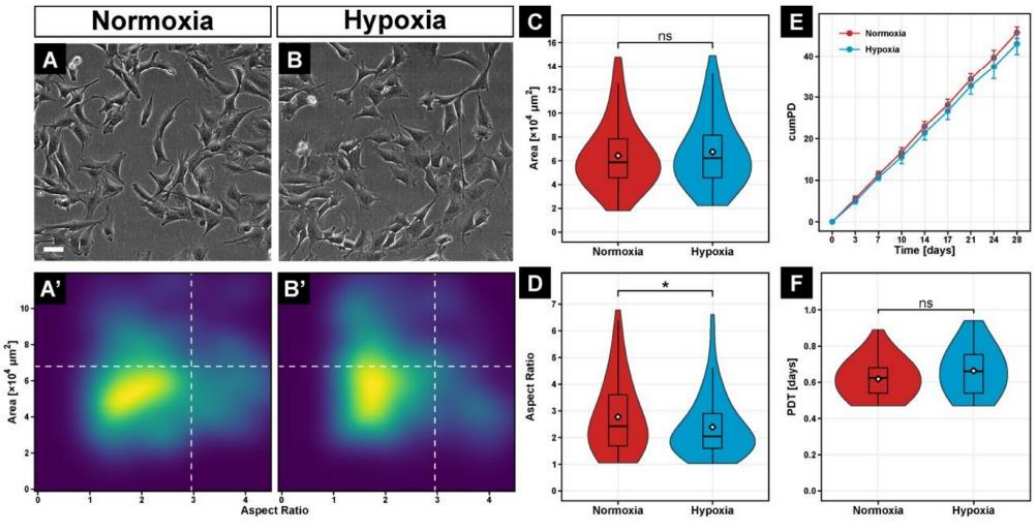

Figure 1. Phase-contrast images of C2C12 cells grown continuously for 28 days at 21% O_2 (**A**) or 2% O_2 (**B**). Quantification of cell area and aspect ratio illustrates the morphology distribution between normoxic (**A'**) and hypoxic (**B'**) cultured cells. Statistical analysis of individual cell morphology parameters revealed a significant decrease in aspect ratio (**D**) but not area (**C**). The effect of long-term hypoxia on cell proliferation, evaluated by cumulative population doublings (cumPD) (**E**) and population doubling time (PDT) (**F**) over a period of 28 days showed no significant differences between the two oxygen levels. Box plots represent the median, quartiles, range, and mean (white diamond). Scale bar: 100 µm. Significance level *: $p \leq 0.05$, ns—not significant.

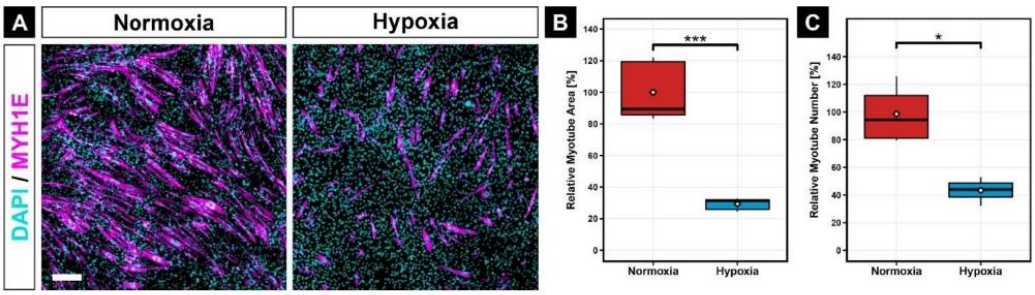

Figure 2. Immunocytochemistry against MYH1E (magenta) after 7 days of myogenic differentiation at 2% O_2 showed a great reduction of myotube formation compared to 21% O_2 (**A**). Quantification of relative myotube area (**B**) and relative myotube number (**C**) revealed significantly lower values in hypoxia than in normoxia. Scale bar: 200 µm. Box plots represent the median, quartiles, range and mean (white diamond). Significance levels: * equals $p \leq 0.05$; *** equals $p \leq 0.001$.

3.3. Development of a Novel Myoblast Fusion Assay to Analyze Interplay of Normoxic- and Hypoxic-Conditioned Myoblasts

After muscle injury, myoblasts are exposed to different oxygen partial pressures depending on the extent of vasculature damage. To investigate the fusion of normoxic- and hypoxic-conditioned myoblasts, we generated C2C12 cell lines stably expressing a green (GFP, used for normoxic C2C12 myoblasts) or red (RFP, used for hypoxic-preconditioned C2C12 myoblasts) fluorescence protein using the sleeping beauty transposon system. After a short selection period in normoxia, one-third of the cells with the highest fluorescence were sorted by FACS (Figure 3A,A'). Afterwards, $C2C12^{GFP}$ cells were exclusively cultured

in 21% O_2, while C2C12^{RFP} cells were grown in 2% O_2. A mixture of normoxic-conditioned GFP-positive and hypoxic-conditioned RFP-positive myoblasts was then used for differentiation assays. In these assays, the green, yellow, and red colors indicate the extent to which GFP- or RFP-positive myoblasts fused into myotubes (Figure 3B). Myoblasts cultured in 21% O_2 were labeled with 'N' (normoxia) and those cultured in 2% O_2 with 'H' (hypoxia). While the first letter denotes normoxic or hypoxic conditioning of C2C12 myoblasts, the letter after the arrow reflects the oxygen treatment applied during subsequent differentiation. For example, N&H▶Diff-H refers to a mixture of normoxic- (N) and hypoxic-conditioned (H) myoblasts that were subsequently differentiated in 2% O_2 (Figure 3B).

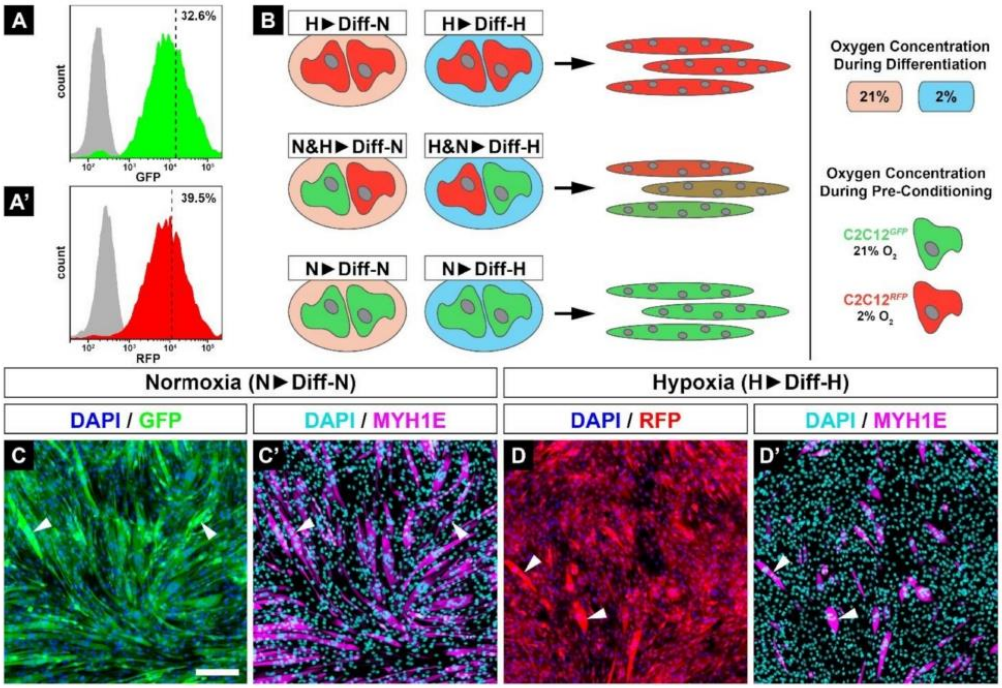

Figure 3. C2C12 cells were stably transfected with fluorescence proteins, sorted for high GFP (**A**) or RFP (**A'**) fluorescence intensity by FACS, and afterwards continuously cultured at 21% (C2C12^{GFP}) or 2% O_2 (C2C12^{RFP}). Myogenic differentiation assays were performed with single or mixed colored cell lines. Thus, coloring depends on the fusion of various myoblasts populations, resulting in green (C2C12^{GFP}), red (C2C12^{RFP}), or dual-colored (C2C12$^{GFP/RFP}$) myotubes (**B**). Immunocytochemistry against MYH1E shows that the newly generated reporter C2C12 cell lines kept their fusion ability (**C'**,**D'**) and C2C12^{RFP} cells showed fusion deficiency in hypoxia (**D**,**D'**) when compared with C2C12^{GFP} (**C**,**C'**). Scale bar: 200 µm.

To exclude a potential loss of myogenic differentiation ability of C2C12 cells due to stable insertion of the respective fluorophore coding sequence into the genomic DNA, we repeated the fusion experiments and found no significant differences for C2C12^{GFP} in 21% (Figure 3C,C') or C2C12^{RFP} in 2% O_2 (Figure 3D,D') compared with non-transfected C2C12 cells (Figure 2A). Moreover, fusion of myoblasts leads to an obvious accumulation of fluorescence intensity (Figure 3C,D, arrowheads).

3.4. Abrupt Change of Oxygen Concentration Differentially Affects Myogenic Differentiation of Normoxic- and Hypoxic-Preconditioned Myoblasts

To analyze how the switch from normoxia to hypoxia or vice versa affects myogenic differentiation, we differentiated long-term, hypoxic-conditioned C2C12^{RFP} myoblasts in normoxia (H▶Diff-N) and normoxic-conditioned C2C12^{GFP} cells in 2% hypoxia (N▶Diff-H). Interestingly, when we directly compared H▶Diff-N (Figure 4A,A′) and N▶Diff-H (Figure 4C,C′) myotubes, we could not find significant differences in overall myogenic efficiency (Figure 4E), number of myotubes (Figure 4F), or size of myotubes (Figure 4G).

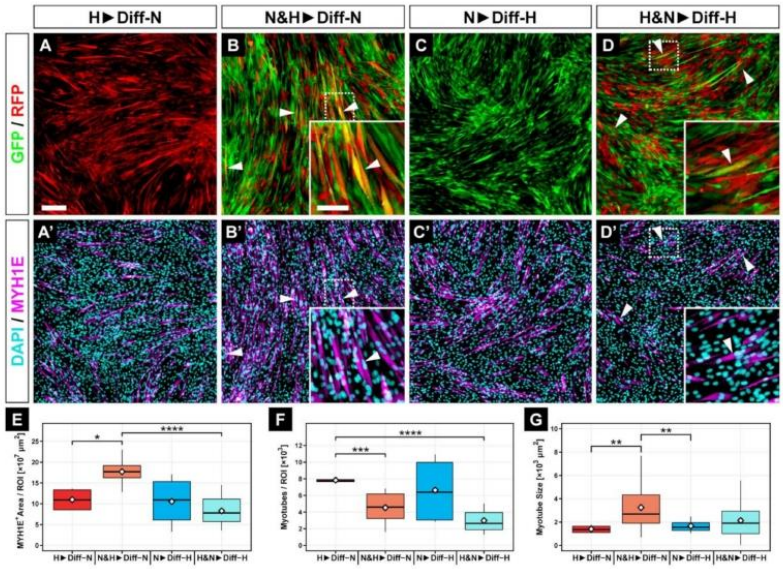

Figure 4. Representative fluorescence microscope images for GFP/RFP (**A**–**D**) and for MYH1E and DAPI (**A′**–**D′**). C2C12^{RFP}, hypoxic-conditioned cells transferred to 21% O_2 (H▶Diff-N, **A**,**A′**) or mixed C2C12 cultures in 2% O_2 (H&N▶Diff-H, **D**,**D′**) showed less myoblast fusion compared with normoxic cells differentiated in hypoxia (N▶Diff-H, **C**,**C′**) or mixed C2C12 cultures differentiated in normoxia (N&H▶Diff-N, **B**,**B′**). Moreover, C2C12^{GFP} and C2C12^{RFP} cells were able to fuse in mixed culture settings (**B**,**D**, arrowheads). While the mixed group had the largest MYH1E^{+} area (**E**) and the greatest myotube size at 21% O_2 (**G**), the myotube number did not increase with mixing of the two cell populations (**F**). Scale bars: 200 µm. Bar plots represent the median, quartiles, range, and mean (white diamond). * $p \leq 0.05$. ** $p \leq 0.01$. *** $p \leq 0.001$. **** $p \leq 0.0001$.

However, when we compared hypoxic-preconditioned cells differentiated in hypoxia (H▶Diff-H) (Figure 3D,D′) or normoxia (H▶Diff-N) (Figure 4A,A′), we detected a 5% and 19% increase in the efficiency of myogenic differentiation and the number of myotubes, respectively, and a 13% larger myotubes size in the H▶Diff-H group compared with H▶Diff-N myotubes (Figure 5).

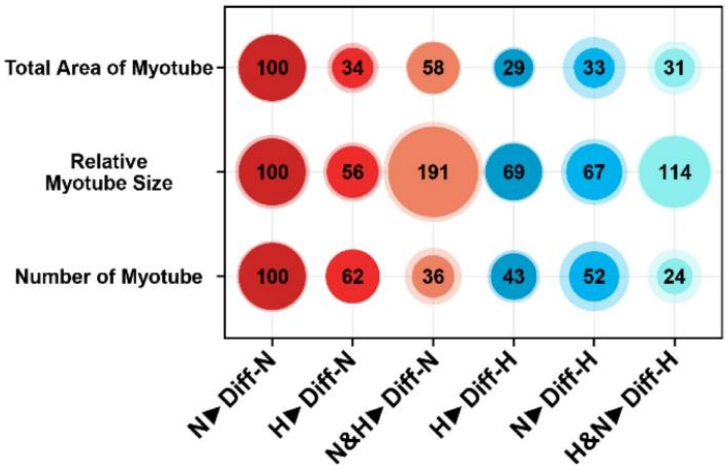

Figure 5. Bubble plots of all investigated groups normalized to N▶Diff-N. Mixed cell cultures showed the greatest relative myotube size, independent of their oxygen environment, even though the number of myotubes was decreased compared with the other groups. Despite low number of myotubes, the total area was greater within N&H▶Diff-N compared with all other groups.

In contrast, differentiation of normoxic myoblasts in 2% hypoxia (N▶Diff-H) reduced myogenic differentiation (Figure 4C,C′) compared with N▶Diff-N (Figure 3C,C′). Specifically, the total myotube area was 67% lower, there were 48% fewer myotubes, and they were 33% smaller compared with the N▶Diff-N myotubes group (Figure 5).

Collectively, our data suggest that (1) the negative effect of hypoxia on myogenic differentiation is reversible to some extent and (2) hypoxia leads to less but significant larger myotubes and is therewith partially involved in the hypertrophy of myotubes.

3.5. Fusion of Hypoxic-Conditioned Myoblasts with Normoxic-Conditioned Myoblasts Results in Larger Myotubes

Next, we investigated how a mixture of hypoxic- and normoxic-conditioned myoblasts under either normoxia or hypoxia affects myogenic differentiation. We found that a mixed population of myoblasts formed fewer myotubes when differentiated under hypoxia (H&N▶Diff-H, Figure 4D,D′) compared with normoxia (N&H▶Diff-N, Figure 4B,B′). Interestingly, mixed myoblasts differentiated in normoxia showed a 187% higher differentiation capacity (N&H▶Diff-N, $p \leq 0.0001$, Figure 4E) when compared with myoblasts that were differentiated in hypoxia (N&H▶Diff-H, Figure 4E). In addition, there were 73% less N&H▶Diff-H myotubes and 162% less H&N▶Diff-H myotubes compared with myoblasts conditioned in hypoxia and differentiated under normoxia (H▶Diff-N, $p \leq 0.001$, Figure 4F). However, when we differentiated a mixture of hypoxic- and normoxic-conditioned myoblasts under normoxia (N&H▶Diff-N), we found 239% or 285% larger myotubes ($p \leq 0.01$) compared with either hypoxic-conditioned myoblasts differentiated under normoxia (H▶Diff-N) or normoxic myoblasts differentiated under hypoxia, respectively (N▶Diff-H, Figure 4G).

We made several additional observations. First, mixing hypoxic-preconditioned cells with normoxic cells inhibited myoblast fusion under normoxic differentiation (N&H▶Diff-N), as judged by the 42% reduction in total $MYHE^+$ area (Figure 5). Second, there were 64% fewer myotubes compared with normoxic-precultured myoblasts differentiated under normoxia (N▶Diff-N). Third, mixed myoblasts were 14% larger when differentiated under hypoxia (H&N▶Diff-H) and 91% larger when differentiated under normoxia (N&H▶Diff-N) compared with normoxic myoblasts differentiated in normoxia (N▶Diff-N) (Figure 5).

Finally, the mixture of long-term, hypoxic-conditioned and normoxic myoblasts (N&H▶Diff-N and H&N▶Diff-H) fused the least, resulting in the lowest number of myotubes (Figure 5).

3.6. Oxygen Tension Differentially Influences Cell Fusion among Different Precultured Cell Populations

To better understand the interaction between long-term, hypoxic-preconditioned and normoxic myoblasts during myogenic differentiation in hypoxia or normoxia, respectively, we divided the fused myotubes (MT) into three subgroups depending on which myoblasts were involved in the fusion process: MT^{GFP}, MT^{RFP}, and $MT^{GFP/RFP}$. In addition to quantifying absolute values (Figure 6D–F), we calculated the relative abundance of MT^{GFP}, MT^{RFP}, and $MT^{GFP/RFP}$ within each experimental group (Figure 6A–C), as the oxygen concentration during differentiation might differentially affect the fusion properties of subpopulations.

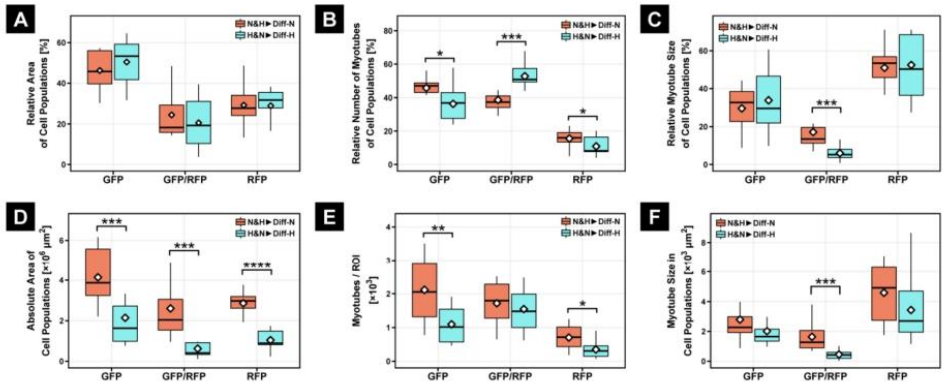

Figure 6. Within the subpopulation, there was no significant difference in relative area of cell population (**A**); however, quantification of the absolute area of all subpopulations at 21% O_2 (N&H▶Diff-N) showed a significant increase compared with H&N▶Diff-H (**D**). While the relative number of mixed myotubes under hypoxic differentiation condition (H&N▶Diff-H) revealed a significant increase in double-fluorescent myotubes compared with differentiation in normoxia (N&H▶Diff-N; **B**), the absolute number of myotubes did not show similar results (**E**). The size of myotubes at 21% O_2 was significantly greater within mixed myotubes, regardless of absolute or relative view, when compared with the H&N▶Diff-H group (**C**,**F**). Bar plots represent the median, quartiles, range, and mean (white diamond). * $p \leq 0.05$. ** $p \leq 0.01$. *** $p \leq 0.001$. **** $p \leq 0.0001$.

Determination of the relative area of individual myotube populations in mixed cultures revealed no differences between normoxic (N&H▶Diff-N) and hypoxic (H&N▶Diff-H) differentiation (Figure 6A). However, within the absolute area, each myotube population showed a significant increase in normoxic differentiation (N&H▶Diff-N) compared with differentiation in hypoxia (H&N▶Diff-H), reflected by a 128% minimum increase of the absolute $MYH1E^{+}$ area in MT^{GFP} and a 316% maximum increase of the absolute $MYH1E^{+}$ area in $MT^{GFP/RFP}$ (Figure 6D).

Intriguingly, quantification of the relative number of myotube types showed a significant difference in myoblast fusion under normoxic (N&H▶Diff-N) and hypoxic conditions (H&N▶Diff-H) (Figure 6B), as indicated by the relative increase of $MT^{GFP/RFP}$ and relative decrease of MT^{GFP} and MT^{RFP} myotubes compared with myoblast fusion of mixed cultures in 21% O_2 (N&H▶Diff-N). However, the determination of absolute myotube number indicated that double-fluorescent myotubes did not differ between the differentiation in normoxia (N&H▶Diff-N) and hypoxia (H&N▶Diff-H), although the absolute numbers of MT^{GFP} and MT^{RFP} myotubes were significant lower in the H&N▶Diff-H group compared with the N&H▶Diff-N group (Figure 6E).

Moreover, the relative and absolute myotube size of $MT^{GFP/RFP}$ was approximately 70% smaller in hypoxic differentiation (H&N▶Diff-H) compared with normoxic differentiation (N&H▶Diff-N) of mixed cultures (Figure 6C,F).

3.7. Hypoxia Leads to Delayed Expression of Genes Encoding Regulators of Myogenic Differentiation

To gain insight into the effect of oxygen on the molecular regulation of myoblasts and their differentiation into myotubes, we performed total RNA-sequencing of myotubes derived from a mixture of normoxic- and hypoxic-conditioned myoblasts that were subsequently differentiated under normoxia and hypoxia (N&H▶Diff-N and H&N▶Diff-H). RNA-Seq was performed at 24, 48, 72, 96, and 144 h after the onset of differentiation. To evaluate potential clustering, we performed a principal component analysis (PCA), which showed the clear separation of a time-dependent first principal component (PC1, Figure 7A, colored spheres) and a second, group-dependent principal component (PC2, Figure 7A, shapes). Moreover, the overall transcriptional landscape of the hypoxic-differentiated mixed C2C12 cells (H&N▶Diff-H, Figure 7A dots) is slightly delayed compared with the N&H▶Diff-N group (Figure 7A, triangles). While the 100 genes that contributed most to PC1 were myogenic-related marker genes (Figure S1A), PC2 revealed segregation of genes associated with adaptation to hypoxia (Figure S1B).

Differential gene expression (DEG) analysis revealed that 177 out of 6740 genes showed significantly different regulation between H&N▶Diff-H and N&H▶Diff-N groups at all time points (Figure 7B). All significant differentially expressed genes are shown in Supplementary Table S1. In addition, gene set enrichment analysis (GSEA) demonstrated that the three gene set hallmarks 'hypoxia', 'glycolysis', and 'myogenesis' were regulated at all time points (Figure 7C). All significant regulated gene set hallmarks are shown in Supplementary Figure S2. Interestingly, at 72 and 96 h after the initiation of differentiation, a significant decrease in the 'myogenesis' gene set further highlighted an adaptive phase for the H&N▶Diff-H group compared with the normoxic mixed myoblast culture (N&H▶Diff-N, Figure 7C, lower panel).

To further investigate which genes are associated with differences of myogenic fusion at different oxygen concentrations of mixed myoblast cultures, we performed a hierarchical cluster analysis (HCA) for the top 50 genes out of the 177 continuously differentially regulated genes (Figure 7D). Intriguingly, HCA showed a clear separation of essential (increased expression over time) or inhibitory (decreased expression over time) myogenic genes in a temporal manner (Figure 7D). The nine most promising genes in this separation are as follows: *Adm* (adrenomedullin), encoding a vasodilator peptide hormone [15]; *Apln* (Apelin), known for the regulation of cell proliferation in smooth muscle cells [16]; *Car9* (Carboxy anhydrase 9), one of the most highly expressed genes in the hypoxic environment of solid tumors [17]; *Grp35* (G-protein related receptor 35), encoding an orphan receptor involved in ERK1/2 activation [18]; *Scara5* (Scavenger receptor class A member 5), encoding a ferritin receptor necessary for cell growth [19]; *Ptgfr* (prostaglandin F receptor), encoding a G-protein-coupled receptor involved in prostaglandin signaling; *Ankrd1* (Ankyrin repeat domain 1), mainly expressed in type 1 skeletal muscle fibers [20]; *Ldb3* (LIM domain binding 3), encoding for Z-band alternatively spliced PDZ-motif protein [21]; *Pdlim3* (PDZ And LIM Domain 3), involved in p38 MAPK activation (Figure 7E) [22].

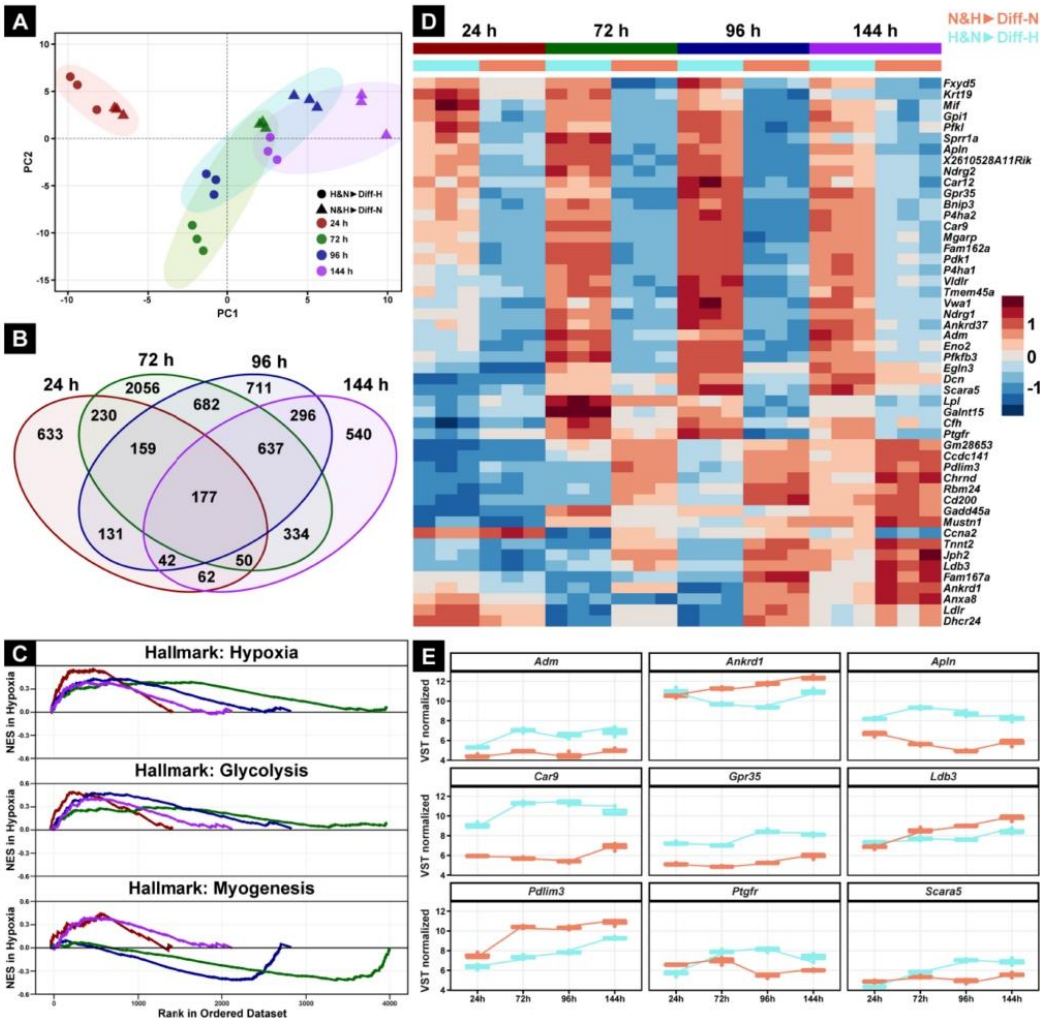

Figure 7. Comparison of gene expression between N&H▶Diff-N and H&N▶Diff-H. The first principal component (PC1) and second principal component (PC2) cluster analysis showed no initial difference between N&H▶Diff-N and H&N▶Diff-H 24 h after the onset of myogenic differentiation (**A**). The Venn diagram shows 177 genes present at all analyzed time points (**B**). Visualization of hypoxic-dependent hallmarks over 144 h shows the most positively (NES > 0) or negatively (NES < 0) regulated gene sets in the myoblast group H&N▶Diff-H compared with the normoxic group, N&H▶Diff-N (**C**). The heat map (**D**) includes the top 50 genes with the greatest variance within 144 h out of the 177 genes shown in (**B**). A positive value indicates higher expression; a negative value indicates lower expression. The nine most promising genes were extrapolated from the heat map and their activation under both oxygen conditions was assessed and directly compared over 144 h. (**E**) Genes are sorted alphabetically. NES—normalized enrichment score.

4. Discussion

The main findings of this study are that chronic exposure to hypoxia or normoxia has a differential effect on myoblast differentiation and that a mixture of normoxic- and hypoxic-conditioned myoblasts forms larger myotubes than when myoblasts are conditioned in

normoxia or hypoxia alone. Additionally, we identified genes whose expression changes significantly in response to hypoxia and/or during differentiation.

4.1. Long-Term Hypoxia Has No Significant Impact on Myoblast Morphology or Proliferation but Leads to Reduced Myogenesis

During somitogenesis, a community effect of 30–40 mesodermal cells is required so that these cells differentiate into myoblasts [23]. Studies have shown that myogenesis is dependent on the expression cell–cell adhesion molecules as N-cadherin (CDH2), which promote the stable expression of myogenic factors [24] and the accumulation of p21 and p27 cyclin-dependent kinase inhibitors, involved in cell cycle withdrawal [25–27]. As several cadherins, including CDH2, were differentially regulated between N&H▶Diff-N and H&N▶Diff-H from 24 h upwards (Table S1), we suggest that the changes in the cell aspect ratio as well as the reduced myoblast fusion under hypoxic conditions are, at least partially, dependent on the expression of hypoxia-sensitive cadherin genes.

Furthermore, while short-term hypoxia can induce an increased proliferation of mouse satellite cells [28] or human primary myoblasts [29] at 2% O_2 in vitro, long-term hypoxic culture of human primary myoblast led to an adjustment of proliferation between normoxic and hypoxic conditions [29], which is consistent with our data showing no significantly different proliferation of C2C12 cells between 21% and 2% O_2.

As previously described by Di Carlo et al., severe acute hypoxia (<1% O_2) leads to accelerated degradation of MYOD and thereby inhibits differentiation of C2C12 myoblasts [30]. Here, we demonstrated that an oxygen level of 2% O_2 over a period of 4 days likewise results in reduced myotube formation, indicating a very quick adjustment to hypoxia. Interestingly, our data showed that not only hypoxic differentiation of hypoxic-precultured myoblasts (H▶Diff-H) led to a reduction in myotube size and number of 40–60%, but we also showed that this negative effect of hypoxia is largely irreversible in differentiation in normoxia (H▶Diff-N).

Myoblast fusion is highly dependent on available energy sources such as ATP [31] and ATP synthesis is impaired in hypoxia [32]. Compared with myoblasts, which are mainly dependent on glycolytic energy production [33], myotubes are less able to maintain ATP levels and turnover, and thus, die within hours [34]. Therefore, the reduction of myogenesis under hypoxic conditions is a multimodal process consisting of at least reduced fusion and subsequent cell death due to energy restrictions.

4.2. Hypoxia Leads to Increased Synergy between Hypoxia- and Normoxia-Cultured Myoblasts

In the case of acute ischemic events, it has been established that regeneration can only occur if blood flow to the affected area is restored [11] and stemlike satellite cells can migrate into (re-)oxygenated tissue [35]. Interaction of myoblasts/satellite cells also occurs after intramuscular transplantation of satellite cells, as shown by a potential novel therapy approach for ischemic muscle injuries [36–38]. Thus, our study mainly focused on the interaction of normoxic and hypoxic precultured myoblasts during the fusion process in normoxic and hypoxic environments.

Intriguingly, both mixed myoblast groups (N&H▶Diff-N and H&N▶Diff-H), regardless of their environmental oxygen exposure, showed a smaller total myotube area and number of myotubes, and a remarkably greater relative myotube size compared with standardized N▶Diff-N group (Figure 5). This suggests that the leading mechanism in the mixed myoblast fusion process is hypertrophy, which results in fewer but larger fused myotubes in an oxygen-dependent manner. Moreover, this hypertrophy seems to depend on the direct fusion of normoxic- and hypoxic-preconditioned myoblasts, suggesting a synergistic effect.

4.3. Hypoxic Transcriptional Changes Are Partially Reversible during Myogenic Differentiation

The potential of myoblasts to fuse was not completely lost within the hypoxic environment, as MTORC1 signaling involved in myoblast proliferation and differentiation [39] was still expressed in the H&N▶Diff-H group.

During prolonged hypoxia, locally released proinflammatory cytokines induce an anabolic response in skeletal muscle cells, which ultimately results in muscle damage and atrophy [40]. However, short hypoxic periods of inflammation are also crucial for adaptive remodeling of skeletal muscle tissue. For example, prostaglandins (PGs), members of inflammatory mediators, have been implicated in multiple stages of myogenesis in vitro, including proliferation, differentiation [41], myoblast survival [42] and fusion [43], and prostaglandin 2α (PGF2α) leads to muscle hypertrophy via the PI3K/ERK/mTOR signaling pathway in C2C12 myotubes [44]. Interestingly, our new data identified *Ptges3* (Prostaglandin E Synthase 3) and *Ptges3l* (Prostaglandin E Synthase 3 Like) as novel candidates that are involved in oxygen-dependent hypertrophy.

In addition, we also identified hypoxia-dependent regulation of *Apln* within the mixed hypoxic group (H&N▶Diff-H). However, *Apln* has exclusively been associated with hypoxia in cardiomyocytes [45] or age-related muscle wasting (sarcopenia) in rodents and humans [46]. Thus, it can be hypothesized that the regulation of APLN is, at least partially, oxygen-driven, as the oxidative capacity of skeletal muscles is reduced during aging [47] and APLN is associated with energy metabolism [48].

Compared with myogenic differentiation of mixed myoblasts in hypoxia, myoblasts/myotubes of the N&H▶Diff-N group showed a significantly faster and higher upregulation of LIM domains, which are known to be involved in myogenesis [49,50]. Intrudingly, we identified *Pdlim3* and *Ldb3* as oxygen-sensitive genes that are associated with hypertrophic cardiomyopathies [51,52].

In vivo, transcriptional changes of whole muscles exposed to moderate hypoxia (11.2%) have been reported after 48 h [53], which is consistent with our results showing a transcriptional change between 24 and 72 h of myogenic differentiation in hypoxia. However, as the transcriptional response to hypoxia is relatively fast in vitro, further time points should be evaluated in future experiments. Moreover, we observed a partial delayed myogenic differentiation of the H&N▶Diff-H within a period of 6 days, assuming that differentiation in hypoxia leads to an initial "hypoxic shock", which seems to be partially reversible. Thus, the investigation of longer observation periods would be necessary.

4.4. Within Hypoxia, Skeletal Muscle Hypertrophy Shows Parallels to Cancer Cell Behavior

Recent studies have revealed increased glycolysis and metabolic reprogramming of skeletal muscle cells during hypertrophy [54], which are similar to those in cancer cells [55]. Our results sustain those findings, as upregulation of several cancer-associated genes was found within mixed myoblast cultured in a hypoxic environment. For example, *Car9*, a well-studied gene in solid tumors such as renal clear cell carcinoma [56], which is mainly associated with tumor-related hypoxia, was upregulated in H&N▶Diff-H over all time points. *Car9* has an upstream hypoxia-responsive element (HRE) binding site [56] that appears to be epigenetically active in zebrafish muscles in response to hypoxia [57].

Although no association with skeletal muscle cells has been reported to date for the KRAS-pathway, its upregulation was observed in the mixed hypoxic myoblast group (H&N▶Diff-H). The KRAS-pathway is known to be involved in cellular proliferation associated with colon, pancreatic, and lung cancer [58] and has previously been shown to have an influence on HIF1A translational regulation within hypoxia [59]. Moreover, the *Scara5* gene, which is associated with tumor suppression in liver [60], lung [61], and breast cancer [62], and osteosarcoma [63], showed upregulation in the H&N▶Diff-H group. It has been reported to have a negative correlation with VEGFA, one of the major target genes of HIF1A, leading to downregulation of angiogenesis. Further investigations revealed a SCARA5-dependent decrease of AKT and ERK phosphorylation [62], which are both also involved in hypoxic-adjustment of skeletal muscle cells [1].

Remarkably, many of the genes found in our study interact with the PI3K/ART/mTOR pathway, for example, SCARA5 and GPR35 (G-coupled receptor 35) [18,62]. In addition, muscle hypertrophy and cancer cells show increased IGF-AKT1-mTORC1 or reduced myostatin signaling [55]. Thus, the mTOR pathway may also play a major role in hypoxic-adjustment of skeletal muscle cells.

5. Conclusions

Taken together, the interaction of hypoxic and normoxic myoblasts leads to a decrease in the total number of myotubes but is likely to result in more hypertrophic myotubes when fused together. This hypertrophic process is possibly based in part on cance-like metabolic reprogramming strategies during hypoxic myogenesis. However, additional loss- and gain-of-function experiments with the promising candidate genes are necessary to reveal further confirmations.

Supplementary Materials: The following supporting information can be downloaded at https://www.mdpi.com/article/10.3390/cells11061059/s1. Figure S1: Top 50 Genes of the PC1 and PC2; Figure S2: Hallmark gene sets over time. Table S1: Differentially expressed genes.

Author Contributions: Conceptualization, T.P. and M.M.S.; methodology, T.P. and M.M.S.; software, T.P., E.A. and M.M.S.; validation, T.P., A.A. and M.M.S.; formal analysis, T.P., E.A. and M.M.S.; investigation, T.P. and M.M.S.; resources, A.A. and H.W.; data curation, M.M.S.; writing—original draft preparation, T.P., H.W. and M.M.S.; writing—review and editing, T.P., H.W., E.A., A.A., W.B. and M.M.S.; visualization, T.P. and M.M.S.; supervision, M.M.S. All authors have read and agreed to the published version of the manuscript.

Funding: This research received no external funding.

Institutional Review Board Statement: Not applicable.

Informed Consent Statement: Not applicable.

Data Availability Statement: Gene expression data are deposited at https://www.ncbi.nlm.nih.gov/geo. All in vitro data are available from the corresponding author upon reasonable request.

Acknowledgments: We thank Simon Wölzmüller, Martina Burggraf, and Zsuzsanna Farkas for technical assistance.

Conflicts of Interest: The authors declare no conflict of interest.

References

1. Pircher1, T.; Wackerhage, H.; Aszodi, A.; Kammerlander, C.; Böcker, W.; Saller, M.M. Hypoxic Signaling in Skeletal Muscle Maintenance and Regeneration: A Systematic Review. *Front. Physiol.* **2021**, *12*, 684899. [CrossRef] [PubMed]
2. Parmar, K.; Mauch, P.; Vergilio, J.-A.; Sackstein, R.; Down, J.D. Distribution of hematopoietic stem cells in the bone marrow according to regional hypoxia. *Proc. Natl. Acad. Sci. USA* **2007**, *104*, 5431–5436. [CrossRef] [PubMed]
3. Śliwicka, E.; Cisoń, T.; Kasprzak, Z.; Nowak, A.; Pilaczyńska-Szcześniak, Ł. Serum irisin and myostatin levels after 2 weeks of high-altitude climbing. *PLoS ONE* **2017**, *12*, e0181259.
4. Bracken, C.P.; Whitelaw, M.L.; Peet, D.J. The hypoxia-inducible factors: Key transcriptional regulators of hypoxic responses. *Cell. Mol. Life Sci.* **2003**, *60*, 1376–1393. [CrossRef] [PubMed]
5. Wackerhage, H. (Ed.) *Molecular Exercise Physiology*; Routledge: Oxfordshire, UK, 2014; ISBN 9781136477034.
6. Park, J.J.; Campbell, K.; Mercuri, J.J.; Tejwani, N.C. Updates in the management of orthopedic soft-tissue injuries associated with lower extremity trauma. *Am. J. Orthop.* **2012**, *41*, E27–E35.
7. Scalea, T.M.; DuBose, J.; Moore, E.E.; West, M.; Moore, F.A.; McIntyre, R.; Cocanour, C.; Davis, J.; Ochsner, M.G.; Feliciano, D. Western Trauma Association critical decisions in trauma: Management of the mangled extremity. *J. Trauma Acute Care Surg.* **2012**, *72*, 86–93. [CrossRef]
8. Belkin, M.; Brown, R.D.; Wright, J.G.; LaMorte, W.W.; Hobson, R.W. A new quantitative spectrophotometric assay of ischemia-reperfusion injury in skeletal muscle. *Am. J. Surg.* **1988**, *156*, 83–86. [CrossRef]
9. Parker, M.H.; Seale, P.; Rudnicki, M. Looking back to the embryo: Defining transcriptional networks in adult myogenesis. *Nat. Rev. Genet.* **2003**, *4*, 497–507. [CrossRef]
10. Berkes, C.A.; Tapscott, S.J. MyoD and the transcriptional control of myogenesis. *Semin. Cell Dev. Biol.* **2005**, *16*, 585–595. [CrossRef]
11. Kalogeris, T.; Baines, C.P.; Krenz, M.; Korthuis, R.J. Cell Biology of Ischemia/Reperfusion Injury. *Int. Rev. Cell Mol. Biol.* **2012**, *298*, 229–317. [CrossRef]

12. Schindelin, J.; Arganda-Carreras, I.; Frise, E.; Kaynig, V.; Longair, M.; Pietzsch, T.; Preibisch, S.; Rueden, C.; Saalfeld, S.; Schmid, B.; et al. Fiji: An open-source platform for biological-image analysis. *Nat. Methods* **2012**, *9*, 676–682. [CrossRef]
13. Kowarz, E.; Löscher, D.; Marschalek, R. Optimized Sleeping Beauty transposons rapidly generate stable transgenic cell lines. *Biotechnol. J.* **2015**, *10*, 647–653. [CrossRef] [PubMed]
14. Mátés, L.; Chuah, M.K.L.; Belay, E.; Jerchow, B.; Manoj, N.; Acosta-Sanchez, A.; Grzela, D.; Schmitt, A.; Becker, K.; Matrai, J.; et al. Molecular evolution of a novel hyperactive Sleeping Beauty transposase enables robust stable gene transfer in vertebrates. *Nat. Genet.* **2009**, *41*, 753–761. [CrossRef] [PubMed]
15. Guidolin, D.; Albertin, G.; Spinazzi, R.; Sorato, E.; Mascarin, A.; Cavallo, D.; Antonello, M.; Ribatti, D. Adrenomedullin stimulates angiogenic response in cultured human vascular endothelial cells: Involvement of the vascular endothelial growth factor receptor 2. *Peptides* **2008**, *29*, 2013–2023. [CrossRef] [PubMed]
16. Li, F.; Li, L.; Qin, X.; Pan, W.; Feng, F.; Chen, F.; Zhu, B.; Liao, D.; Tanowitz, H.; Albanese, C.; et al. Apelin-induced vascular smooth muscle cell proliferation: The regulation of cyclin D1. *Front. Biosci.* **2008**, *13*, 3786–3792. [CrossRef] [PubMed]
17. Chafe, S.C.; Lou, Y.; Sceneay, J.; Vallejo, M.; Hamilton, M.J.; McDonald, P.C.; Bennewith, K.L.; Möller, A.; Dedhar, S. Carbonic Anhydrase IX Promotes Myeloid-Derived Suppressor Cell Mobilization and Establishment of a Metastatic Niche by Stimulating G-CSF Production. *Cancer Res.* **2015**, *75*, 996–1008. [CrossRef] [PubMed]
18. Zhao, P.; Sharir, H.; Kapur, A.; Cowan, A.; Geller, E.B.; Adler, M.W.; Seltzman, H.H.; Reggio, P.H.; Heynen-Genel, S.; Sauer, M.; et al. Targeting of the Orphan Receptor GPR35 by Pamoic Acid: A Potent Activator of Extracellular Signal-Regulated Kinase and β-Arrestin2 with Antinociceptive Activity. *Mol. Pharmacol.* **2010**, *78*, 560–568. [CrossRef]
19. Li, J.Y.; Paragas, N.; Ned, R.M.; Qiu, A.; Viltard, M.; Leete, T.; Drexler, I.R.; Chen, X.; Sanna-Cherchi, S.; Mohammed, F.; et al. Scara5 Is a Ferritin Receptor Mediating Non-Transferrin Iron Delivery. *Dev. Cell* **2009**, *16*, 35–46. [CrossRef]
20. Tsukamoto, Y.; Senda, T.; Nakano, T.; Nakada, C.; Hida, T.; Ishiguro, N.; Kondo, G.; Baba, T.; Sato, K.; Osaki, M.; et al. Arpp, a New Homolog of Carp, Is Preferentially Expressed in Type 1 Skeletal Muscle Fibers and Is Markedly Induced by Denervation. *Lab. Investig.* **2002**, *82*, 645–655. [CrossRef] [PubMed]
21. Zhou, Q.; Ruiz-Lozano, P.; Martone, M.E.; Chen, J. Cypher, a Striated Muscle-restricted PDZ and LIM Domain-containing Protein, Binds to α-Actinin-2 and Protein Kinase C. *J. Biol. Chem.* **1999**, *274*, 19807–19813. [CrossRef]
22. Yin, H.; Zhao, J.; He, H.; Chen, Y.; Wang, Y.; Li, D.; Zhu, Q. Gga-miR-3525 Targets PDLIM3 through the MAPK Signaling Pathway to Regulate the Proliferation and Differentiation of Skeletal Muscle Satellite Cells. *Int. J. Mol. Sci.* **2020**, *21*, 5573. [CrossRef] [PubMed]
23. Cossu, G.; Kelly, R.; Di Donna, S.; Vivarelli, E.; Buckingham, M. Myoblast differentiation during mammalian somitogenesis is dependent upon a community effect. *Proc. Natl. Acad. Sci. USA* **1995**, *92*, 2254–2258. [CrossRef] [PubMed]
24. Holt, E.C.; Lemaire, P.; Gurdon, J.B. Cadherin-mediated cell interactions are necessary for the activation of MyoD in Xenopus mesoderm. *Proc. Natl. Acad. Sci. USA* **1994**, *91*, 10844–10848. [CrossRef] [PubMed]
25. Goichberg, P.; Geiger, B. Direct Involvement of N-Cadherin–mediated Signaling in Muscle Differentiation. *Mol. Biol. Cell* **1998**, *9*, 3119–3131. [CrossRef]
26. Gavard, J.; Marthiens, V.; Monnet, C.; Lambert, M.; Mège, R.M. N-cadherin activation substitutes for the cell contact control in cell cycle arrest and myogenic differentiation: Involvement of p120 and beta-catenin. *J. Biol. Chem.* **2004**, *279*, 36795–36802. [CrossRef]
27. Charrasse, S.; Meriane, M.; Comunale, F.; Blangy, A.; Gauthier-Rouvière, C. N-cadherin-dependent cell-cell contact regulates Rho GTPases and beta-catenin localization in mouse C2C12 myoblasts. *J. Cell Biol.* **2002**, *158*, 953–965. [CrossRef]
28. Urbani, L.; Piccoli, M.; Franzin, C.; Pozzobon, M.; De Coppi, P. Hypoxia Increases Mouse Satellite Cell Clone Proliferation Maintaining both In Vitro and In Vivo Heterogeneity and Myogenic Potential. *PLoS ONE* **2012**, *7*, e49860. [CrossRef]
29. Koning, M.; Werker, P.M.; van Luyn, M.J.; Harmsen, M.C. Hypoxia Promotes Proliferation of Human Myogenic Satellite Cells: A Potential Benefactor in Tissue Engineering of Skeletal Muscle. *Tissue Eng. Part A* **2011**, *17*, 1747–1758. [CrossRef]
30. Di Carlo, A.; De Mori, R.; Martelli, F.; Pompilio, G.; Capogrossi, M.C.; Germani, A. Hypoxia Inhibits Myogenic Differentiation through Accelerated MyoD Degradation. *J. Biol. Chem.* **2004**, *279*, 16332–16338. [CrossRef]
31. O'Connor, R.S.; Steeds, C.M.; Wiseman, R.W.; Pavlath, G.K. Phosphocreatine as an energy source for actin cytoskeletal rearrangements during myoblast fusion. *J. Physiol.* **2008**, *586*, 2841–2853. [CrossRef]
32. Hogan, M.C.; Gladden, L.B.; Grassi, B.; Stary, C.M.; Samaja, M. Bioenergetics of contracting skeletal muscle after partial reduction of blood flow. *J. Appl. Physiol.* **1998**, *84*, 1882–1888. [CrossRef] [PubMed]
33. Matsuki, N.; Inaba, M.; Ono, K. Catabolism of Cytoplasmic and Intramitochondrial Adenine Nucleotides in C2C12 Skeletal Myotube under Chemical Hypoxia. *J. Veter. Med Sci.* **2002**, *64*, 341–347. [CrossRef] [PubMed]
34. Dehne, N.; Kerkweg, U.; Otto, T.; Fandrey, J. The HIF-1 response to simulated ischemia in mouse skeletal muscle cells neither enhances glycolysis nor prevents myotube cell death. *Am. J. Physiol. Integr. Comp. Physiol.* **2007**, *293*, R1693–R1701. [CrossRef] [PubMed]
35. Mohyeldin, A.; Garzon-Muvdi, T.; Quinones-Hinojosa, A. Oxygen in stem cell biology: A critical component of the stem cell niche. *Cell Stem Cell* **2010**, *7*, 150–161. [CrossRef]
36. Frudinger, A.; Kolle, D.; Schwaiger, W.; Pfeifer, J.; Paede, J.; Halligan, S. Muscle-derived cell injection to treat anal incontinence due to obstetric trauma: Pilot study with 1 year follow-up. *Gut* **2009**, *59*, 55–61. [CrossRef]

37. Frudinger, A.; Pfeifer, J.; Paede, J.; Kolovetsiou-Kreiner, V.; Marksteiner, R.; Halligan, S. Autologous skeletal muscle-derived cell injection for anal incontinence due to obstetric trauma: A five-year follow-up of an initial study of ten patients. *Color. Dis.* **2015**, *17*, 794–801. [CrossRef]
38. Frudinger, A.; Marksteiner, R.; Pfeifer, J.; Margreiter, E.; Paede, J.; Thurner, M. Skeletal muscle-derived cell implantation for the treatment of sphincter-related faecal incontinence. *Stem Cell Res. Ther.* **2018**, *9*, 233. [CrossRef]
39. Hauerslev, S.; Vissing, J.; Krag, T.O. Muscle Atrophy Reversed by Growth Factor Activation of Satellite Cells in a Mouse Muscle Atrophy Model. *PLoS ONE* **2014**, *9*, e100594. [CrossRef]
40. Agrawal, A.; Rathor, R.; Kumar, R.; Suryakumar, G.; Ganju, L. Role of altered proteostasis network in chronic hypobaric hypoxia induced skeletal muscle atrophy. *PLoS ONE* **2018**, *13*, e0204283. [CrossRef]
41. Ms, C.L.M.; Tatsumi, R.; Allen, R.E. Role of cyclooxygenase-1 and -2 in satellite cell proliferation, differentiation, and fusion. *Muscle Nerve* **2004**, *30*, 497–500. [CrossRef]
42. Jansen, K.M.; Pavlath, G.K. Prostaglandin F2α promotes muscle cell survival and growth through upregulation of the inhibitor of apoptosis protein BRUCE. *Cell Death Differ.* **2008**, *15*, 1619–1628. [CrossRef]
43. Shen, W.; Prisk, V.; Li, Y.; Foster, W.; Huard, J. Inhibited skeletal muscle healing in cyclooxygenase-2 gene-deficient mice: The role of PGE2and PGF2α. *J. Appl. Physiol.* **2006**, *101*, 1215–1221. [CrossRef] [PubMed]
44. Markworth, J.F.; Cameron-Smith, D. Prostaglandin F2α stimulates PI3K/ERK/mTOR signaling and skeletal myotube hypertrophy. *Am. J. Physiol. Cell Physiol.* **2011**, *300*, C671–C682. [CrossRef] [PubMed]
45. Hou, J.; Wang, L.; Long, H.; Wu, H.; Wu, Q.; Zhong, T.; Chen, X.; Zhou, C.; Guo, T.; Wang, T. Hypoxia preconditioning promotes cardiac stem cell survival and cardiogenic differentiation in vitro involving activation of the HIF-1α/apelin/APJ axis. *Stem Cell Res. Ther.* **2017**, *8*, 215. [CrossRef] [PubMed]
46. Vinel, C.; Lukjanenko, L.; Batut, A.; Deleruyelle, S.; Pradère, J.-P.; Le Gonidec, S.; Dortignac, A.; Geoffre, N.; Pereira, O.; Karaz, S.; et al. The exerkine apelin reverses age-associated sarcopenia. *Nat. Med.* **2018**, *24*, 1360–1371. [CrossRef]
47. Russ, D.W.; Kent-Braun, J.A. Is skeletal muscle oxidative capacity decreased in old age? *Sports Med.* **2004**, *34*, 221–229. [CrossRef]
48. Hu, G.; Wang, Z.; Zhang, R.; Sun, W.; Chen, X. The Role of Apelin/Apelin Receptor in Energy Metabolism and Water Homeostasis: A Comprehensive Narrative Review. *Front. Physiol.* **2021**, *12*, 632886. [CrossRef]
49. Han, S.; Cui, C.; Wang, Y.; He, H.; Liu, Z.; Shen, X.; Chen, Y.; Li, D.; Zhu, Q.; Yin, H. Knockdown of CSRP3 inhibits differentiation of chicken satellite cells by promoting TGF-β/Smad3 signaling. *Gene* **2019**, *707*, 36–43. [CrossRef]
50. Pomiès, P.; Pashmforoush, M.; Vegezzi, C.; Chien, K.R.; Auffray, C.; Beckerle, M.C. The Cytoskeleton-associated PDZ-LIM Protein, ALP, Acts on Serum Response Factor Activity to Regulate Muscle Differentiation. *Mol. Biol. Cell* **2007**, *18*, 1723–1733. [CrossRef]
51. Bagnall, R.D.; Yeates, L.; Semsarian, C. Analysis of the Z-disc genes PDLIM3 and MYPN in Patients with Hypertrophic Cardiomyopathy. *Int. J. Cardiol.* **2010**, *145*, 601–602. [CrossRef]
52. Tucholski, T.; Cai, W.; Gregorich, Z.R.; Bayne, E.F.; Mitchell, S.D.; McIlwain, S.J.; de Lange, W.J.; Wrobbel, M.; Karp, H.; Hite, Z.; et al. Distinct hypertrophic cardiomyopathy genotypes result in convergent sarcomeric proteoform profiles revealed by top-down proteomics. *Proc. Natl. Acad. Sci. USA* **2020**, *117*, 24691–24700. [CrossRef] [PubMed]
53. Ji, W.; Wang, L.; He, S.; Yan, L.; Li, T.; Wang, J.; Kong, A.-N.T.; Yu, S.; Zhang, Y. Effects of acute hypoxia exposure with different durations on activation of Nrf2-ARE pathway in mouse skeletal muscle. *PLoS ONE* **2018**, *13*, e0208474. [CrossRef] [PubMed]
54. Verbrugge, S.A.J.; Gehlert, S.; Stadhouders, L.E.M.; Jacko, D.; Aussieker, T.; de Wit, M.J.G.; Vogel, I.S.P.; Offringa, C.; Schönfelder, M.; Jaspers, R.T.; et al. PKM2 Determines Myofiber Hypertrophy In Vitro and Increases in Response to Resistance Exercise in Human Skeletal Muscle. *Int. J. Mol. Sci.* **2020**, *21*, 7062. [CrossRef] [PubMed]
55. DeBerardinis, R.J.; Chandel, N.S. Fundamentals of cancer metabolism. *Sci. Adv.* **2016**, *2*, e1600200. [CrossRef]
56. Wykoff, C.C.; Beasley, N.J.; Watson, P.; Turner, K.J.; Pastorek, J.; Sibtain, A.; Wilson, G.; Turley, H.; Talks, K.L.; Maxwell, P.; et al. Hypoxia-inducible expression of tumor-associated carbonic anhydrases. *Cancer Res.* **2000**, *60*, 7075–7083. [PubMed]
57. Esbaugh, A.J.; Perry, S.F.; Gilmour, K.M. Hypoxia-inducible carbonic anhydrase IX expression is insufficient to alleviate intracellular metabolic acidosis in the muscle of zebrafish, Danio rerio. *Am. J. Physiol. Integr. Comp. Physiol.* **2009**, *296*, R150–R160. [CrossRef]
58. Vogelstein, B.; Kinzler, K.W. Cancer genes and the pathways they control. *Nat. Med.* **2004**, *10*, 789–799. [CrossRef]
59. Kikuchi, H.; Pino, M.S.; Zeng, M.; Shirasawa, S.; Chung, D.C. Oncogenic KRAS and BRAF Differentially Regulate Hypoxia-Inducible Factor-1α and -2α in Colon Cancer. *Cancer Res.* **2009**, *69*, 8499–8506. [CrossRef]
60. Huang, J.; Zheng, D.; Qin, F.-S.; Cheng, N.; Chen, H.; Wan, B.; Wang, Y.-P.; Xiao, H.-S.; Han, Z.-G. Genetic and epigenetic silencing of SCARA5 may contribute to human hepatocellular carcinoma by activating FAK signaling. *J. Clin. Investig.* **2010**, *120*, 223–241. [CrossRef]
61. Yan, N.; Zhang, S.; Yang, Y.; Cheng, L.; Li, C.; Dai, L.; Dai, L.; Zhang, X.; Fan, P.; Tian, H.; et al. Therapeutic upregulation of Class A scavenger receptor member 5 inhibits tumor growth and metastasis. *Cancer Sci.* **2012**, *103*, 1631–1639. [CrossRef]
62. You, K.; Su, F.; Liu, L.; Lv, X.; Zhang, J.; Zhang, Y.; Liu, B. SCARA5 plays a critical role in the progression and metastasis of breast cancer by inactivating the ERK1/2, STAT3, and AKT signaling pathways. *Mol. Cell. Biochem.* **2017**, *435*, 47–58. [CrossRef] [PubMed]
63. Wen, X.; Dong, C.; Wang, N.; Zhang, F. Overexpression of SCARA5 inhibits tumor proliferation and invasion in osteosarcoma via suppression of the FAK signaling pathway. *Mol. Med. Rep.* **2016**, *13*, 2885–2891. [CrossRef] [PubMed]

Acknowledgments

First of all, I would like to thank all members in Musculoskeletal University Munich individually for believing and supporting me at every step. It has been a huge opportunity for me to work with people from different backgrounds in an international environment.

A few months after I started my Ph.D. study on December 2019, Corona pandemic has just started. I felt so anxious and nervous about how to continue with my studies. I am so glad that during that period my supervisor Dr. rer.nat. Maximilian Saller and PD Dr. Attila Aszodi trusted in me to perform Bioinformatics analysis of other lab members. It improved me so much that at the end of my Ph.D. I have 5 co-authorships that were published and at least 1 more on the way. I would like to thank them both for guiding my doctoral thesis, scientific manuscripts and for every opportunity they created for me. Also, I would like to thank Dr. rer. nat Veronika Schönitzer for being my co-supervisor who did the funding application in the first place which creates the initial opportunity for me to move to Munich.

Furthermore, I would like to thank Prof. Hanna Taipaleenmäki and Dr. Hiroaki Saito for their generous contribution to my research without any hesitation. They lead me in the right direction when I needed the most.

Another person I owe my sincere gratitude to Prof. Dr. Susanne Mayer. It has been a great honor for me to work with her and I feel so lucky that I met such a successful yet so friendly woman in science. I truly wish I would like to be like her in the future.

Finally, throughout my doctorate, I believe I cannot be able to come to the finishing line without the help of my husband, Berkay Ölken. We started together this journey by moving to Munich in September 2019. He has always been there when I felt lost, demotivated and deeply whenever I have “imposter syndrome”. I cannot able to survive without him or my family, my lovely father Eren Akova, my mother Seyhan Akova and my mother-in-law Zerrin Ölken. Even we can only see each other once or twice a year they were all there to give me hand and support me. I am so glad to meet their expectations and hopefully keep continue to make them proud.